

# Single Molecule Study of Polymer–Surfactant Interactions

DISSERTATION

for the award of academic degree of

Doctor of Natural Science

– Dr. rer. nat. –

from the faculty of Biology, Chemistry and Geosciences

University of Bayreuth

Submitted by

**John Bosco Stanislaus**

born in Kalugumalai, Tamil Nadu/India

Bayreuth, 2007



# **Single Molecule Study of Polymer–Surfactant Interactions**

## **DISSERTATION**

zur Erlangung des akademischen Grades eines  
Doktors der Naturwissenschaften (Dr. rer. nat.)  
im Fach Chemie der Fakultät für Biologie, Chemie und Geowissenschaften  
der Universität Bayreuth

vorgelegt von

**John Bosco Stanislaus**

Geboren in Kalugumalai, Tamil Nadu/India

Bayreuth, 2007

Die vorliegende Arbeit wurde in der Zeit von März 2003 bis Mai 2007 in Bayreuth am Lehrstuhl Physikalische Chemie II unter Betreuung von Herrn Prof. Dr. Georg Krausch angefertigt.

Vollständiger Abdruck der von der Fakultät für Biologie, Chemie und Geowissenschaften der Universität Bayreuth genehmigten Dissertation zur Erlangung des akademischen Grades eines Doktors der Naturwissenschaften (Dr. rer. nat.).

Promotionsgesuch eingereicht am	15.05.2007
Zulassung durch die Promotionkommission	23.05.2007
Wissenschaftliches Kolloquium	17.07.2007

Amtierender Dekan: Prof. Dr. Carl Beierkuhnlein

Prüfungsausschuß:

*Prof. Dr. Matthias Ballauff (Erstgutachter)*

*Prof. Dr. Georg Krausch (Zweitgutachter)*

*Prof. Dr. Helmut G. Alt (Vorsitzender)*

*Prof. Dr. Axel H.E. Müller*

## **To my parents**

*Experiments never  
deceive. It is our  
judgement that deceives  
itself because it expects  
results which experiments  
do not give.*

Leonardo da Vinci  
15th century



# Table of Contents

<b>1. Introduction</b>	<b>1</b>
1.1 Motivation . . . . .	2
1.2 Outline . . . . .	3
<b>2. Theory and Background</b>	<b>5</b>
2.1 Polymers . . . . .	5
2.1.1 The Influence of Degree of Substitution on Solubility . . . . .	8
2.2 Surfactants . . . . .	9
2.2.1 Classification of Surfactants . . . . .	9
2.2.1.1 Anionic Surfactants. . . . .	10
2.2.1.2 Cationic Surfactants . . . . .	10
2.2.1.3 Zwitterionic Surfactants . . . . .	11
2.2.1.4 Nonionic Surfactants . . . . .	11
2.2.2 Theoretical Basics for Surfactant Self-Assembly . . . . .	11
2.2.2.1 Typical CMC values . . . . .	16
2.2.2.2 The Krafft Point. . . . .	17

2.3	Polymer-Surfactant Interactions in Aqueous Solution.	18
2.3.1	Classification	19
2.3.2	Critical Aggregation Concentration (CAC).	20
2.3.3	Characterization	22
2.3.3.1	Classical Physico-Chemical Methods.	22
2.3.3.2	Spectroscopic Methods.	22
2.3.4	Important Inferences	25
2.3.5	Other Factors Affecting the Complex Formation	26
2.3.6	Interactions Between Nonionic Polymer and Anionic Surfactants	26

### **3. Materials and Methods 29**

3.1	Materials	29
3.1.1	Polymer	29
3.1.1.1	Purification of Polymer	29
3.1.2	Surfactant and Dye	30
3.1.3	Preparation of Solutions	31
3.2	Methods	31
3.2.1	Fluorescence Correlation Spectroscopy	31
3.2.1.1	Experimental Setup.	33
3.2.1.2	Theoretical Concept	35
3.2.1.3	Sample Chamber and Temperature Control Setup	43
3.2.2	Rheology	44
3.2.3	Cryo-Transmission Electron Microscopy	49
3.2.4	Turbidity Measurements	51

<b>4. Results and Discussion</b>	<b>53</b>
4.1 Concentration Dependent Studies. . . . .	53
4.1.1 Fluorescence Correlation Spectroscopy . . . . .	53
4.1.1.1 Critical Micelle Concentration . . . . .	53
4.1.1.2 Critical Aggregation Concentration . . . . .	59
4.1.2 Rheology . . . . .	69
4.1.3 Cryo-Transmission Electron Microscopy . . . . .	72
4.2 Temperature Dependent Studies . . . . .	79
4.2.1 Fluorescence Correlation Spectroscopy . . . . .	79
4.2.2 Rheology . . . . .	86
4.2.3 Turbidity . . . . .	89
<b>5. Summary</b>	<b>95</b>
<b>6. Zusammenfassung</b>	<b>99</b>
<b>7. Bibliography</b>	<b>103</b>



# List of Figures

2.1	Cyclopyranose structure of glucose. . . . .	6
2.2	Methylcellulose . . . . .	8
2.3	Schematic diagram of monomer and micelle concentration as a function of total concentration of surfactants . . . . .	15
2.4	Illustration of the dramatic changes in physical properties beyond the critical micellar concentration . . . . .	16
2.5	Schematic diagram of the temperature dependence of surfactant solubility in the region of the Krafft point . . . . .	18
2.6	A schematic plot of the concentration dependence of the surface tension for polymer–surfactant solutions . . . . .	20
2.7	Schematic diagram of association between homopolymer and a surfactant in wide range of concentration regions . . . . .	25
3.1	(a) Sulphoradamine B (b) Rhodamine B base . . . . .	30
3.2	Schematic drawing of illuminated volume. . . . .	32
3.3	Schematic diagram of confocal FCS setup . . . . .	34
3.4	Shape of the confocal volume element. Here $w_{xy}$ and $w_z$ represents half of the short and long axis respectively. . . . .	36
3.5	The fluctuation signal (fluorescence intensity) in the course of measurement time . . . . .	38

3.6	Typical autocorrelation curve of freely diffusing dye molecule with the triplet fraction . . . . .	41
3.7	Illustration of Temperature control setup with sample chamber .	44
3.8	Simple shear flow of a fluid trapped between two parallel plates.	45
3.9	(a) Schematic illustration of piezoelectric axial vibrator in longitudinal view (b) PAV used in this study . . . . .	48
4.1	Diffusion time of SDS for Sulphoradamine B, Rhodamine 6G , Cresyl violet perchlorate . . . . .	54
4.2	Characteristic diffusion times of Cresyl violet perchlorate as a function of SDS concentration in the absence of MC . . . . .	55
4.3	Normalized autocorrelation curves of SDS solutions . . . . .	57
4.4	Number of Cresyl violet perchlorate dye molecules in the excitation volume for various SDS concentrations . . . . .	58
4.5	Diffusion time of dye molecules as a function of methyl cellulose concentration in the absence of SDS . . . . .	59
4.6	FCS measurements of 1 wt % MC with SDS under different laser powers . . . . .	61
4.7	Diffusion times of the dye molecules determined for 1 wt % MC and various SDS concentration . . . . .	62
4.8	Normalized autocorrelation curves of 1 wt % MC and SDS concentrations . . . . .	63
4.9	Diffusion times of the dye molecules determined for $c_{MC} = 0.5$ (a), and 0.25 (b), as a function of SDS concentration . . . . .	65
4.10	Normalized autocorrelation curves of 0.5 wt % MC (a) and 0.25 wt % MC with various SDS concentrations . . . . .	66
4.11	Location of the SDS concentration leading to the maximum diffusion time of the dye molecules for different MC . . . . .	68
4.12	Number of dye molecules in excited volume for $c_{MC} = 0.25, 0.5,$	

	and 1.0 wt % with various $c_{\text{SDS}}$ . . . . .	68
4.13	(a) Flow curves of 1wt % MC and various $c_{\text{SDS}}$ mixtures.	
	(b) Zero shear viscosity of 1 wt %MC and SDS mixtures. . . . .	70
4.14	CryoTEM image of 1 wt% MC and $2.0 \times 10^{-2}$ M SDS . . . . .	71
4.15	CryoTEM micrographs of 1 wt% MC and $2.0 \times 10^{-2}$ M SDS. . . . .	72
4.16	Cryo-TEM micrograph of 0.4 M SDS solution . . . . .	73
4.17	Cryo-TEM image of 0.4 M SDS + 1 wt % MC solution . . . . .	74
4.18	Schematic diagram explaining the MC/SDS complex formation with increasing concentration of SDS . . . . .	78
4.19	Diffusion time of $c_{\text{dye}}=10^{-8}$ M alone and with $c_{\text{SDS}} = 2.0 \times 10^{-3}$ M, $8.0 \times 10^{-3}$ M, $2.0 \times 10^{-2}$ M, $5.0 \times 10^{-2}$ M, and $2.0 \times 10^{-1}$ M at various temperatures . . . . .	80
4.20	The hydrodynamic radii of SDS solution in different temperatures.	81
4.21	The change in diffusion time of $c_{\text{dye}}=10^{-8}$ M alone and with 1 wt % MC . . . . .	82
4.22	Diffusion time of $c_{\text{dye}}=10^{-8}$ M alone and with $c_{\text{SDS}} = 2.0 \times 10^{-3}$ M, 1 wt % MC, and MC/SDS mixture at various temperatures . . . . .	83
4.23	FCS measurements of 1 wt% MC and $c_{\text{SDS}} = 2.0 \times 10^{-2}$ M at various temperatures . . . . .	84
4.24	Diffusion time of $c_{\text{dye}}=10^{-8}$ M alone and with $c_{\text{SDS}} = 2.0 \times 10^{-1}$ M, 1 wt % MC, and MC/SDS mixture . . . . .	85
4.25	Elastic and loss modulus of 1.0 wt % MC at different temperatures measured with PAV . . . . .	87
4.26	Elastic and loss modulus of $c_{\text{SDS}} = 2.0 \times 10^{-3}$ M and 1.0 wt % MC mixture at different temperatures measured with PAV . . . . .	87
4.27	Elastic and loss modulus of $c_{\text{SDS}} = 2.0 \times 10^{-2}$ M and 1.0 wt % MC mixture at different temperatures measured with PAV . . . . .	88
4.28	Visual inspection of 1 wt % MC and SDS mixtures at different	

	temperatures . . . . .	. 90
4.29	Turbidity measurement of 1 wt % MC alone . . . . .	. 91
4.30	Turbidity curve for the mixtures of $c_{\text{SDS}} = 2.0 \times 10^{-2}$ M and 1 wt %MC, $c_{\text{SDS}} = 2.0 \times 10^{-3}$ M and 1 wt % MC . . . . .	. 91
4.31	Turbidity curve for the mixtures of $c_{\text{SDS}} = 2.0 \times 10^{-1}$ M and 1 wt % MC . . . . .	. 93
4.32	Selected data of Turbidity curve between 20 and 60 °C for the mixtures of $c_{\text{SDS}} =$ no SDS $2.0 \times 10^{-3}$ M, $2.0 \times 10^{-2}$ M, $2.0 \times 10^{-1}$ M, with 1 wt % MC . . . . .	. 93

# List of Tables

2.1	The possible polymer-surfactant combinations based on the charge of the system.. . . . .	19
4.1	Diffusion coefficients from diffusion time of MC/SDS mixtures.	76



# List of Abbreviations

AGU	anhydroglucose units
AOTF	acousto-optical tunable filter
APD	avalanche photodiode
C <sub>12</sub> E <sub>5</sub>	pentaethylene glycol monododecyl ether
CAC	critical aggregation concentration
CEVS	controlled environment vitrification system
CMC	critical micelle concentration
c <sub>MC</sub>	concentration of methyl cellulose
cryo-TEM	cryogenic transmission electron microscopy
c <sub>SDS</sub>	concentration of sodium dodecyl sulfate
CTAB	cetyltrimethylammonium bromide
<i>D</i>	self-diffusion coefficient
$\delta$	duration of gradient pulses
DP	degree of polymerization
DS	degree of substitution
DSC	differential scanning calorimetry
EOA	end of aggregation
ESR	electron spin resonance
<i>F(t)</i>	fluorescence fluctuation function
FCS	fluorescence correlation spectroscopy
FFT	fast Fourier transform

$\gamma$	proton magnetogyric
G	shear-modulus
$G(t)$	correlation function
$G'$	storage modulus
$G''$	loss modulus
HLB	hydrophobic-lipophilic-balance
HPC	hydroxylpropylcellulose
HPMC	hydroxylpropylmethylcellulose
$I_0$	excitation intensity amplitude
$I_{ex}$	spatial distribution of the excitation energy
IPT	incipient precipitation temperature
JR400	cellulose,2-hydroxyethyl 2-[2-hydroxy-3-(trimethylammonio)propoxyl]ethyl 2-hydroxy-3-(trimethylammonio)propyl ether, chloride
$k_B$	Boltzmann constant
MC	methyl cellulose
Mw	weight average molecular weight
N	particle number
NA	numerical aperture
PAA	polyacrylic acid
PAV	piezoelectric axial vibrator
PEI	polyethyleneimine
PEO	polyethylene oxide
PFG-SE NMR	pulsed field gradient spin-echo nuclear magnetic resonance
pH	$-\log[H^+]$
PSS	polymer-surfactant systems
PT100	temperature sensor based on platinum
$q$	quantum yield
$R_{H,i}$	hydrodynamic radius
$S$	structure parameter
SANS	small angle neutron scattering
SAXS	small angle X-ray scattering

SDS	sodium dodecyl sulfate
$T$	fraction of dye molecules in the triplet state
$T$	absolute temperature
$T_{kr}$	Krafft temperature
$U$	transmittance
$U_0$	transmittance of water
$V$	effective volume
$\delta C$	changes in the local concentration
$\eta$	viscosity of the medium
$\eta_0$	zero shear viscosity
$\eta_i$	number of photon counts
$\kappa$	overall detection efficiency
$\sigma_i$	molecular absorption cross section
$\tau$	relaxation time
$\omega$	frequency
$S(\vec{r})$	optical transfer function of the objective-pinhole combination
$w_z$	lateral distance of the confocal volume
$w_{xy}$	axial distance of the confocal volume
$\phi_i$	fraction of the $i^{\text{th}}$ component
$\tau_i$	lag time of $i^{\text{th}}$ component of autocorrelation analysis
$\gamma$	shear strain
$\sigma$	shear stress
$\dot{\gamma}$	shear rate
$\gamma_0$	amplitude of the strain



# 1

## Introduction

Throughout the last decades the association between polymers and surfactants has attracted much scientific attention due to the fundamental properties in intermolecular interactions and hydrophobic aggregation phenomena. Water soluble polymer/surfactant systems are important for a variety of industrial applications in the areas of cosmetics, personal-care, food, pharmaceuticals, detergents, and mineral processing [1, 2]. In particular, complexes between non-ionic cellulose ethers and ionic surfactants in aqueous solution were investigated in the past [3-16]. Various studies were devoted to characterizing the association process. Most of them employed conventional techniques accessing *macroscopic* solution properties.

During the past few decades fluorescence methods have been used to study polymer dynamics and polymer-surfactant systems with dye-labeled polymers [17-19]. In recent years single molecule fluorescence correlation spectroscopy (FCS) has become very popular for investigating *microscopic* details of diffusion processes and complex formation in macromolecular solutions. Despite their indisputable potential, however, the technique was applied

## 1. Introduction

almost exclusively to biological systems in the past. First applications in the field of synthetic polymers have very recently been reported [20-31]. To study complex formation with FCS, one of the partners is typically covalently labeled with a suitable dye [32, 33]. Since the labeling procedure is often tedious, FCS has not been widely used for the study of synthetic polymers so far. Lately, however, it was shown that covalent labeling is not necessarily needed to study molecular aggregation by FCS. Zettl *et al.* studied various well-known surfactant systems and found that dyes with suitable polarity will spontaneously aggregate with surfactant micelles allowing to precisely follow the aggregation of the surfactant molecules [34]. It turned out that the choice of the proper polarity of the dye molecule is important if covalent labeling is to be avoided. In short: cationic dyes are needed to study anionic surfactants and vice versa. This approach extends to macromolecular complexes.

### 1.1 Motivation

The aim of this work is to use FCS to characterize the polymer/surfactant aggregation at a single molecule level. Moreover, we shall demonstrate the potential of FCS to access the macroscopic as well as microscopic properties of complex systems in detail. As a model system complex formation between hydrophobically modified nonionic polymer, methyl cellulose and the anionic surfactant sodium dodecyl sulfate (SDS) in water was chosen for investigation. We shall show that FCS can follow the motion of individual SDS micelles and single MC/SDS aggregates. Rheology is used to follow the macroscopic properties of the polymer/surfactant systems which will then be compared to the FCS measurements.

Methylcellulose tends to undergo a sol-gel transition at elevated temperature. Therefore temperature dependent measurements are performed by both FCS and rheology. The additives SDS and salts will normally change

## 1. Introduction

the aggregation behavior of MC at the gelation temperature. The changes in diffusion time and aggregation states are studied as a function of temperature. Since the dye molecules are not attached to MC the FCS measurements reveal limited information for MC gelation. Further measurements are in progress to clarify the effect of additives on MC.

### 1.2 Outline

The details of the chapters are discussed as follows:

Chapter 2 provides a detailed discussion about the polymers and the surfactants. Polymer-surfactant interactions are dealt with followed by a discussion about the techniques required to characterize such interactions. A brief literature review on the polymer-surfactant system investigated in this thesis is given at the end of the chapter.

Chapter 3 focuses on the materials under study and experimental methods. The basics, experimental setup, and theory of the FCS technique are discussed. The assumptions made to analyze the FCS data are also presented in detail. To analyze the macroscopic properties, rheology and turbidity measurements are done which is also discussed at a later stage of this chapter followed by details about the cryo-TEM measurements.

Chapter 4 summarizes the results obtained from FCS and other techniques as well as the detailed discussions of all the relevant observations. The first part of this chapter is focused on the MC concentration dependence studies followed by the discussions on temperature dependent measurements. Single molecule FCS results to understand the polymer-surfactant interactions are further supported by rheology data. To view the aggregations, cryo-TEM images are shown and discussed. The effect of temperature on the gelation of MC with additives is also discussed with FCS, rheology and turbidity measurements.

## 1. Introduction

A summary of the thesis is given in chapter 5.

# 2

## Theory and Background

### 2.1 Polymers

In comparison with synthetic polymers the number of commercially available water-soluble polymers is small even if one adds water-soluble biopolymers and their synthetic derivatives. The solubility of a polymer in water is determined by the balance between the intermolecular interactions of the hydrophilic and hydrophobic polymer segments with themselves and with the solvent. Water soluble polymers can be classified broadly into two types: synthetic polymers and biopolymers. Synthetic water-soluble polymers are either non-ionic or charged. While non-ionic polymers can be further classified according to the type of atoms in their backbone which could be either oxygen or nitrogen like in polyethylene oxide (PEO) or polyethyleneimine (PEI), charged polymers can either be anionic like in polyacrylic acid (PAA) or cationic as in polyacrylamide after cationization due to the charge they possess.

## 2. Theory and Background

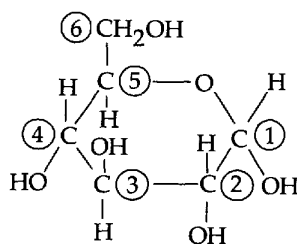


**Figure 2.1** Cyclorpyranose structure of glucose

Biopolymers and their derivatives, on the other hand e.g. cellulose, the primary constituent of wood, paper, and cotton, carbohydrate are made up of chained glucose units.

Cellulose is made up of anhydroglucose units (AGU) having alternating orientation with respect to the bridging oxygen bond. Nonetheless, the degree of polymerization (DP) of cellulose is customarily designated as the number of AGUs in the chain. The structure of cellulose is known as a "beta glucoside" as distinguished from starch, an alpha glucoside, the true polymer of glucose. In starch, the orientation of AGUs with respect to the oxygen bridge does not alternate. For convenient reference, the locations of the carbon atoms in the glucose molecule are numbered as shown in Figure 2.1. Each AGU contains three hydroxyl (OH) groups. At carbon 6, there is a "primary" hydroxyl group; the OH there is attached to a carbon atom having at least two hydrogens. The hydroxyls on carbons 2 and 3 are classified as "secondary" hydroxyl groups; the OHs there are attached to a carbon with only one hydrogen. When cellulose is etherified, the hydroxyls are substituted by the etherifying reagent. The average number of hydroxyls substituted per AGU is known as the degree of substitution (DS), a key aspect in characterizing cellulose ethers. With three OH groups present, the maximum DS is three.

## 2. Theory and Background

Etherifying reagents such as ethylene oxide ( $\text{CH}_2\text{CH}_2\text{O}$ ) and propylene oxide introduce a hydroxyl group. This group can further react with the etherifying reagent, making it possible for each AGU to react with more than three molecules of such a reagent. The total number of alkylene oxide molecules reacting with each AGU is known as molecular substitution (MS). Theoretically, there is no upper limit on MS. For example in the two AGUs, three of the six hydroxyl groups are substituted; hence the degree of substitution (DS) is  $3/6 \times 6/2$  or 1.5. The molecular weight of a cellulose ether molecule depends both on the average degree of polymerization of the cellulose and on the amount of substitution and the molecular weight of the substituent groups. Substitution rarely occurs exclusively on one particular OH group in the AGU. Instead, it occurs at all three positions, yet differing in extent.

Water soluble cellulose ethers and their derivatives are a class of technically important compounds. Therefore hydroxypropylcellulose (HPC), methylcellulose (MC), and hydroxypropylmethylcellulose (HPMC) are most common. These kinds of hydrophobically modified natural derivatives suffer from a lack of fundamental physico-chemical studies. The difficulty mainly arises from the absence of a model polymer sample with the precise distribution of the substitutions.

Among the various non-ionic cellulose ethers, MC is the simplest and most well known. Linear arrangement of MC is formed with  $\beta$ , 1:4 glycosidic linkages (see structure in figure 2.2). It is used as a thickener and emulsifier in various food and cosmetic products, and also as a treatment of constipation. Commercial MC is a heterogeneous polymer consisting of highly substituted hydrophobic zones and less substituted hydrophilic zones resulting in an amphiphilic multiblock copolymer [35]. The amphiphilic nature of the

## 2. Theory and Background

polymer leads to weak inter and intra molecular hydrophobic interactions in aqueous environment.

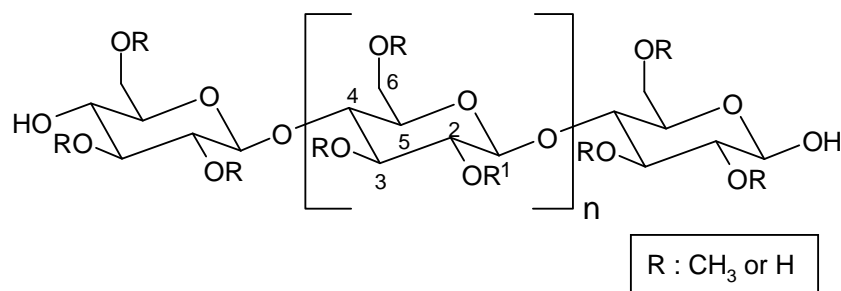


**Figure 2.2** Methylcellulose

### **2.1.1 The influence of the degree of substitution on solubility**

Cellulose ethers of moderate to high molecular weight are insoluble in water. As a rule, the polymers gradually pass through a stage of solubility in dilute alkali (those with a DS of up to about 1.0), then through a water-soluble stage (about DS 1.0-2.3), and finally attain an organic-solvent-soluble stage (DS 2.3-3.0), with increasing DS.

Such DS ranges are, of course, only approximate. The trend toward solubility in organic solvents is gradual and differs for individual ethers. Moreover, the uniformity of substitution along the cellulose chain can have a major influence on solubility.

MC of DS between 0.1 and 1.1 tends to be soluble in dilute (6 to 8%) sodium hydroxide solution. Water solubility is reached between DS=1.4-2.0, a range commercially available and often used by conservators. Almost completely substituted MC (DS=2.4-2.8) is insoluble in water, but soluble in organic solvents. The latter types can often be applied in mixtures of chloroform or methylene dichloride and methanol or ethanol.

## 2. Theory and Background

The range of DS cited in these examples is only approximate because solubility is influenced by the distribution of molecular weights of various fractions in a given product and by the extent and uniformity of substitution within particular products or molecular weight fractions. Sarkar *et al.* provides an excellent discussion of how such factors influence the incipient precipitation temperature (IPT) and the cloud point of methyl and hydroxypropylmethyl ethers [36].

### 2.2 Surfactants

Surfactants are of natural or of synthetic origin. Surfactants of natural origin (vegetable or animal) are known as oleo-chemicals and are typically derived from sources such as palm oil or tallow. Surfactants of synthetic origin are known as petro-chemicals and are typically derived from petroleum.

Surfactant is an abbreviation for surface active agent. A surface active chemical tends to accumulate at a surface or interface. An interface is the area of contact between two substances. When the interface is between two substances which are not in the same phase, the interface is usually called a surface.

#### 2.2.1 Classifications of surfactants

Generally, a surfactant molecule consists of two parts having different properties: a 'headgroup' (hydrophilic) with a strong affinity for the solvent and a 'tail' (hydrophobic) with less affinity for the solvent. The head group may carry a negative or positive charge, giving rise to anionic or cationic surfactants, respectively. Alternatively, it may contain ethylene oxide chains or sugar or saccharide type groups, as is the case with nonionic surfactants. The tail part of the molecule is usually a hydrocarbon chain, but may contain

## 2. Theory and Background

aromatic groups. Besides, there is the class of 'zwitterionic' surfactants which alter their ionic behavior according to pH-value of the solvent. Depending on the molecular structure and type, a balance between hydrophilicity and hydrophobicity exists in the surfactant molecule. This is called hydrophobic-lipophilic-balance or HLB, which is important in categorizing surfactants as emulsifiers, detergents, wetting agents, solubilizing agents, micelle forming types, etc. [37]. In short, surfactants having greater hydrophobicity are more surface active.

### **2.2.1.1 Anionic surfactants**

When the head group of the surfactant molecule carries an anion, the molecule is referred to as an anionic surfactant. Anionic surfactants are most widely used for laundering, dishwashing liquids, and shampoos because of their excellent cleaning properties. Important types of anionic surfactants are carboxylates, sulfonates, sulfates and phosphates. Sodium dodecyl sulfate (SDS) is a well known anionic surfactants with a wide range of applications.

### **2.2.1.2 Cationic surfactants**

Surfactants which carry a cationic head group are referred to as cationic surfactants. Cationic surfactants play an important role as antiseptic agents in cosmetics, as general fungicides and germicides, corrosion inhibitors, fuel and lubricating oil additives and in a number of bulk chemical applications. Two common types of cationic surfactants are long chain amines and quaternary amine salts. Alkyl amines chain length  $C_8$  to  $C_{18}$  are the most important surfactants in this category. In the pharmaceutical area, cationic surfactants with pyridinium and piperidinium groups are also used. Pure cationic surfactants such as cetyltrimethylammonium bromide (CTAB) have been extensively studied in terms of the fundamental physical chemistry of surface active components.

## 2. Theory and Background

### **2.2.1.3 Zwitterionic surfactants**

These surfactants are very mild, making them particularly suited for use in personal care and household cleaning products. Zwitterionic surfactants are compatible with all other classes of surfactants and are soluble and effective in the presence of high concentrations of electrolytes, acids and alkalies. They exhibit cationic behavior near or below their isoelectric points and anionic behavior at higher pH. The isoelectric point depends on the structure of the surfactant. These surfactants may contain two charged groups of different sign. Whereas the positive charge is almost always ammonium, the source of the negative charge may vary (carboxylate, sulphate, sulphonate). These surfactants have excellent dermatological properties. They are frequently used in shampoos and other cosmetic products, and also in hand dishwashing liquids because of their high foaming properties.

### **2.2.1.4 Nonionic surfactants**

Nonionic surfactants do not carry any electrical charge. They are more stable over the entire pH range. They show lower sensitivity to the presence of electrolytes in the system and they are compatible with other surfactants. They are excellent grease removers used in laundry products, household cleaners, and hand dishwashing liquids. The amphiphilic nature of these surfactants is expressed in terms of an empirical HLB [37]. Water-soluble surfactants have an HLB value higher than 13 and those with poor or no dispersibility in water have HLB values less than 6. Pentaethylene glycol monododecyl ether (C<sub>12</sub>E<sub>5</sub>) is an example for a nonionic surfactant.

## **2.2.2 Theoretical basics of surfactant self-assembly**

The dual character of surfactants is the driving force for their peculiar behavior in the presence of water. When small amounts of surfactant are

## 2. Theory and Background

solubilized in water, alkyl chain/water contacts are energetically unfavorable with respect to water/water contacts. Therefore some surfactants tend to locate at the air/water interface with a specific orientation, thus reducing the free energy and the surface tension of water. With increasing concentration of the surfactant, the air/water interface and walls of the solution container are eventually completely occupied by surfactant molecules. Any additional surfactant molecules then remain in the aqueous phase. In order to reduce the number of alkyl chain/water contacts surfactants self associated into *micelles* at the *critical micelle concentration* (CMC). Depending on the concentration, micelles exit in the shape of spheres, rods, and lamellae. This thesis will focus on spherical micelles. The driving forces for micelle formation are van der Waals, electric double layer, and hydration forces. These are explained in detail by Israelachvili [39].

The self-assembly of surfactants is explained theoretically using thermodynamic equations [38-40]. To attain the thermodynamic equilibrium, the chemical potential  $\mu$  of a surfactant molecule in a micelle should be identical with a non-associated surfactant molecule.

$$\mu = \underbrace{\mu_1^0 + kT \log X_1}_{\text{monomers}} = \underbrace{\mu_2^0 + \frac{1}{2} kT \log \frac{1}{2} X_2}_{\text{dimers}} = \underbrace{\mu_3^0 + \frac{1}{3} kT \log \frac{1}{3} X_3}_{\text{trimers}} = \dots \quad (2.1)$$

where  $X_1$ ,  $X_2$ ,  $X_3$  are the concentration of single surfactant molecules, dimers and trimers respectively. The concentration is the mole fraction or activity of surfactant in the corresponding aggregates. The chemical potential for an aggregate of N surfactants is given by

$$\mu = \mu_N \quad (2.2)$$

## 2. Theory and Background

$$\mu = \mu_N = \mu_N^0 + \frac{kT}{N} \log \left( \frac{X_N}{N} \right) = \text{constant} \quad N = 1, 2, 3, \dots \quad (2.3)$$

where  $\mu_N$  is the mean chemical potential of a molecule in an aggregate of aggregation number  $N$ ,  $\mu_N^0$  is the standard chemical potential in aggregates of aggregation number  $N$  and concentration  $X_N$ . The quantity  $X_N$  is the mole fraction or activity of surfactant (monomer) in  $N$ -aggregates. This concentration,  $X_N$ , can be written by using equation 2.1 as

$$X_N = N \left( X_1 e^{N(\mu_1^0 - \mu_N^0) / kT} \right)^N \quad (2.4)$$

The total concentration of surfactant molecules in the solution is the sum over all concentrations described by equation 2.4

$$C = X_1 + X_2 + X_3 + \dots = \sum_{N=1}^{\infty} X_N \quad (2.5)$$

At equilibrium, the reference or standard chemical potentials  $\mu_N^0$  may be assumed to be about the same if the surfactant monomers in each aggregate experience the same interactions with the surroundings. The essential condition for the formation of larger stable aggregates of surfactant molecules (micelle) is that  $\mu_N^0 < \mu_1^0$  for some value of  $N$ . The detailed dependence of  $\mu_N^0$  upon  $N$  also determines the size distribution (polydispersity) and shape of the resulting aggregates. In order to get an equation for a particular shape of the micelles, the energy term  $\alpha kT$  describing the intermolecular interactions

## 2. Theory and Background

between two surfactant molecules is considered. For the simplest shapes (rods, sheets, and spheres) one obtains

$$\mu_N^0 = \mu_\infty^0 + \frac{\alpha kT}{N^p} \quad (2.6)$$

where  $p$  is a number that depends on the shape of the aggregates (eg.  $1/3$  for spherical micelles). A combination of equation 2.4 and 2.6 leads to

$$X_N = N \left( X_1 e^{\alpha \left( 1 - 1/N^{1/3} \right)} \right)^N \approx N (X_1 e^\alpha)^N \quad (2.7)$$

The concentration of molecules which forms aggregates depends on the parameter  $\alpha$ . For sufficiently low monomer concentrations,  $X_1 e^\alpha$  is much less than unity and thus most of the molecules will be isolated monomers. Since  $X_N$  can never exceed unity, once  $X_1$  reaches a value of  $e^{-\alpha}$  the concentration of monomer can not be increased further: An addition of surfactant rather forms aggregates. The monomer concentration at which this occurs is called *critical micelle concentration* (CMC).

$$(X_1)_{CMC} = CMC \approx e^{-\alpha} \quad (2.8)$$

## 2. Theory and Background

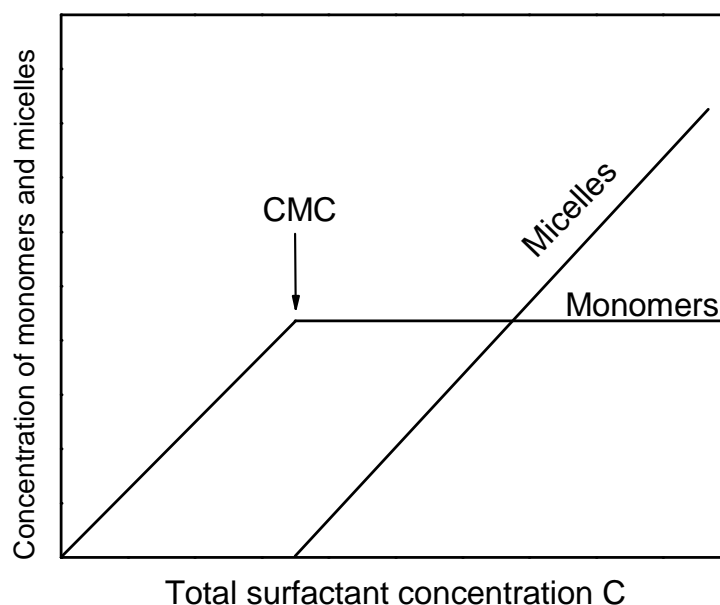


**Figure 2.3** Schematic diagram of monomer and micelle concentrations as a function of total concentration of surfactants. Before CMC, the monomer concentration increases linearly with the surfactant concentration. Micelle concentration increases from the point CMC but the monomer concentration remains the same inspite of an increasing the surfactant concentration [4].

Equation 2.8 is explained in the diagram displayed in figure 2.3. Moreover it explains that the monomer concentration increases up to the CMC and then remains constant upon further addition of surfactant molecules. The concentration of micelles increases with increasing surfactant concentration above the CMC.

At the CMC, many physical properties exhibit abrupt changes as illustrated in Figure 2.4. These changes are mostly sensitive to the micelle concentration, while some of them are sensitive to the monomer concentration, too [2].

## 2. Theory and Background

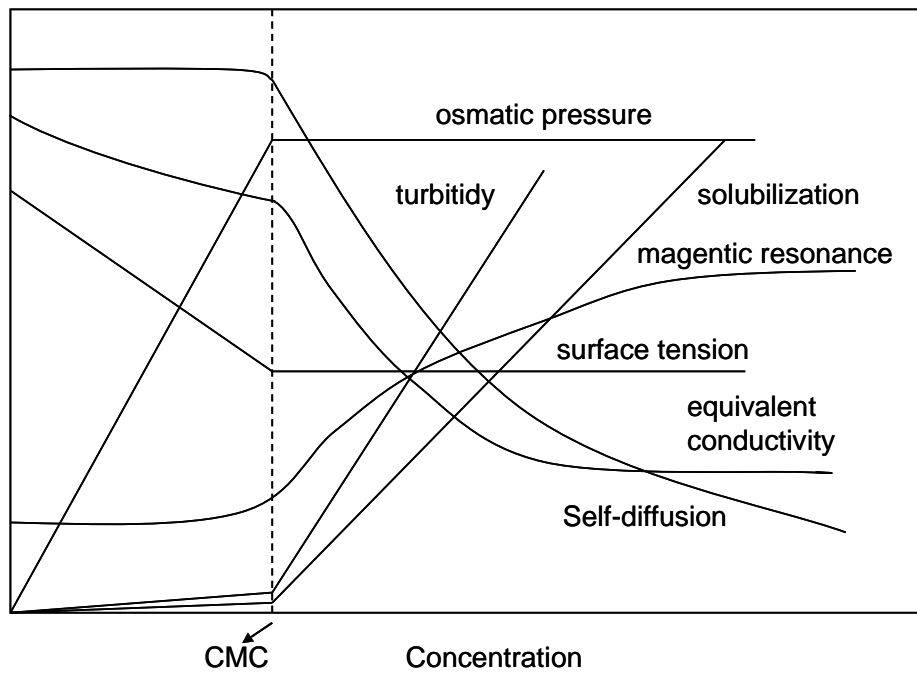


**Figure 2.4** Illustration of the dramatic changes in physical properties beyond the critical micellar concentration [7].

Since the surfactant molecules are in continuous motion, the nature of micelles is dynamic. There is a constant interchange between micelles and solution. The lifetime of a surfactant molecule in a micelle is the order of  $10^{-7}$  seconds, and the half-life for micellar formation or breakdown is usually in the region of  $10^{-3}$  to 1 seconds [41].

### 2.2.2.1 Typical CMC values

Some typical CMC values [42] for low electrolyte concentration at room temperature are

Anionic surfactants:	$10^{-3} - 10^{-2}$ M
Cationic surfactants:	$10^{-3} - 10^{-1}$ M
Zwitterionic surfactants:	$10^{-3} - 10^{-1}$ M
Nonionic surfactants:	$10^{-5} - 10^{-1}$ M

## 2. Theory and Background

Some of the factors affecting the CMC are the nature of hydrophobic [43] and hydrophilic groups, the electrolyte concentration [44], and the temperature. Among these factors, the effect of the temperature is explained in some detail in the following section.

### 2.2.2.2 The Krafft point

Temperature plays an important role for the behavior of surfactant molecules. At lower temperature surfactants often precipitate from the solution as hydrated crystals instead of forming micelles. This results in a different surface behavior due with changing temperature [38]. The point at which the solubility equals the CMC is called the *Krafft temperature* ( $T_{kr}$ ). The solubilities of micelle-forming surfactants show a strong increase above  $T_{kr}$  and a solution of any composition becomes a single homogeneous phase. This phenomenon reflects equilibrium between surfactants in solution and in hydrated crystals (Figure 2.5). The Krafft point increases strongly along with the alkyl chain length. The head group and the counterion of the surfactant strongly influence the Krafft point. Normally, the addition of salt raises the Krafft point [45]. Nonionic surfactants do not exhibit Krafft points. The solubility of nonionic surfactants typically decreases with increasing temperature. These surfactants even may begin to lose their surface activity above a transition temperature referred to as the cloud point [42].

## 2. Theory and Background

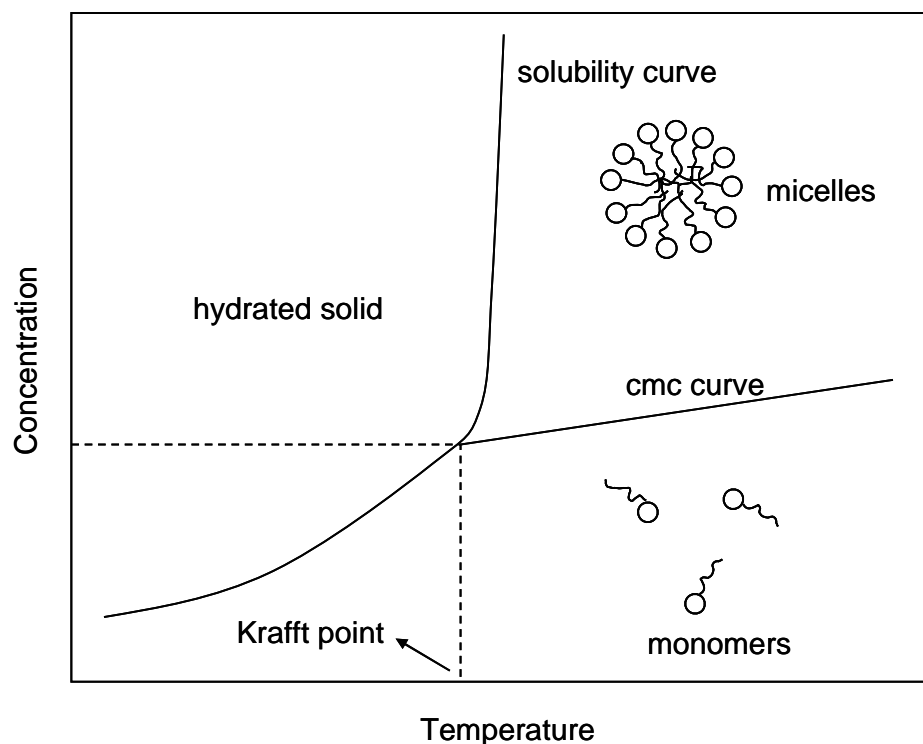


**Figure 2.5** Schematic diagram of the temperature dependence of surfactant solubility in the region of the Krafft point [46].

### 2.3 Polymer–surfactant interactions in aqueous solution

With the understanding of polymers and surfactants, it is straightforward to extend our discussion to polymer–surfactant systems (PSS) in this section. These associated systems are employed to achieve different effects such as emulsification, flocculation, colloidal stability, or rheology control. There have been extensive studies over the last decades on various aspects of how the association of uncharged polymers in dilute aqueous solution occurs. Several extensive reviews are available in this field [1, 2, 45]. Before we discuss the various factors associated with polymer/surfactant interactions, a brief overview shall be given first.

## 2. Theory and Background

Surfactant Polymer	Anionic	Cationic	Nonionic
Anionic	$P^-S^-$	$P^-S^+$	$P^-S^0$
Cationic	$P^+S^-$	$P^+S^+$	$P^+S^0$
Nonionic	$P^0S^-$	$P^0S^+$	$P^0S^0$

**Table 2.1** The possible polymer–surfactant combinations based on the charge of the system.

### 2.3.1 Classification

Conventionally, polymer–surfactant interactions are classified according to polymer or surfactant charge and according to the concentration regime. The possible combinations of polymers and surfactants of different nature are shown in Table 2.1 in a nutshell. For polyelectrolytes and surfactants of opposite charge, surfactant binding is easily observable due to the electrostatic interactions. Water soluble nonionic polymers with charged surfactants have attracted much attention because of the hydrophobic interactions. The interactions between surfactants and nonionic hydrophilic polymers are much stronger for anionic surfactants than for cationic surfactants. The highlighted system in Table 2.1 is the combination of nonionic polymers and anionic surfactant ( $P^0S^-$ ), which is investigated in this thesis. In terms of concentration related classifications, the studies focused on the surfactant binding to polymers at low polymer concentration and phase equilibria, while phase diagrams are typically studied at higher concentration.

## 2. Theory and Background

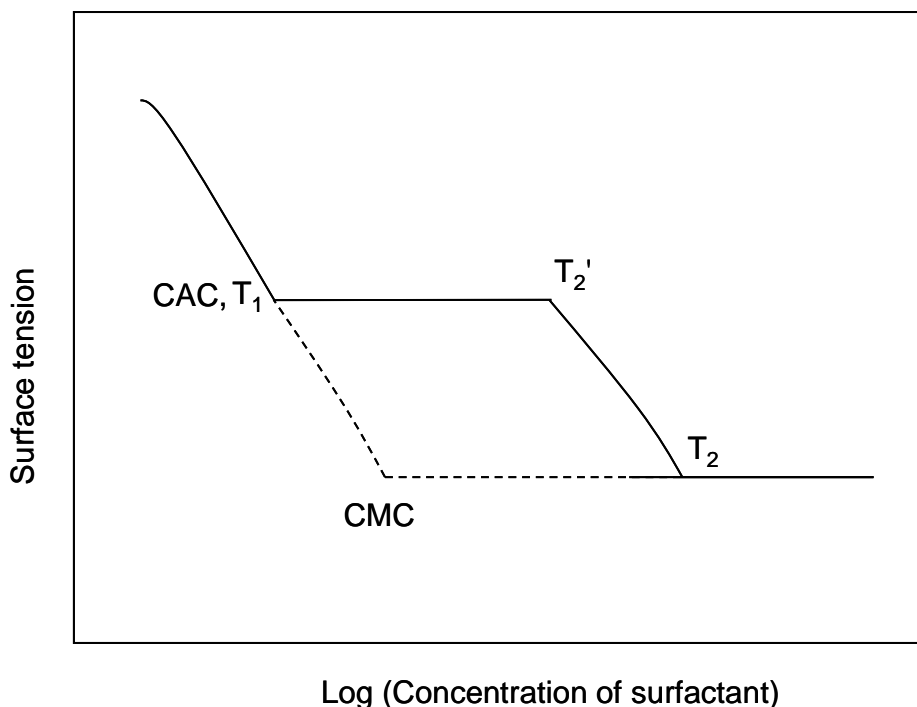


**Figure 2.6** A schematic plot of the concentration dependence of the surface tension for polymer-surfactant solutions [47].  $T_1$  is the critical aggregation concentration,  $T_2'$  – polymer saturation with micelles and  $T_2$  – surfactant free micelle formation.

### 2.3.2 Critical aggregation concentration (CAC)

An addition of polymer to a surfactant solution induces aggregation of the surfactants. The onset of surfactant binding to the polymer molecules is the so-called critical aggregation concentration (CAC) referred to as  $T_1$  in figure 2.6. To understand the CAC in detail its influence on the surface tension is used in figure 2.6. The solid line represents the surface tension of the solution in the presence of polymers whereas the dotted line represents it in the presence of surfactant alone. In the presence of polymers, aggregations form below the surfactants' CMC and reaching a point  $T_2'$  where polymers are

## 2. Theory and Background

saturated with micelles. With increasing concentration of the surfactant, additional free micelles are formed starting at the point  $T_2$ . Other techniques such as binding isotherms, conductivity measurements etc., can be used to characterize the association behavior of surfactants to the polymers.

Based on the experimental observations, in polymer–surfactant systems the CAC is lower than CMC [48].

$$\varphi_{CAC} < \varphi_{cmc} \quad (2.9)$$

Diament [48] classified PSS into two categories based on the CAC, such as (i) systems whose CAC is much smaller than CMC.

$$\varphi_{CAC} \ll \varphi_{cmc} \quad (2.10)$$

and (ii) systems where CAC is lower than yet comparable with CMC

$$\varphi_{CAC} \leq \varphi_{cmc} \quad (2.11)$$

The first category is connected with  $P^+S^-$  or  $P^-S^+$  (Table 2.1) as polyelectrolytes and charged surfactant systems. The strong electrostatic attraction between the two species cause a CAC several order magnitude lower than the normal CMC of charged surfactant. The interactions between the cationic polymer JR400 and the anionic surfactant SDS is an example for this category. The latter case usually corresponds to nonionic polymers and ionic surfactant. The system containing the nonionic polymer MC and the anionic surfactant SDS ( $P^0S^{-1}$ ) is the best studied example for the second category. Therefore, this system has been chosen as a model system in the

## 2. Theory and Background

present thesis. The mixture of polyelectrolytes and nonionic surfactants also belongs to the second category. As classified in the preceding section, systems where both species are neutral, exhibit only a very weak effect.

### **2.3.3 Characterization**

To understand the physico-chemical properties of these PSS a large variety of methods has been used. For reasons of convenience the experimental methods are classified as 'classical' physico-chemical methods and spectroscopic methods.

#### **2.3.3.1 Classical physico-chemical methods**

Binding isotherms, phase equilibrium, conductance and potentiometry, surface tension, viscometry, dye solubilization, calorimetry, chromatographic and other separation techniques, micellar relaxation kinetics are important physico-chemical methods to characterize PSS. The determination of binding isotherms is useful to know the amount of bound surfactant as function of the free surfactant concentration. It allows exploring the nature of the binding process and the structure of aggregates. As discussed in section 2.3.2 the measurement of the surface tension is useful to determine the CAC. The dye solubilization method can also be used to determine CAC values. Separation methods such as electrophoresis [49, 50], capillary electrophoresis, gel filtration or size exclusion chromatography (SEC) [51], ultracentrifugation can be applied for studying PSS.

#### **2.3.3.2 Spectroscopic Methods**

Spectroscopic methods are very useful to determine the local structure and the environment of the component system, the aggregation number, diffusion coefficients, and kinetic parameters in PSS. The notable methods to study PSS include pulsed field gradient spin-echo nuclear magnetic resonance

## 2. Theory and Background

(PFG-SE NMR)[14-16, 52-55], electron spin resonance (ESR)[56, 57], Infra-Red and Raman spectroscopy, light scattering, uv-visible spectroscopy, fluorescence, cryo-transmission electron microscopy (cryo-TEM) [58-60], small angle neutron scattering (SANS), small angle X-ray scattering (SAXS)[61]. The cryo-TEM method visualizes the microscopic structure of different aggregates in solution. The gelation of cellulose ethers with surfactants have also been studied in detail with cryo-TEM in Talmon's research group [62]. Each technique has its own limitations and advantages. In the following PFG-SE NMR is discussed briefly because the information thus obtained complements the information from the proposed technique of this thesis.

### **Pulsed field gradient spin-echo NMR spectroscopy**

NMR experiments reveal information on the dynamics of the polymer chain, as well as on the surfactant entities. A detailed knowledge of the nature of polymer-surfactant interactions thus can be inferred from chemical shifts, line widths and relaxation time measurements on  $^1\text{H}$ ,  $^{13}\text{C}$ , and other nuclei. Monitoring the chemical shift changes as a function of solution composition would be the simplest NMR-based approach [63]. Södermann *et al.* explained the basic spin relaxation approach in PSS to obtain detailed information on (picosecond to microsecond) local molecular dynamics and order of alkyl chains, water or counter ions [64]. But the overall molecular displacement on a much longer time scale (on the order of 100 milliseconds) can be obtained from the multi-component self-diffusion approach [65]. Self diffusion coefficients of the species present in the system can be obtained from PFG-SE NMR measurements as well as some indirect information on the average size of polymer-surfactant complexes. Signal intensity for the surfactants in the case of free (Gaussian) diffusion is given by Stejskal-Tanner equation [16]

## 2. Theory and Background

$$I(K) = I_0 e^{(-kD)} \quad (2.12)$$

where  $D$  is the self-Diffusion coefficient and  $k$  is defined as

$$k = (\gamma g \delta)^2 \left( \Delta - \frac{\delta}{3} \right) \quad (2.12)$$

where  $\gamma$  is the proton magnetogyric ( $\gamma = 2.6752 \times 10^8 \text{ rad T}^{-1} \text{ s}^{-1}$ ),  $\delta$  is the duration of gradient pulses, and  $\Delta$  is the time between the leading edges of the gradient pulses. The  $^1\text{H}$  signal from the surfactant displays a single-exponential decay when the surfactant signal intensity (from the methyl group) is plotted against  $k$  in accordance with equation 2.12.

The signal intensity of polymer or mixed PSS is more complex. Due to the polydispersity of the polymers, there will be a distribution of the self-diffusion coefficient resulting in a curved signal decay in a Stejskal-Tanner plot. The signal intensity decays are interpreted in terms of a distribution of diffusing species with respect to

$$I(k) = \int P(D) e^{(-kD)} dD \quad (2.13)$$

where  $P(D)$  is the normalized distribution of self-diffusion coefficients  $D$ . The observed surfactant self-diffusion coefficient  $D_{obs}$  is interpreted as a population weighted average over the diffusion coefficients of the free monomeric surfactant and the polymer bound surfactant. Binding isotherms is written in a two-site model  $D_{obs}$  as

$$D_{obs} = (1 - p_{bound}) D_{free} + p_{bound} D_{bound} \quad (2.14)$$

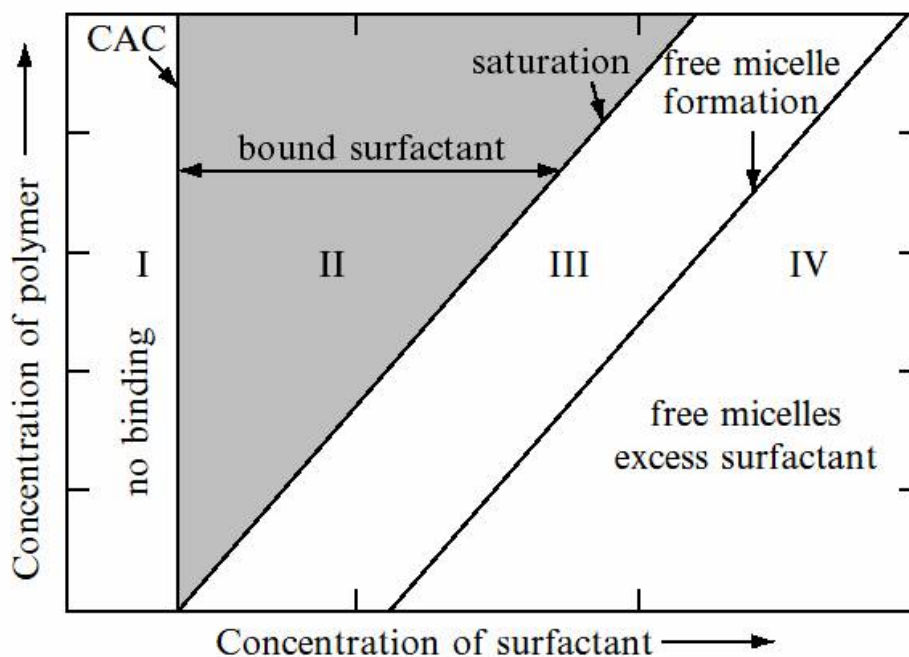


**Figure 2.7** Schematic diagram of association between homopolymer and a surfactant in wide range of concentration regions. Reproduced from [47]. (I) at low surfactant concentration, there is no significant association in any polymer concentration; (II) above the CAC, the surfactant associating with polymer increases up to certain surfactant concentration, which develops linearly with polymer concentration; (III) association is saturated and the surfactant concentration increases; (IV) free micelles and surfactant aggregated polymer coexist.

where  $p_{bound}$  is the fraction of surfactant bounded with polymer, and  $D_{bound}$  is the diffusion coefficient of the bound surfactants.  $D_{bound}$  is given by the diffusion of polymer.

### 2.3.4 Important Inferences

From the various experimental binding studies, a schematic diagram is drawn in figure 2.7. Though the picture is schematic, it well describes the mixtures of an ionic surfactant and nonionic homopolymer [45]. It shows that  $CAC/CMC$  is weakly dependent on polymer concentration over wide ranges and

## 2. Theory and Background

independent of the polymer molecular weight down to low values. The plateau binding increases with the polymer concentration.

### 2.3.5 Other factors affecting the complex formation

The precise structure of a polymer/surfactant complex will depend on the hydrophobicity and molecular weight of the polymer, and the charge and shape of the surfactant. The addition of salt (inorganic electrolyte) generally depresses the  $T_l$  values and promotes the formation of complexes. With increasing (hydrophobic tail) chain length of the surfactant the binding with the polymer strengthens. This suggests the linear relationship between  $\log T_l$  and  $n$ , the number of alkyl chain carbons [2]. The interactions between uncharged water-soluble polymers is much more facile with anionic surfactants than with cationic surfactants [66]. For anionic surfactants, Breuer and Robb list polymers in the following order of increasing reactivity: PVOH < PEO < MC < PVAc  $\leq$  PPO  $\sim$  PVP; and for cationic surfactants: PVP < PEO < PVOH < MC < PVAc < PPO.

### 2.3.6 Interactions between nonionic polymers and anionic surfactants

Among the various types of PSS, only nonionic polymer and anionic surfactant system are reviewed in this section. MC is the simplest cellulose ether which shows inter and intra molecular hydrophobic interactions in aqueous solutions. The addition of an anionic surfactant is expected to lead to aggregation in the hydrophobic zones of MC. Earlier studies on nonionic polymer and anionic surfactant system have dealt with the adsorption of SDS on MC, poly(vinyl alcohol) and vinyl alcohol–acetate copolymers in aqueous solution using viscosity measurements and equilibrium dialysis [67, 68]. Later studies on MC/SDS interactions include pressure-jump experiments [69] and

## 2. Theory and Background

steady state fluorescence probe techniques [70] aiming at investigating the micellar stability and the microviscosity. Thermodynamic aspects have been studied in detail by Sing et al. for SDS and nonionic cellulose ethers having different hydrophobicity [12].

Kundu et al. have studied the effect of salts and surfactants on the gelation of extremely dilute solutions of MC [71]. On heating, thermoreversible gelation and phase separation are the interesting common phenomena with MC. This has been studied using DLS, SANS [72], SAXS [73],  $^{13}\text{C}$  NMR [74], DSC [75-77], and rheology [77, 78]. The mechanism of gelation of MC has been studied recently [79-82]. Influence of hydroxyl groups [83], salt [71, 84-87] have been investigated in detail which has led to several conclusions. A salt-out salt can lower the gelation temperature of MC whereas a salt-in salt delays the formation of MC gelation. Nishinari et al proved that the increase in gelation with the molecular weight [88]. Savage has analyzed the temperature-viscosity relationship with various degree of substituted MC and concluded that MC for DS 1.7 to 1.9, association started near 45°C and gelation occurred at 55°C [89]. Apart from this the addition of SDS on MC gelation was studied by Wang et al[90]. They claimed that the gelation of MC occurred with salt-in and salt-out effects of SDS.

In this work, FCS has been explicitly used to characterize the polymer/surfactant aggregation at a single molecular level and the results are quite intriguing as will be discussed in the subsequent chapters.

## 2. Theory and Background

# 3

## Materials and Methods

### 3.1 Materials

#### 3.1.1 Polymer

Methylcellulose (figure 2.4) was purchased from Sigma Aldrich, Germany. The manufacture's specifications indicate that the viscosity of a 2 wt % solution is 4.0 Pa·s at 20°C and that the methoxyl content and the degree of substitution are 27.5–31.5 wt % and 1.6–1.9, respectively. The weight-average molecular weight ( $M_w$ ) is 313 800 g/mol as determined by static light scattering.

##### 3.1.1.1 Purification of polymer

Since MC is manufactured via an etherification reaction of cellulose, impurities are inevitable. Therefore it was purified by dialysis. Approximately a 2 wt % MC solution was prepared in Milli-Q water and allowed to stir for 2

### 3. Materials and Methods

days to get a homogeneous solution. The standard procedure for preparing stock solutions is reported elsewhere [91]. This solution was in a Spectra/Por dialysis membrane which has carried out until the conductivity of water became equal to that of the pure Milli-Q water. Subsequently, the solution was freeze-dried.

#### 3.1.2 Surfactant and dye

The anionic surfactant SDS (figure 3.1e) was purchased from Fluka and used without further purification. The anionic dye Sulphoradamine B (figure 3.1a) and the nonionic dye Rhodamine B (figure 3.1b) base were purchased from Sigma-Aldrich GmbH. The cationic laser dyes Rhodamine 6G (figure 3.1c) and cresyl violet perchlorate (figure 3.1d) were purchased from Lamda Physik (Lambdachrome,  $\lambda_{exc} = 601$  nm,  $\lambda_{emiss} = 632$  nm) and used without further purification.

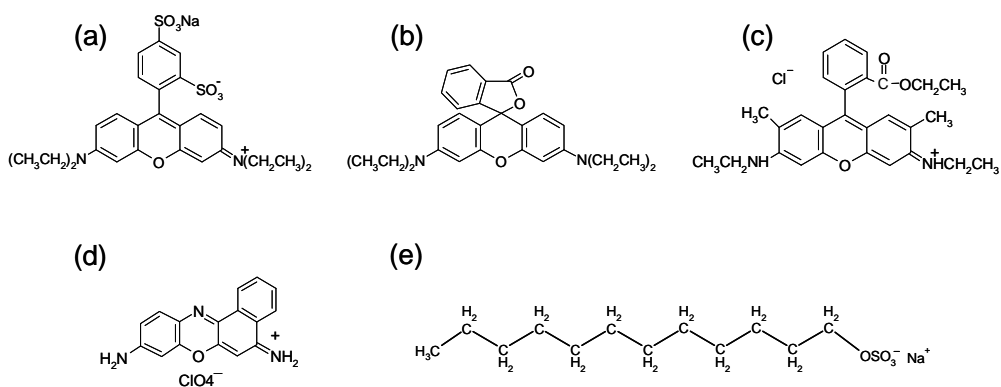


**Figure 3.1** (a) Sulphoradamine B (b) Rhodamine B base (c) Rhodamine 6G (d) Cresyl violet perchlorate. (e) Sodium dodecyl sulfate (SDS)

### 3.1.3 Preparation of solutions

1 wt % and 2 wt % MC stock solutions were prepared by the standard procedure [91]. A weighed amount of MC was mixed with approximately  $\frac{1}{4}$  of the total amount of water, heated to 80°C. This solution was shaken in warm water bath for half an hour. The rest of the water was cooled to 0°C and then added. The mixture was stirred in an ice bath for about 4 h in order to get homogenous solution.

SDS stock solutions of three different concentrations were prepared by Milli-Q water. All the other SDS solutions were prepared by diluting the stock solutions with Milli-Q water. A constant cresyl violet perchlorate concentration of  $c_{\text{dye}} = 10^{-8}$  M was prepared by diluting appropriate stock solutions and used for FCS measurements.

## 3.2 Methods

### 3.2.1 Fluorescence correlation spectroscopy

The theoretical background and the experimental setup of FCS was proposed in the early 1970s by Magde, Elson, and Webb [92, 93]. A very tiny, diffraction-limited illuminated volume is created by a laser which forms the hardcore conceptual basis of FCS (figure 3.2). FCS monitors the motion of single dye molecules via the observation of spontaneous intensity fluctuations of the fluorescence light when molecules are in thermal motion through the illuminated volume (Brownian motion) [94]. Intensity fluctuations may arise from diffusion of the fluorescent molecules, different fluorescent yield of fluorescence molecules, or by chemical or photophysical reactions. By reducing the concentration of dye solutions down to nanomolar, 1 femtoliter

### 3. Materials and Methods

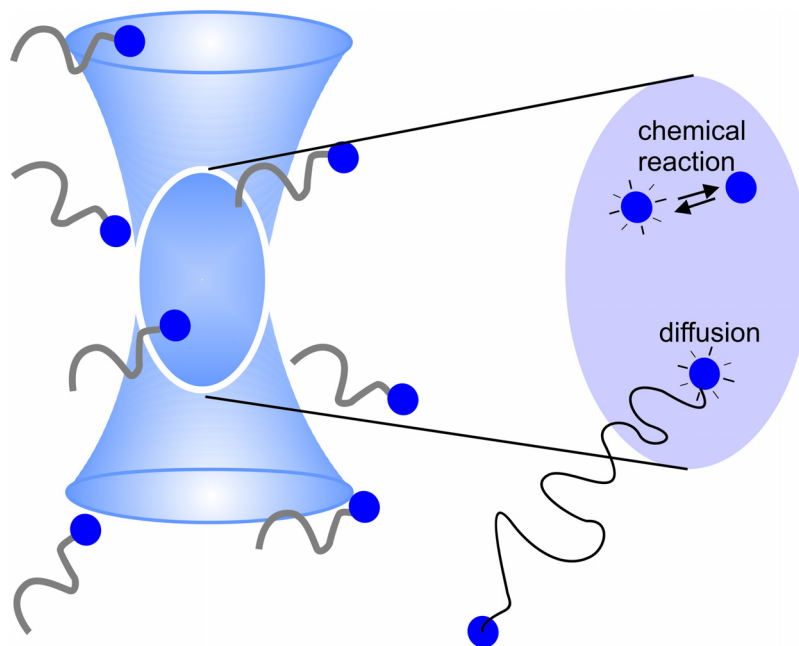


**Figure 3.2** Schematic drawing of illuminated volume. The confocal volume is enlarged for clarity. Fluorescence intensity fluctuations are due to particle movement (diffusion), chemical reactions (photophysical reactions) and conformational changes (not shown here).

illuminated volume contains some 0.6 molecules on average [95]. The fluctuations are quantified by temporally autocorrelating the recorded intensity signal. Autocorrelation analysis provides a measure for the self similarity of a time-series signal and thereby describes the persistence of the information it carries [96]. It is obvious that intensity fluctuations are associated with the diffusion process of the molecule. It is also possible to determine the local concentrations of samples, diffusion coefficients, number of molecules and kinetic parameters like equilibrium constant.

### 3.2.1.1 Experimental setup

The FCS experiments were carried out using a commercial Zeiss ConfoCor 2 spectrometer (Carl Zeiss AG, Jena). A schematic diagram of the confocal FCS setup is shown in figure 2. It consists of three parts viz.: the observation unit, the detection unit, and the laser unit. The observation unit consists of an inverted optical microscope with a cover slip corrected C-Apochromat 40× water immersion objective. The detection unit holds an avalanche photodiode (APD) in single photon counting mode. The laser unit contains an Ar ion laser in combination with a pinhole diameter of 74  $\mu\text{m}$  for excitation. This experimental setup allows FCS studies with confocal optics.

The desired laser line is selected by an acousto-optical tunable filter (AOTF) and passes via a collimation lens as an expanded parallel laser beam, which is reflected with by a a dichroic mirror acting as a beam splitter, [95]. Further, a water immersion objective with high numerical aperture ( $\text{NA} > 0.9$ ) focuses the laser beam and creates an illuminated volume in a drop of a sample which resides on the cover slide. The emitted light of fluorescent molecules passes through the same objective, dichroic mirror, and motor driven adjustable pinholes. Finally, the APD single photon detector records the photons. The emission filters and pinholes are used to reduce contributions from Raman scattering and fluorescence light not originating from the confocal volume respectively [97]. A good signal-to-noise ratio is maintained with the help of emission filters. Fluctuations in the fluorescence signal from the dye molecules are quantified by temporally auto correlating the fluorescence intensity signal. The autocorrelation functions of the measurements were evaluated by a homemade routine performing least-squares fits.

### 3. Materials and Methods

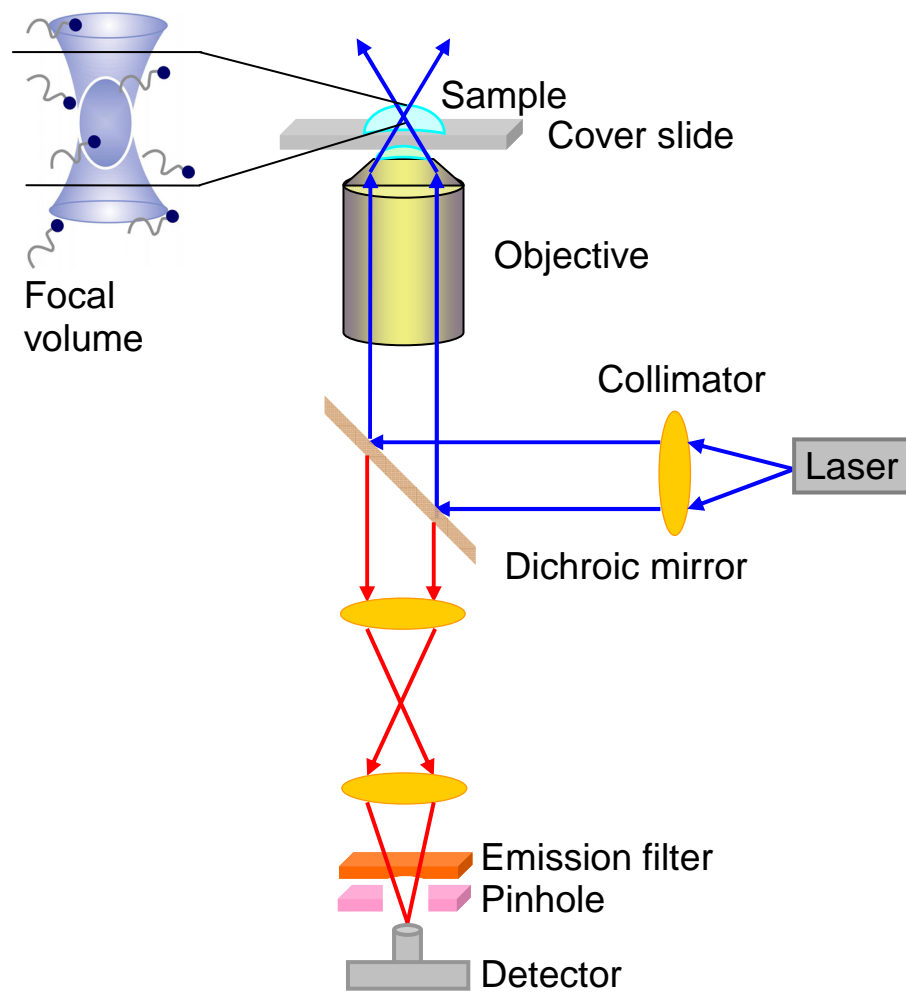


**Figure 3.3** Schematic diagram of confocal FCS setup.

Cresyl violet perchlorate (Lambdachrome,  $\lambda_{\text{exc}} = 601 \text{ nm}$ ,  $\lambda_{\text{emiss}} = 632 \text{ nm}$ ) was chosen as a dye. The diffusion coefficients and the hydrodynamic radii were calculated based on the beam waist radius calibrated by Rhodamine 6G in water (for details see ‘data analysis’). The waist radius for all the measurements is  $w_{xy} \approx 195 \text{ nm}$ .

### 3.2.1.2 Theoretical concept

The number of molecules contained within the focal volume at any time is governed by a Poissonian distribution [98]. Hence, the root mean square fluctuation of the particle number  $N$  is given by

$$\frac{\sqrt{\langle(\delta N)^2\rangle}}{\langle N\rangle} = \frac{\sqrt{\langle(N-\langle N\rangle)^2\rangle}}{\langle N\rangle} = \frac{1}{\sqrt{\langle N\rangle}} \quad (3.1)$$

In order to increase the relative fluctuations, it is most important to minimize the number of fluorescence molecule in the focal volume. This can be achieved by combining two ways viz. a) reducing the concentration of fluorescence molecule (laser dye), and b) minimizing the focal volume. Obviously, the fluorescence signal should be higher than the residual background signal. This can be accomplished by laser-dyes which have higher quantum yields. Roughly, the temporal average of the particle number should be between 0.1 and 10 (maximum 1000). At concentrations between  $10^{-9}$  M –  $10^{-8}$  M only a few fluorescence molecules pass through the focal volume at any given time.

The fluorescence light emitted by the molecules in the focal volume is recorded as individual photons. The number of photon counts  $\eta_i$  for the single molecule  $i$ , depends on various photophysical parameters viz. the molecular absorption cross section  $\sigma_i$ , the quantum yield  $q$ , the overall detection efficiency  $\kappa$ , and the excitation intensity amplitude  $I_0$ . Therefore  $\eta_i$  can be written as

$$\eta_i = \sigma_i q_i \kappa I_0 \quad (3.2)$$

This parameter  $\eta_i$  can be a measure for the signal-to-noise ratio of the measurement and therefore is often used for a quick comparison regarding the quality of the different adjustments or setups. Further, the spatial distribution

### 3. Materials and Methods

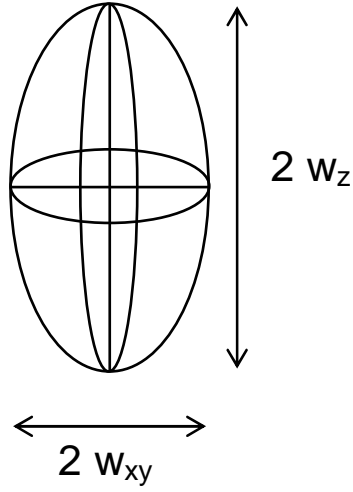


**Figure 3.4** Shape of the confocal volume element. Here  $w_{xy}$  and  $w_z$  represents half of the short and long axis respectively.

of the emitted light should be considered. It is described in the the molecule detection function of the optical setup  $W(\vec{r})$  which is given as

$$W(\vec{r}) = \frac{I_{ex}(\vec{r})}{I_0} S(\vec{r}) = \exp\left(-\frac{2(x^2 + y^2)}{w_{xy}^2}\right) \exp\left(-\frac{2z^2}{w_z^2}\right) \quad (3.3)$$

where  $I_{ex}$  is the spatial distribution of the excitation energy with maximum amplitude  $I_0$  (central intensity) and  $S(\vec{r})$  is optical transfer function of the objective-pinhole combination. Moreover  $S(\vec{r})$  determines the spatial collection efficiency of the setup. Often  $W(\vec{r})$  is approximated by a three dimensional Gaussian, which is characterized by two lateral and axial distances  $w_{xy}$  and  $w_z$ , where the intensity drops to  $\frac{1}{e^2}$ . It gives the shape of an ellipsoid (figure 3.4).

### 3. Materials Methods

Knowing the above two parameters  $\eta_i$  and  $W(\vec{r})$ , the fluorescence fluctuation calculation is simple. The fluctuations of the fluorescence signal are due to the changes in the local concentration  $\delta C$  caused by diffusion, changes of the photophysics of the fluorescent molecules and chemical reactions like conformational changes and aggregation (figure 3.2). The fluorescence fluctuations of molecules at time  $t$  and within the effective volume  $V$  are written as

$$\delta F_i(t) = \int_V W(\vec{r}) \eta_i c_i(\vec{r}, t) . dV \quad (3.4)$$

Incorporating equation 3.2 and 3.3 with 3.4 leads to

$$\delta F_i(t) = \int_V I_{ex}(\vec{r}) S(\vec{r}) \delta(\sigma_i q_i \kappa) \delta c_i(\vec{r}, t) . dV \quad (3.5)$$

The molecular absorption cross section  $\sigma_i$  and the quantum yield  $q$  are assumed constant during the experiment, so equation 3.5 can be rewritten

$$\delta F_i(t) = \kappa \int_V I_{ex}(\vec{r}) S(\vec{r}) \sigma_i q_i \delta c_i(\vec{r}, t) . dV \quad (3.6)$$

The fluctuations of the fluorescence signal (figure 3.5) are defined as the deviations from the temporal average of the signal

$$\delta F(t) = F(t) - \langle F(t) \rangle \quad (3.7)$$

Therefore the fluorescence signal is the sum of time-dependent average fluorescence intensity and the time-dependent fluorescence fluctuations.

$$F(t) = \langle F(t) \rangle + \delta F(t) \quad (3.8)$$

### 3. Materials and Methods

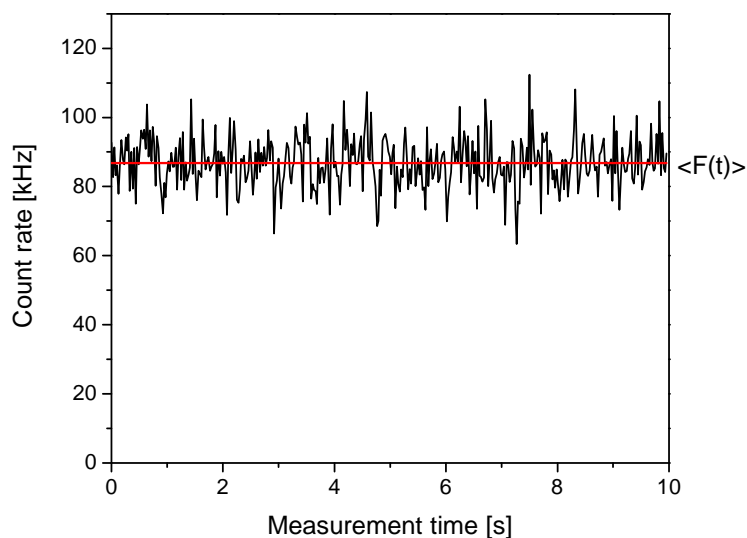


**Figure 3.5** The fluctuation signal (fluorescence intensity) in the course of measurement time is shown. The horizontal red line indicates the average intensity of the signal.

In order to extract information about the time required for a molecule to diffuse through the focal volume, the signal at a given (but arbitrary) time  $t$ ,  $F(t)$ , is compared to the fluorescence intensity  $F(t + \tau)$  after the lag time  $\tau$  by multiplying both values. If  $t$  is sufficiently small, the product will be high since the molecule has not yet left the detection volume. For a large value of  $t$ , when the molecule has left the volume,  $F(t + \tau)$  is zero and so is the product. The autocorrelation analysis measures the self-similarity of the time-series fluorescence signal after the lag time  $\tau$  [98].

$$G(\tau) = \langle F(t)F(t + \tau) \rangle \quad (3.9)$$

### 3. Materials Methods

The normalized autocorrelation function is defined as

$$G(\tau) = \frac{\langle F(t)F(t+\tau) \rangle}{\langle F(t) \rangle^2} = \frac{\langle F(t)F(t+\tau) \rangle}{\langle F(t) \rangle^2} + 1 \quad (3.10)$$

In the equilibrium state, the concentration of fluorescent molecules undergoes fluctuations around its constant mean value [92, 98, 99]:

$$C(\vec{r}, t) = \langle C \rangle + \delta C(\vec{r}, t) \quad (3.11)$$

The concentration fluctuation  $\delta C(\vec{r}, t)$  can be described by free diffusion of particles in three dimensions, using Fick's diffusion equation

$$\frac{\partial \delta C_j(\vec{r}, t)}{\partial t} = D_j \nabla^2 \delta C_j(\vec{r}, t) \quad (3.12)$$

where  $D_j$  is the diffusion coefficient of component  $j$ . The number density autocorrelation term can be calculated as:

$$\langle \delta C(\vec{r}, 0) \delta C(\vec{r}', \tau) \rangle = \langle C \rangle \frac{1}{(4\pi D \tau)^{3/2}} e^{-\frac{(\vec{r}-\vec{r}')^2}{4D\tau}} \quad (3.13)$$

The autocorrelation function of freely diffusing molecules is obtained by combining the equations from (3.3), (3.6), and (3.13) into equation (3.10) as follows

$$G(t) = \frac{1}{\langle N \rangle} \frac{1}{1 + \frac{\tau 4D}{w^2_{xy}}} \frac{1}{\sqrt{1 + \frac{\tau 4D}{w^2_z}}} + 1 = \frac{1}{\langle N \rangle} \frac{1}{1 + \frac{\tau}{\tau_D}} \frac{1}{\sqrt{1 + \frac{\tau}{S^2 \tau_D}}} + 1 \quad (3.14)$$

### 3. Materials and Methods

where  $\langle N \rangle$  is the average number of fluorescent molecule in the focal volume,  $S$  is the structure parameter ( $S=w_z/w_{xy}$ ) which describes the focal volume characterized by the radii  $w_{xy}$  and  $w_z$  and the average time to diffuse the focal volume is

$$\tau_D = \frac{w_{xy}^2}{4D} \quad (3.14)$$

To get the equation 3.14, it is assumed that the fluorophore's fluorescence properties do not change while passing the focal volume. But for real dyes this assumption is not valid. There is a 'flickering' in the fluorescence intensity while the transition of dye to the first excited triplet state. Since this process is forbidden by quantum mechanics, the dye needs more time to relax before reaching the ground state. In other words, the dye cannot emit any fluorescence light when it is in triplet excited state. To consider this into autocorrelation analysis, the triplet dynamics is separated from the diffusion dynamics [100]:

$$G(\tau) = G_{diffusion}(\tau) G_{triplet}(\tau) \quad (3.15)$$

The triplet blinking can be described by a simple exponential decay.

$$G_{triplet}(\tau) = 1 - T + T e^{-\frac{\tau}{\tau_{triplet}}} \quad (3.16)$$

where  $T$  is the fraction of molecules in the triplet state and  $\tau_{triplet}$  is the decay time of the triplet state. Combining the equations (3.16) and (3.14) gives the overall function for a freely diffusing dye.

$$G(\tau) = \left( 1 - T + T e^{-\frac{\tau}{\tau_{triplet}}} \right) \frac{1}{\langle N \rangle} \frac{1}{1 + \frac{\tau}{\tau_D}} \frac{1}{\sqrt{1 + \frac{\tau}{S^2 \tau_D}}} + 1 \quad (3.17)$$

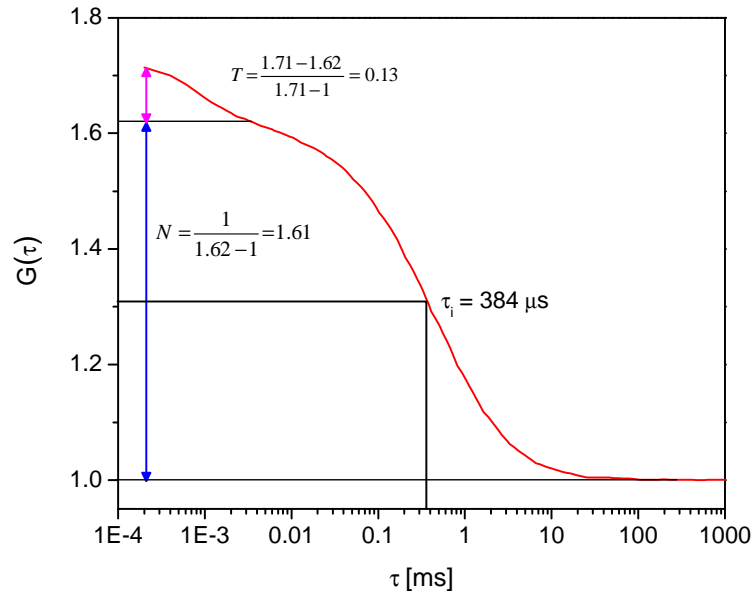


**Figure 3.6** Typical autocorrelation curve of freely diffusing dye molecule with the triplet fraction  $T = 0.13$ , an average number of particle  $N = 1.61$  and the diffusion time  $\tau_i = 384 \mu\text{s}$

A typical autocorrelation curve is shown in figure 3.6 which includes the triplet excitation fraction, number of particle in the focal volume  $N$ , and diffusion time  $\tau_i$  for the fraction  $i$ .

#### Data analysis:

The diffusion of a single fraction of dye molecules is described by equation (3.17). To analyze  $K$  different fractions of dye molecules including triplet states, the extended autocorrelation function is written as follows [100].

### 3. Materials and Methods

$$G(\tau) = \frac{1 + \frac{T}{1-T} \cdot e^{-\frac{\tau}{\tau_0}}}{N} \cdot \sum_{i=1}^K \frac{\phi_i}{1 + \frac{\tau}{\tau_i}} \frac{1}{\sqrt{1 + \frac{\tau}{S^2 \tau_i}}} + 1 \quad (3.18)$$

where  $\phi_i$  is the fraction of the  $i^{\text{th}}$  component. The characteristic diffusion time of the  $i^{\text{th}}$  fraction  $\tau_i$  is the average time required to pass the focal volume and it is related to the diffusion coefficient  $D_i$  of this fraction by the equation

$$\tau_i = \frac{w_{xy}^2}{4D_i} \quad (3.19)$$

The diffusion coefficient of Rhodamine 6G in water is known as  $2.8 \times 10^{-10} \text{ m}^2\text{s}^{-1}$  [93]. By using the equation (3.19), with the experimental value  $\tau_i$  and the known diffusion coefficient, the radius  $w_{xy}$  is calibrated. This value of  $w_{xy}$  is then used to calculate the *a priori* unknown diffusion coefficients of the micelles or aggregates. From the Stokes-Einstein equation the hydrodynamic radius can be calculated.

$$R_{H,i} = \frac{k_B T}{6\pi\eta D_i} \quad (3.20)$$

where  $k_B$  is Boltzmann constant,  $T$  is absolute temperature and  $\eta$  is viscosity of the medium. The autocorrelation functions were fitted the using equation 3.18 for quantitative data analysis. This procedure is performed with the home made Levenberg-Marquardt algorithm [101]. The data were fitted allowing either for a single fraction of dye molecules diffusing at the same rate ( $K = 1$ ) or for two fractions of dye molecules diffusing at different rates ( $K = 2$ ). The former assumes that all dye molecules are in a similar environment, i.e. all dye molecules diffuse freely or all dye molecules are bound to a micelle or all

### 3. Materials Methods

dye molecules are bound to a complex of well-defined size. The latter assumes two different fractions of dye molecules bound to complexes of sufficiently different size, thereby diffusing at different average speed. In the latter case, the value of the parameter *fraction* quantifies the relative population of the different groups. An F-test with a 5 % confidence level was applied to statistically quantify which of the two models fits the experimental data better [102-105]. All FCS measurements discussed here were analyzed both by the single fraction and by the two fraction model. The assumption that each dye diffusion time relates to a well-defined microscopic environment of the dye molecule in turn is based on the assumption that no exchange processes between the dye and different complexes happen during the observation time window. In contrast to other techniques probing considerably longer time scales (e.g. PFG-SE NMR), this assumption seems reasonable given the short time scale probed by FCS.

#### **3.2.1.3 Sample chamber and temperature control setup**

The calibration and other normal FCS measurements were done on a 140  $\mu\text{m}$  thick cover glass (Marienfeld No.1). For the temperature dependent measurements a closed sample chamber was designed [106] as illustrated in figure 3.7. The chamber is made of stainless steel and has maximum volume of 150  $\mu\text{L}$ . The bottom of this sample volume is glued (epoxy glue) with cover glass (Marienfeld No.1). The temperature is controlled by a Peltier element linked to a PRG RS H 100 control unit (Peltron) and PT100 temperature sensors. One of the temperature sensors was placed near by the sample and the other one close to the Peltier element to control the temperature precisely. To assure a good heat conductivity, all the parts of setup were fit together with thermal conducting paste.

### 3. Materials and Methods

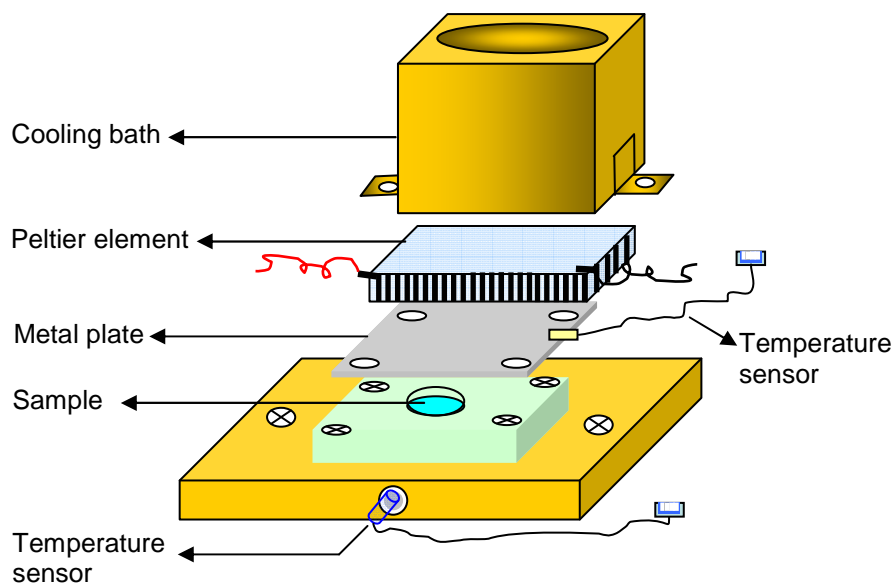


**Figure 3.7** Illustration of Temperature control setup with sample chamber.

A cooling bath was put on top of the setup to remove excess heat from Peltier element. The signals from the temperature sensors were measured by a Keithley 2000 multimeter. The control unit PRG and the Keithly multimeter were controlled by a homemade Labview program.

#### **3.2.2 Rheology**

Rheology is the science of deformation and flow. It accesses the linear and non-linear behavior and macroscopic properties of the viscoelastic fluids. The basics of rheology can be explained by two plates system as shown in figure 3.8.

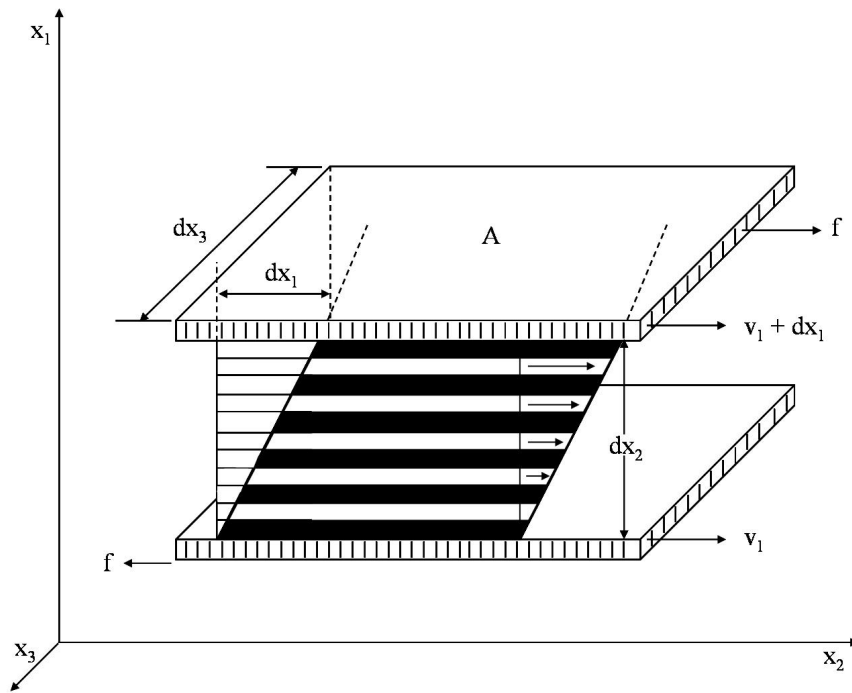


**Figure 3.8** Simple shear flow of a fluid trapped between two parallel plates [107].

The fluid is placed between two large parallel plates of area  $A$  separated by a small gap  $dx_2$ . The lower plate is moving at constant velocity  $v_1$  whereas the upper plate is moving as a constant velocity of  $v_1 + dv_1$  under the applied force  $f$ . From this one can get three important parameters as follows: shear stress  $\sigma$  (force per unit area,  $\frac{f}{A}$ ), shear strain  $\gamma$  (relative deformation,  $\frac{dx_1}{dx_2}$ ), and shear rate  $\dot{\gamma} (= \frac{d\gamma}{dt})$ . The flow characteristics (viscosity) of simple fluids are described with Newton's law of viscosity, a linear constitutive relation between shear stress and shear rate:

$$\sigma = \eta \cdot \dot{\gamma} \tag{3.21}$$

### 3. Materials and Methods

According to the Hookean law, the simplest constitutive relation of elastic solids can be written as

$$\sigma = G \cdot \gamma \quad (3.22)$$

where  $G$  is shear-modulus. Polymers show elastic and viscous behavior (viscoelastic nature) dependent on the temperature and time scale of applied deformation. Therefore it is not possible to describe the mechanical properties of polymers with only one constitutive relation (Hooke or Newton). Thus different combinations of these two ideal properties are used to model the polymer rheological behavior phenomenologically. Maxwell and Voigt-Kelvin models are the basis of available generalized models. The Maxwell model consists of a spring and a dashpot in series, while the Voigt-Kelvin model consists of a spring and a dashpot in parallel arrangement. The time dependent relaxation modulus  $G^0(t)$  is from the Maxwell model:

$$G^0(t) = G \cdot \exp(-t/\tau) \quad (3.23)$$

where  $\tau$  is the relaxation time. In polymer systems there is usually some distribution of relaxation times and thus the real behavior cannot be described by using only one model. The generalized Maxwell model leads to a parallel sequence of individual Maxwell elements. The generalization of the Voigt-Kelvin model consists of a serial array of different Voigt-Kelvin elements.

Concentration dependent rheological measurements were performed with a RFS II spectrometer from Rheometrics Scientific. A Couette system (cup diameter: 34 mm; bob diameter: 32 mm; bob length: 33 mm) was used. The sample was kept at 20 °C for half an hour and sealed to prevent evaporation of the solvent. Steady shear flow experiments were performed from 0.02 to

### 3. Materials Methods

$1000 \text{ s}^{-1}$ . The Zero shear viscosity  $\eta_0$  was determined by extrapolation of the flow curves to the zero shear (equation 3.25).

In a continuous shear field the viscosity of the solution is given by:

$$\eta(t) = \frac{\sigma(t)}{\dot{\gamma}(t)} \quad (3.24)$$

where  $\dot{\gamma}$  is the shear rate and  $\eta$  is the viscosity

$$\lim_{\dot{\gamma} \rightarrow 0} \eta(t) = \eta_0 \quad (3.25)$$

Temperature dependent linear viscoelasticity was probed with a piezoelectric axial vibrator (PAV), which is a squeeze-flow rheometer working at frequencies between 1 and 4000 Hz. It is built by the Institute for Dynamic Materials Testing, University of Ulm, Germany. A scheme of the PAV is shown in figure 3.9. Here, the four piezoelectric elements are attached to two opposite walls of the tube in order to maintain the vibrations while four additional piezoelectric elements are attached to the remaining sides in order to pick up the signal. This whole setup was thermostated with an accuracy of  $\pm 0.02 \text{ }^\circ\text{C}$ . Crassous *et al.* explained the details in [108]. The linear viscoelasticity was ensured by limiting the experiment to sufficiently small amplitudes of the oscillation. PAV has several advantages for gelation measurements e.g. it requires a minimum amount of the sample ( $100 \mu\text{L}$ ), it does not show any evaporation problem at higher temperature, and the gelation rheogram is also accessible.

### 3. Materials and Methods

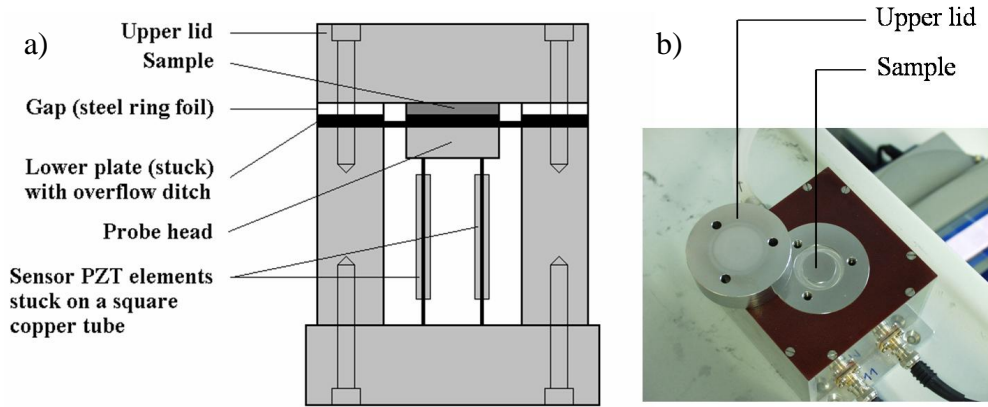


**Figure 3.9** (a) Schematic illustration of piezoelectric axial vibrator in longitudinal view (b) PAV used in this study.

The sample is deformed periodically (oscillating deformation with frequency  $\omega=2\pi f$ ):

$$\gamma = \gamma_0 \sin(\omega t) \quad (3.26)$$

where  $\gamma_0$  is the amplitude of the strain. If the sample shows only elasticity and obeys Hookean's law, the stress and strain would be exactly in phase

$$\sigma = G \cdot \gamma = G \cdot \gamma_0 \cdot \sin(\omega t) = \sigma_0 \cdot \sin(\omega t) \quad (3.27)$$

where  $\sigma_0$  is the amplitude of the stress. The strain rate is given by:

$$\frac{d\gamma}{dt} = \dot{\gamma} = \omega \gamma_0 \cdot \cos(\omega t) \quad (3.28)$$

If the sample behaves like a Newtonian liquid, the stress is

### 3. Materials Methods

$$\sigma = \eta \cdot \frac{d\gamma}{dt} = \eta\omega\gamma_0 \cdot \cos(\omega t) \quad (3.29)$$

Comparing this result with the Hooke system (equation 3.27) shows that elastic and viscous forces – occurring separately – are 90° out of phase. In a viscoelastic material both forces occur simultaneously, leading to a phase shift  $\delta$  (phase angle) between stress and deformation.

$$\sigma = \sigma_0 \sin(\omega t + \delta) = \underbrace{\sigma_0 \sin(\omega t) \cos \delta}_{\text{in phase with } \gamma} + \underbrace{\sigma_0 \sin \delta \cos(\omega t)}_{\text{in phase with } \dot{\gamma}} \quad (3.30)$$

Dividing by the deformation amplitude  $\gamma_0$ ,  $G^*$  can be calculated with

$$G^* = \frac{\sigma^*}{\gamma^*} = \frac{\sigma_0}{\gamma_0} \cos \delta + i \frac{\sigma_0}{\gamma_0} \sin \delta = G' + iG'' \quad (3.31)$$

The complex modulus includes the storage modulus  $G'$  and loss modulus  $G''$ . The storage modulus  $G'$  is the imaginary part of the complex viscosity and is to be considered as the elastic contribution to the complex functions and it measures the energy storage. Similarly, the loss modulus  $G''$  is the viscous contribution and measures the energy dissipation.

#### 3.2.3 Cryogenic transmission electron microscopy

Cryo-TEM is a natural tool to elucidate the microstructures that appear in the systems. It provides direct images of the many different coexisting assemblies found in the systems.

For cryo-TEM studies, a drop of the sample (2  $\mu\text{L}$ ) was put on an untreated bare copper transmission electron microscopy (TEM) grid (600 mesh, Science Services, Munich, Germany), where most of the liquid was removed with blotting paper leaving a thin film covering the grid holes. The specimens were

### 3. Materials and Methods

instantly shock frozen by rapid immersion into liquid ethane and cooled to approximately  $-183\text{ }^{\circ}\text{C}$  by liquid nitrogen in a temperature-controlled freezing unit (Zeiss Cryobox, Zeiss NTS GmbH, Oberkochen, Germany). The temperature was monitored and kept constant in the chamber during all the sample preparation steps. After freezing the specimens, the remaining ethane was removed using blotting paper. The specimen was inserted into a cryotransfer holder (CT3500, Gatan, Munich, Germany) and transferred to a Zeiss EM922 EFTEM (Zeiss NTS GmbH, Oberkochen, Germany). Examinations were carried out at temperatures around  $-183\text{ }^{\circ}\text{C}$ . The TEM was operated at an acceleration voltage of 200kV. Zero-loss filtered images ( $\Delta E=0\text{ eV}$ ) were taken under reduced dose conditions ( $100 - 1000\text{ e/nm}^2$ ). All images were registered digitally by a bottom mounted CCD camera system (Ultrascan 1000, Gatan, Munich, Germany) combined and processed with a digital imaging processing system (Digital Micrograph 3.10 for GMS 1.5, Gatan, Munich, Germany).

Most of the measurements were repeated in the group of Prof. Talmon at the Technion, Haifa, Israel. The sample preparation followed a different protocol and the imaging was performed on a different instrument. Vitrified specimens for cryo-TEM were prepared in a controlled environment vitrification system (CEVS) at  $25\text{ }^{\circ}\text{C}$  and 100% relative humidity, as previously described [60]. CEVS was used to prevent the evaporation during the specimen preparation. In brief, a drop of the solution to be imaged was applied onto a perforated carbon film supported on an electron microscopy copper grid, held by the CEVS tweezers. The sample was blotted by filter paper, and immediately plunged into liquid ethane at its freezing point ( $-183\text{ }^{\circ}\text{C}$ ). The vitrified samples were then stored under liquid nitrogen ( $-196\text{ }^{\circ}\text{C}$ ), transferred to an Gatan 626 cooling holder via its “work station”, and kept in

### 3. Materials Methods

a FEI T12 G2 microscope at about -180 °C. Images were recorded at 120 kV acceleration voltage, in the low-dose mode, to minimize electron-beam radiation-damage. We used a Gatan US1000 cooled CCD camera, with the Digital Micrograph software package, to acquire the images. Images were recorded at nominal underfocus of about 2 micrometer to enhance phase-contrast.

#### 3.2.4 Turbidity measurements

Turbidity measurements were performed utilizing an *in-situ* photometer operating at a wavelength  $\lambda = 523$  nm (Spectrosense, 6.1109.110, Metrohm) and connected to a Titrand 806 system (Metrohm). This whole system was controlled by the Metrohm Tiamo™ computer software. The turbidity as a function of temperature was measured in a 50 mL tall-form jacketed glass cell tempered by a computer controlled thermostat (EcoLine RE 306, Lauda). Solution temperatures were monitored with a PT1000 temperature sensor (6.1110.110, Metrohm) calibrated to an accuracy of  $\pm 0.02$  °C. The turbidity,  $\tau$ , may be calculated as

$$\tau = \left(-\frac{1}{L}\right) \ln\left(\frac{I_t}{I_0}\right) \quad (3.32)$$

where  $L$  is the light path length of the photometer ( $L = 22$  mm),  $I_t$  is the transmitted light intensity, and  $I_0$  is the incident light intensity.

### 3. Materials and Methods

# 4

## Results and Discussion

### 4.1 Concentration dependent studies<sup>‡</sup>

The single molecule approach for the characterization of the polymer-surfactant systems (PSS) is applied for methylcellulose (MC), sodium dodecyl sulfate (SDS) system. The concentration of MC dependent measurements were studied by FCS, rheology and cryoTEM. The detailed discussion about the FCS measurements followed by other techniques to support the FCS data is reported in this chapter.

#### 4.1.1 Fluorescence correlation spectroscopy

##### 4.1.1.1 Critical micelle concentration

Before investigating the interactions between MC and SDS the detailed FCS investigations of SDS solutions in the absence of MC are discussed.

---

<sup>‡</sup> Parts of the results presented in this section have been published [117]

## 4. Results and Discussion

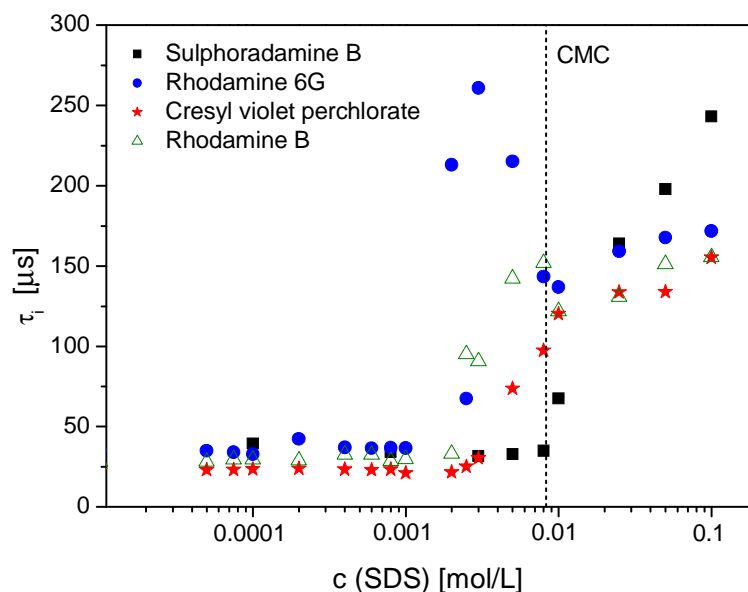


**Figure 4.1** Diffusion time of SDS for Sulphoradamine B ■(anionic), Rhodamine 6G ●, Cresyl violet perchlorate ★(cationic) and Rhodamine B △(nonionic) laser dyes. The data result from single-fraction fit ( $K = 1$ ). More scattering of diffusion time is observed with all dyes except Cresyl violet perchlorate. Increasing of diffusion time starts at  $c_{\text{SDS}} = 2.5 \times 10^{-3}$ . The dotted vertical line represents the classical CMC of SDS.

The anionic surfactant SDS is measured with the anionic dye Sulphordamine B, and cationic dyes, Rhodamine 6G, Cresyl violet perchlorate and nonionic dye Rhodamin B at a constant concentration of  $c_{\text{Dye}} = 10^{-8}$  M. This concentration relates to approximately a single dye molecule in the femtoliter sized focal volume. The characteristic diffusion time of the dye molecules at various SDS concentrations is shown in figure 4.1. The results from the single-fraction fit ( $K=1$ ) throughout the entire SDS concentration range.

## 4. Results and Discussion

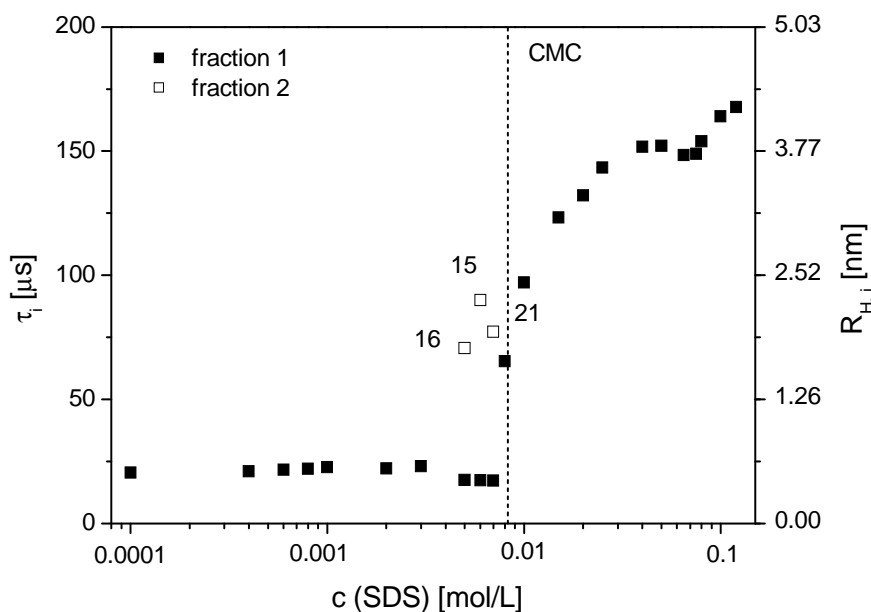


**Figure 4.2** Characteristic diffusion times of Cresyl violet perchlorate as a function of SDS concentration in the absence of MC. The dotted line indicates the CMC of SDS as determined by classical techniques[109]. Only free dye molecules with  $\sim 20 \mu\text{s}$  are detected at low SDS concentration. The data result from a single-fraction fit ( $K = 1$ ) to the autocorrelation data. A second fraction of populations with diffusion time  $70 \mu\text{s}$  appears at  $c_{\text{SDS}} = 5.0 \times 10^{-3} \text{ M}$ . The corresponding hydrodynamic radii are shown at the right hand axis. For the calculation of the hydrodynamic radii, the spherical micelles are assumed to diffuse in a solution of viscosity  $0.001 \text{ Pa}\cdot\text{s}$  and temperature  $20 \text{ }^\circ\text{C}$ . The numbers refer to the population of fraction 2 in per cent. The population of fraction 1 can be calculated as the complement to 100%.

The dashed vertical line shows the critical micelles concentration (CMC) obtained by “classical techniques” such as conductivity, surface tension etc. [109]. Rhodamine 6G and Rhodamine B base give more scattered diffusion time. Sulphordamine B does not provide any characteristic changes of diffusion time near CMC supposedly because of the repulsive electrostatic interactions between Sulphordamine B and SDS. At higher concentration of

#### 4. Results and Discussion

SDS more scattered diffusion time is observed as well as an increase of diffusion time below the classical CMC of SDS irrespective of dyes. It is at  $c_{\text{SDS}} = 2.5 \times 10^{-3}$  that diffusion time starts to increase. Out of the two cationic laser dyes, Cresyl violet perchlorate was chosen to be used for further investigations. The diffusion time of Cresyl violet perchlorate with SDS is shown in figure 4.2. At SDS concentrations below  $c_{\text{SDS}} = 5.0 \times 10^{-3}$  M the diffusion time is constant at the value observed in the absence of SDS, i.e.  $\tau_{\text{Dye}} = 21.5 \pm 1.0 \mu\text{s}$ . This value relates to free dye molecules. At around  $c_{\text{SDS}} = 5.0 \times 10^{-3}$  M the diffusion time significantly increases and slowly reaches  $\tau_{\text{Dye}} \sim 150 \mu\text{s}$  at  $c_{\text{SDS}} = 4.0 \times 10^{-2}$  M characteristic of dye molecules bound to an SDS micelle. Except for the transition region the data are best fitted by assuming a single fraction ( $K = 1$ ) of molecules. Between  $c_{\text{SDS}} = 5.0 \times 10^{-3}$  and  $7.0 \times 10^{-3}$  M a two fraction fit yields better results indicating the presence of two different fractions. One fraction has the same diffusion behavior as free dye molecule while the second is much slower and represents dye molecules bound to SDS micelles. F-test is used to verify the suitability of the chosen model i.e the single or two-fraction model with a 5 % confidence level. This finding of 'pre-micellar aggregates' is most probably due to the ultra-high sensitivity of the FCS technique which can detect as little as  $10^{-9}$  M micelles.

At SDS concentrations below CMC the dye molecules diffuse freely without significant changes in diffusion time as a function of SDS concentration. The increase in the diffusion time of the dye in SDS solutions close to the CMC indicates that the dye molecules are physically bound to SDS micelles. The lowest SDS concentration at which the FCS autocorrelation function can be well represented by a single fraction of dye molecules bound to micelles can be defined as CMC of SDS from FCS measurements.

## 4. Results and Discussion

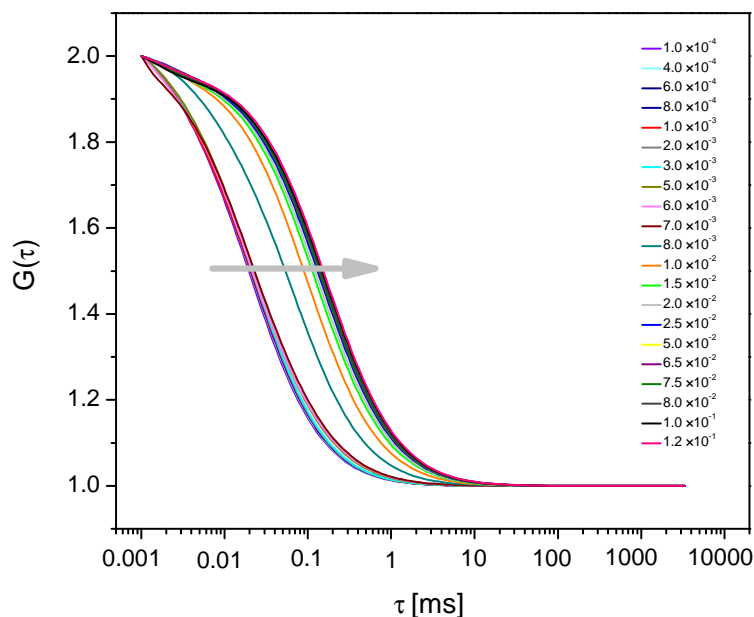


**Figure 4.3** Normalized autocorrelation curves of SDS solutions. The arrow shows the increasing SDS concentration. The diffusion time starts to increase at  $c_{\text{SDS}} = 5.0 \times 10^{-3}$  M. In this concentration region two fractions with different diffusion are observed. The position of the autocorrelation curves shifted towards higher time when SDS approaching higher concentration.

This value coincides with the CMC of SDS determined by “classical techniques” such as conductivity, surface tension etc. [109]. The normalized autocorrelation curves are shown in figure 4.3. Below CMC there aren’t any characteristic changes in the autocorrelation curves. With further increase in the SDS concentration diffusion time increases and the autocorrelation curves position also changes accordingly.

The numbers of dye molecules are available in the illuminated volume during the FCS measurements as given in figure 4.4. After CMC the number

## 4. Results and Discussion

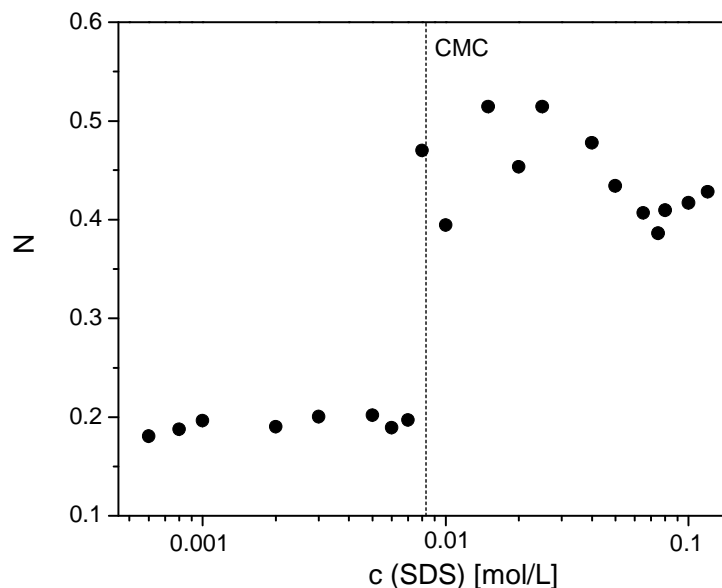


**Figure 4.4** Number of Cresyl violet perchlorate dye molecules in the excitation volume for various SDS concentrations. The dye concentration is  $c_{\text{dye}} = 10^{-8}$  M. There is a characteristic change in the number of particles after CMC of SDS.

of dye molecule almost doubles in the illuminated volume and there isn't any remarkable change before the highest concentration of SDS solution is attained. The increasing number of dye molecules in the illuminated volume could be explained by the solubilization of dye molecules in the micelles. The dyes are attached to the cover glass reaching the solution during micelle formation. The concentration of dye does not influence the changing the micelle formation of SDS [34].

Uniform intensity fluctuations indicate a single dye molecule being attached to a single micelle. Compared to  $c_{\text{SDS}} = 1.0 \times 10^{-1}$  M, dye concentration is several orders lesser in magnitude. Therefore, few micelles may not bind with

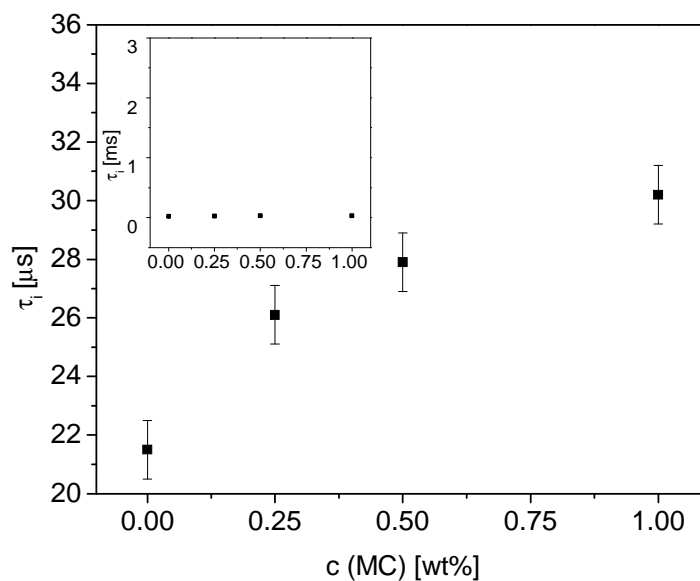


**Figure 4.5** Diffusion time of dye molecules as a function of methyl cellulose concentration in the absence of SDS. The inset has the same y-scale as in figure 4.9b for comparison.

the dye molecules, at higher concentration of SDS which can not be observed in the FCS measurements.

#### 4.1.1.2 Critical aggregation concentration

So far our results resemble the findings of Zettl *et al* on similar surfactant system [34]. It can be precisely follow the micelle formation without covalent labeling of dye with SDS. In order to investigate MC/SDS interactions, we have repeated the above experiment in the presence of different amounts of MC, i.e. at  $c_{MC} = 1, 0.5$  and  $0.25$  wt%.

The SDS concentration varied between  $4.0 \times 10^{-4}$  M and  $2.0 \times 10^{-1}$  M. The dye concentration was kept constant at  $c_{Dye} = 10^{-8}$  M. Before we discuss the

## 4. Results and Discussion

MC/SDS mixtures, the influence of MC on the diffusion time of the dye molecules needs to be considered. Indeed, the diffusion time of the free dye molecules does increase slightly with increasing MC concentration (figure 4.5). However, plotting the data on the same scales as the data obtained on MC/SDS mixtures (inset to figure 4.5) reveals that the effect of MC is negligible when compared to the effect of SDS. The data clearly indicate that the significant change of the diffusion behavior of the dye molecules in MC/SDS mixtures is *not* induced by the presence of MC alone. One may conclude from this finding that the interaction between nonionic MC and the cationic dye is not strong enough to enable the formation of stable complexes. We note in passing that the observed small increase of the Cresyl violet diffusion time is an interesting finding in itself as it suggests that the dye molecules are able to probe the presence of the MC chains even at these low MC concentrations. The finding is to some extent in contrast to earlier reports on dye labeled polymers using pyrene as a dye [110, 111]. The different observation may well be due to the considerably longer life-time of Cresyl violet. This issue, however, is beyond the scope of our present study.

We start our discussion with the data obtained at the highest MC concentration  $c_{MC} = 1.0$  wt % with SDS. The figure 4.6 summarizes the results obtained with different laser intensity. This experiment was to show that the apparent diffusion time does not depend on the laser intensity. The trend of changing diffusion time is observed near CMC and beyond. Though two fraction fit is valid for most of the measurements, only single-fraction fit is considered here. The rather long diffusion times may potentially lead to photo bleaching of the dye during its passage time through the focal volume. This effect is observed at  $c_{SDS} = 2.5 \times 10^{-2}$  M very clearly.

## 4. Results and Discussion

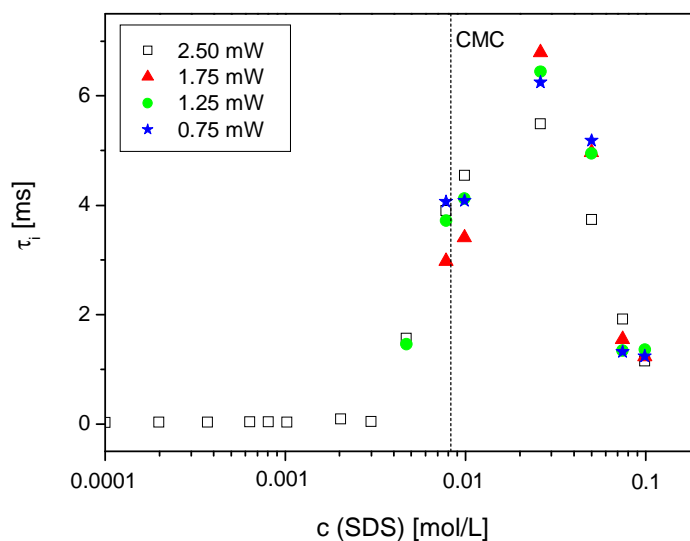


**Figure 4.6** FCS measurements of 1 wt % MC with SDS under different laser powers. The increasing trend of diffusion time with laser power is observed while photobleaching causes an abnormal diffusion time with higher laser power. This analysis shows that the right laser power for the measurements needs to be chosen. The results are drawn from single fraction fit.

The diffusion time increases with increasing laser power 1.75 mW. Because of photo bleaching, diffusion time decreases remarkably when laser power increases to 2.5 mW. Therefore for incoming all the measurements the optimum laser power has chosen as 1.25 mW. The detailed description for 1 wt % MC with SDS is going to be discussed further and results are shown in figure 4.6. At low SDS concentrations, the FCS data is well represented by a single fraction fit yielding a rather constant diffusion time similar to the value observed for free dye molecules. At SDS concentrations between  $c_{\text{SDS}} = 2.0 \times 10^{-3}$  M and  $1.2 \times 10^{-1}$  M the F-Test indicates that a two-fraction fit is needed to reliably describe the data.

#### 4. Results and Discussion

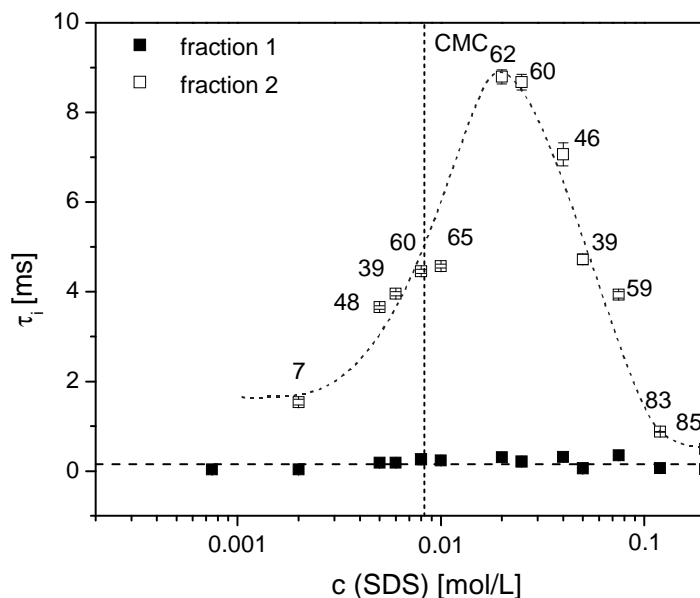


**Figure 4.7** Diffusion times of the dye molecules determined for 1 wt % MC and various SDS concentration. The dotted vertical line indicates the location of the CMC of SDS as determined by “classical” techniques. The dashed horizontal lines indicates the maximum diffusion time of the dye molecules with SDS in the absence of MC. The dotted curves are guides-to-the-eye. The population of the fraction 2 is included (in per cent). The population of fraction 1 can be calculated as the complement to 100%.

A second fraction of dye molecules is observed characterized by a considerably longer diffusion time. With increasing SDS concentration the diffusion time of this second fraction decreases again. The per cent of dye fraction is mentioned in figure 4.7 as numerical number near by the slow diffusing fraction points. The per cent of fraction 2 is increasing with the diffusion time until  $c_{\text{SDS}} = 2.0 \times 10^{-2}$  M and decreasing further. This decreasing tendency ends at  $c_{\text{SDS}} = 5.0 \times 10^{-2}$  M. Afterwards it increases again further.

## 4. Results and Discussion

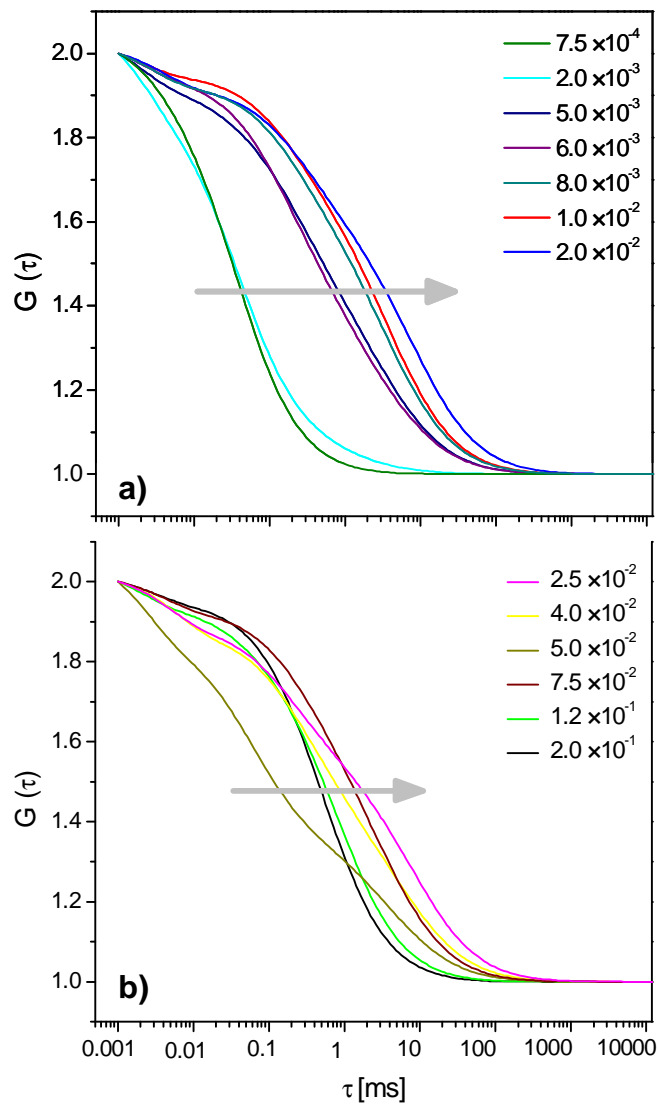


**Figure 4.8** Normalized autocorrelation curves of 1 wt % MC and SDS concentrations. a) The shape of the autocorrelation curves varies largely. This graph shows the results up to  $c_{\text{SDS}} = 2.0 \times 10^{-2}$  M. The two fractions exist from the  $c_{\text{SDS}} = 2.0 \times 10^{-3}$  M. The increasing SDS concentration mentioned as an arrow. b) Greater changes are found at  $c_{\text{SDS}} = 5.0 \times 10^{-2}$  M. All other curves show a similar trend in their behavior. The increasing diffusion time is mentioned as an arrow.

#### 4. Results and Discussion

The normalized autocorrelation curves of 1 wt % MC and SDS are summarized in figure 4.8. The shape of the curve gives the information about slow and fast diffusing fractions. The beginning and end of the autocorrelation curve attributes the fast diffusing fraction 1 and slow diffusing fraction 2 respectively. Increasing SDS concentration leads to maximum diffusion time at  $c_{\text{SDS}} = 2.0 \times 10^{-2}$  M and figure 4.8a shows its autocorrelation curve's shape. The decreasing tendency of diffusion time is shown by autocorrelation curves in figure 4.8b. Upon increasing SDS concentration the shape of the autocorrelation curves changes towards inside.

The similar behavior of 1 wt % MC/SDS was observed at lower MC concentrations. Single fraction is considered at very low SDS concentrations and the diffusion time attributes the free dye molecules. For  $c_{\text{MC}} = 0.5$  wt %, at SDS concentrations between  $c_{\text{SDS}} = 3.0 \times 10^{-3}$  M and  $5.0 \times 10^{-2}$  M two fractions are available (figure 4.9a). Above  $c_{\text{SDS}} = 5.0 \times 10^{-2}$  M the data is again well described by a single fraction fit indicating that all dye molecules diffuse at the same, however somewhat longer, diffusion time as compared to the free dye molecules observed at low SDS concentrations. A second fraction of considerably slower dye molecules is observed around the CMC of SDS. Again, its diffusion time increases and eventually decreases again at sufficiently high SDS concentrations.

For  $c_{\text{MC}} = 0.25$  wt %, at SDS concentrations between  $c_{\text{SDS}} = 6.0 \times 10^{-3}$  M and  $2.5 \times 10^{-2}$  M the F-test indicates the suitable possibility of two-fraction fit (figure 4.9b). All the other behavior is similar to  $c_{\text{MC}} = 1.0$  and  $0.5$  wt % at very low and high SDS concentrations. The normalized autocorrelation curves of  $c_{\text{MC}} = 0.5$  and  $0.25$  wt % of SDS mixtures are displayed in figure 4.10.

## 4. Results and Discussion

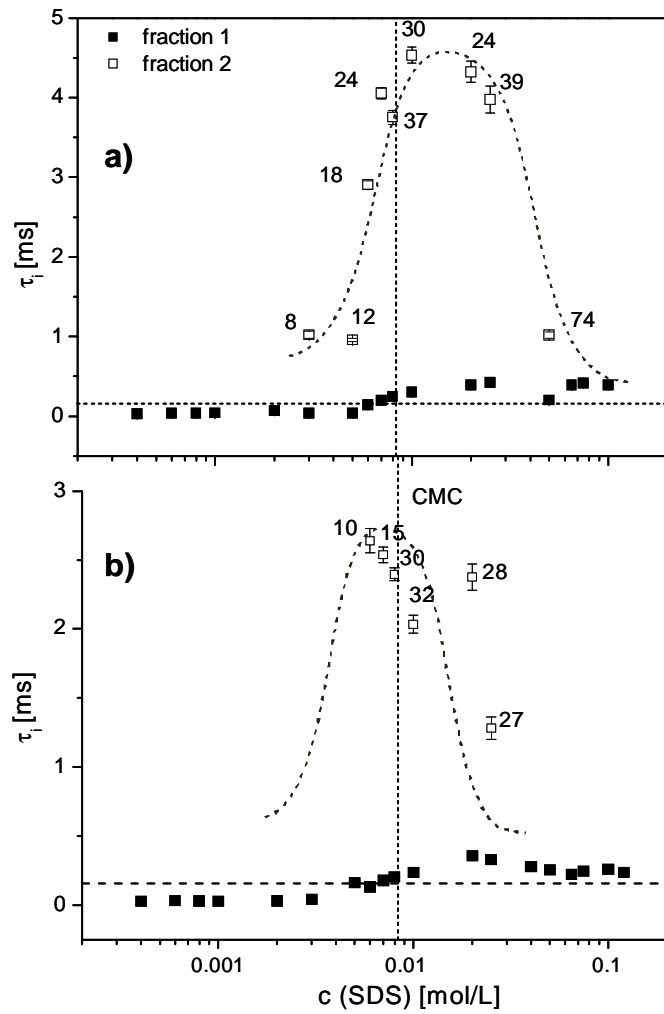


**Figure 4.9** Diffusion times of the dye molecules determined for  $c_{MC} = 0.5$  (a), and 0.25 (b), as a function of SDS concentration. The dotted vertical line indicates the location of the CMC of SDS as determined by “classical” techniques. The dashed horizontal lines indicate the maximum diffusion time of the dye molecules with SDS in the absence of MC. Two-fraction fits ( $K = 2$ ) are applied around the CMC.

## 4. Results and Discussion

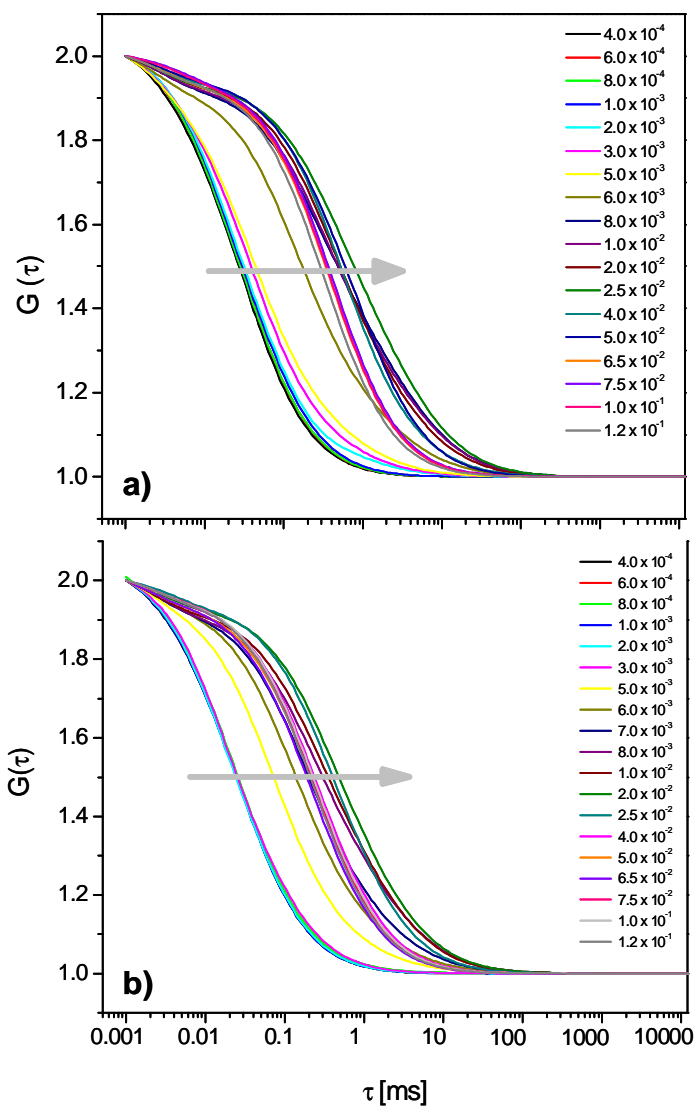


**Figure 4.10** Normalized autocorrelation curves of 0.5 wt % MC (a) and 0.25 wt % MC with various SDS concentrations. The arrows show the increasing diffusion time. The shift in position of the autocorrelation curve is seen with the same x and y-scales.

The trend to change its shape is not exactly the same as in 1 wt % MC but rather smooth. With the comparison of same x and y scale of  $c_{MC} = 0.5, 0.25$

## 4. Results and Discussion

wt %, the shift in the autocorrelation curves of 0.5 wt % MC is observable. The location of the maximum diffusion time of second fraction shifts to higher SDS concentrations with increasing MC concentration as can be seen in figure 4.11. The concentration at which the diffusion time reaches maximum is roughly proportional to the MC concentration. The number of dye molecules of MC/SDS mixtures, present in the illuminated focal volume is displayed in the figure 4.12. There is more scattering for  $c_{MC} = 0.25$  and 0.5 wt %. The number increases once or twice for  $c_{MC} = 0.25$ , 0.5 wt % and  $c_{MC} = 1.0$  wt % respectively.

From the experiments on SDS solutions in the absence of MC (figure 4.2) we know that the Cresyl violet perchlorate dye behaves like a fluorescent label attached to the SDS micelles. In the presence of MC, SDS molecules are expected to form complexes with the hydrophobic zones of the MC chains by virtue of hydrophobic interactions [12, 67]. Therefore we expect them to be able to follow the MC/SDS aggregates through FCS. The availability of second fraction of dye molecules confirms the onset of increasing diffusion time which slightly differs from different concentrations of MC/SDS mixtures. We may define a critical aggregation concentration (CAC) from FCS measurements as the onset of increasing diffusion time. The concentration, at which the diffusion time of second fraction reaches the minimum after the maximum aggregation, refers to the end of aggregation (EOA). It can be  $c_{SDS} = 5.0 \times 10^{-2}$  M for 1 wt % MC and SDS mixtures. EOA will shift to higher with increasing MC concentration. Before CAC the diffusion time of single dye fraction attributes the mobility of dye alone. Indeed, above the CAC of SDS we find that a certain fraction of dye molecules diffuse considerably slower indicating the formation of complexes.

#### 4. Results and Discussion

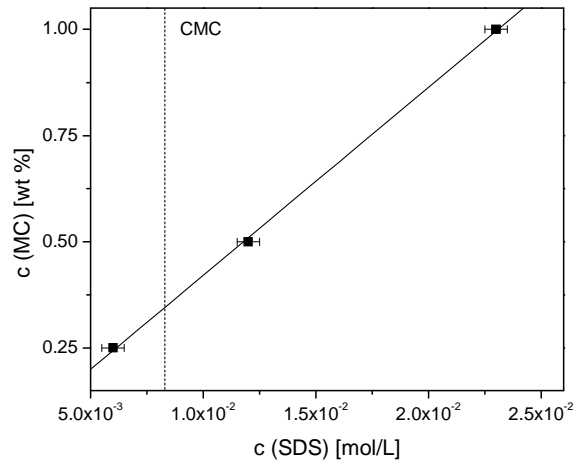


**Figure 4.11** Location of the SDS concentration leading to the maximum diffusion time of the dye molecules for different MC concentration. The required amount of SDS to saturate the association is proportional to the MC concentration.

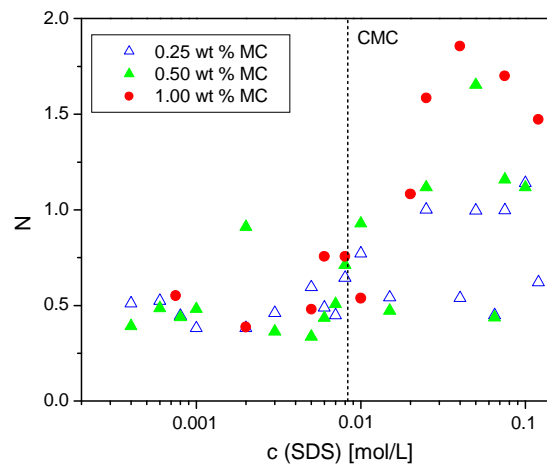


**Figure 4.12** Number of dye molecules in excited volume for  $c_{MC} = 0.25, 0.5,$  and  $1.0$  wt % with various  $c_{SDS}$ .

## 4. Results and Discussion

The absolute diffusion time of this slow fraction of dye molecules is considerably larger than the one observed for SDS micelles indicating the formation of aggregates with rather large hydrodynamic volume. We may assume that these are aggregates between different MC chains bound together via hydrophobic interactions involving SDS molecules. Upon SDS binding, the hydrodynamic volume of polymer chains is expected to increase further due to polyelectrolyte behavior [69]. The largest diffusion time is obtained at the highest MC concentration (1 wt %). Interestingly, the amount of SDS required to form maximum aggregations is proportional to the MC concentration. With higher concentration of MC, more SDS molecules are required to saturate the association as shown in figure 4.11. This behavior coincides with common non-ionic polymer and anionic surfactant systems [45].

### 4.1.2 Rheology

While FCS addresses the microscopic mobility of a single dye molecule either free or bound to a complex, we performed steady shear flow rheological measurements to assess the macroscopic viscosity of the solutions (figure 4.13a). The flow curves are extrapolated to zero shears and zero shear viscosity is obtained for MC/SDS mixtures as shown in figure 4.13b. Here we only emphasize and report on 1 wt % MC/SDS solutions. The solutions are characterized by a zero shear viscosity around 0.4 Pa's both in the absence of SDS and at low enough SDS concentrations. At higher SDS concentration the viscosity increases significantly reaching a maximum of around 1.53 Pa's at  $c_{\text{SDS}} = 2.0 \times 10^{-2}$  M. When the SDS concentration is further increased, the viscosity drops and eventually reaches 0.04 Pa's at and above  $c_{\text{SDS}} = 7.5 \times 10^{-2}$  M. The onset concentration at which the viscosity increases is known as critical aggregation concentration (CAC).

## 4. Results and Discussion

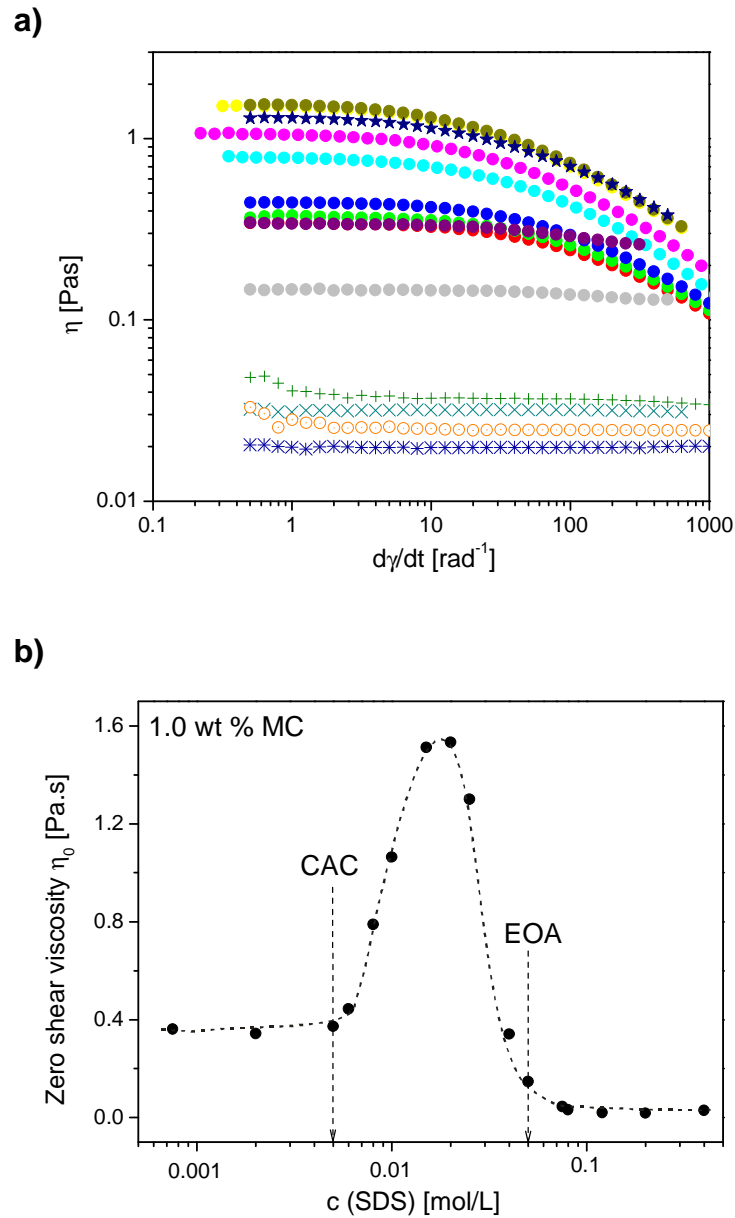


**Figure 4.13** (a) Flow curves of 1wt % MC and various  $c_{\text{SDS}} = 2.0 \times 10^{-3} \text{ M}$  ( $\bullet$ ),  $5.0 \times 10^{-3} \text{ M}$  ( $\bullet$ ),  $6.0 \times 10^{-3} \text{ M}$  ( $\bullet$ ),  $8.0 \times 10^{-3} \text{ M}$  ( $\bullet$ ),  $1.0 \times 10^{-2} \text{ M}$  ( $\bullet$ ),  $1.5 \times 10^{-2} \text{ M}$  ( $\bullet$ ),  $2.0 \times 10^{-2} \text{ M}$  ( $\bullet$ ),  $2.5 \times 10^{-2} \text{ M}$  ( $\star$ ),  $4.0 \times 10^{-2} \text{ M}$  ( $\bullet$ ),  $5.0 \times 10^{-2} \text{ M}$  ( $\bullet$ ),  $7.5 \times 10^{-2} \text{ M}$  ( $+$ ),  $8.0 \times 10^{-2} \text{ M}$  ( $\times$ ),  $1.2 \times 10^{-1} \text{ M}$  ( $\ast$ ), and  $4.0 \times 10^{-1} \text{ M}$  ( $\circ$ ) (b) Zero shear viscosity of 1 wt % MC and SDS mixtures. Curve is drawn as guide- to-the-eye.

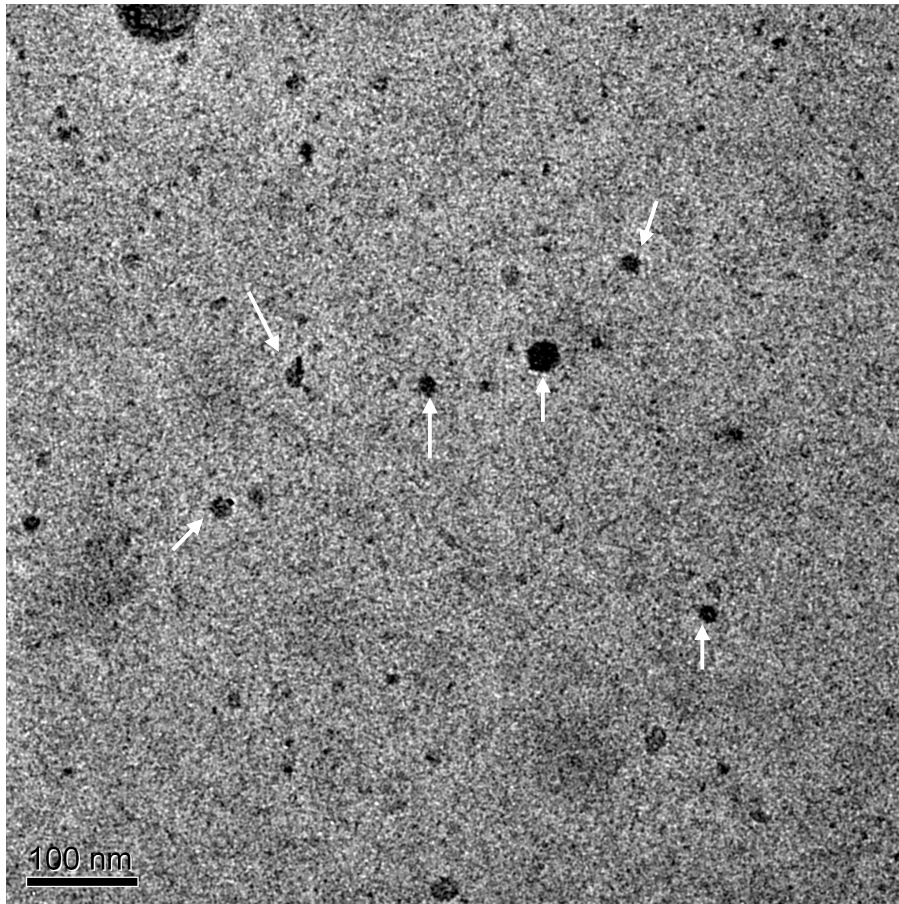


**Figure 4.14** CryoTEM image of 1 wt% MC and  $2.0 \times 10^{-2}$  M SDS. The background is subtracted to minimize thickness variation effects. The various sizes of aggregates are shown selectively with arrows. The scale bar corresponds to 100 nm

The concentration at which the minimum viscosity is reached is denoted as end of aggregation (EOA) concentration in figure 4.13b. The shear thinning effect is not observed after EOA It indicates the separation of MC chains. The behavior of the zero shear viscosity resembles the behavior of the slowly diffusing fraction of dye molecules identified with FCS. This meets the notion that the macroscopic viscosity is dominated by the physical cross links between MC chains strengthened by SDS [112].

## 4. Results and Discussion

### 4.1.3 Cryogenic transmission electron microscopy

To visualize the MC/SDS aggregates, cryoTEM was used. We performed cryoTEM measurements only with 1 wt % MC/SDS systems. Since we observe three different types of behavior in viscosity as well as FCS measurements, cryoTEM measurements were tried selectively from each category viz. before CAC, at maximum aggregation and after EOA. The contrast of MC is equal to water and we can not distinguish from its water

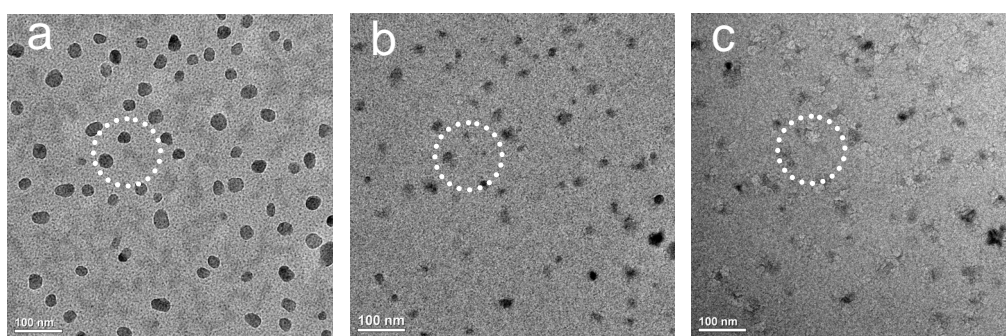


**Figure 4.15** CryoTEM micrographs of 1 wt% MC and  $2.0 \times 10^{-2}$  M SDS. a) image of aggregates b) after less radiation c) after more radiation. The sample undergoes more radiation damage showing the vanishing effect. The white circle is drawn to follow structure reformation with radiolysis. The scale bar corresponds to 100 nm.

background. Even with addition of small amounts of SDS we could not visualize any distinct structure. The maximum aggregation was found with FCS and rheology measurements at  $c_{\text{SDS}} = 2.0 \times 10^{-2}$  M. The same concentration is used to visualize with cryoTEM and the images are shown in figure 4.14 and 4.15. The aggregates can be seen in various sizes as in figure 4.14. The dark parts of the aggregates which are indicated with white arrows are thought to be the MC/SDS aggregates.

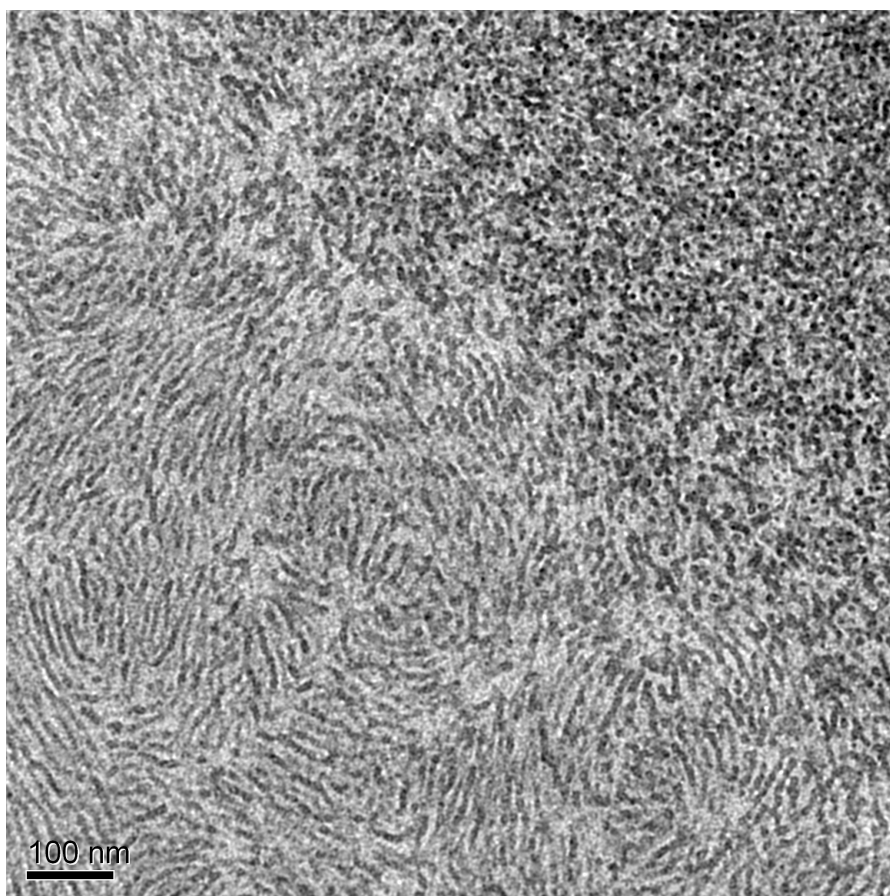


**Figure 4.16** Cryo-TEM micrograph of 0.4 M SDS solution (background subtracted). The scale bar corresponds to 100 nm. High contrast worm like micelles are seen. The superposition of worm like micelles is also showing the spherical shapes in the right top corner of the image.

The same aggregates are not visible anymore after strong radiolysis. The more irradiation reforms the aggregates and by radiation damage could be observed. The shape of the aggregates loses stability after strong irradiation for more time. The size of the aggregates is not uniform in size. To study the behavior of the MC/SDS system after EOA  $c_{\text{SDS}} = 0.4$  M with 1 wt % MC was focused on. The image of 0.4 M SDS alone is shown in figure 4.16

#### 4. Results and Discussion

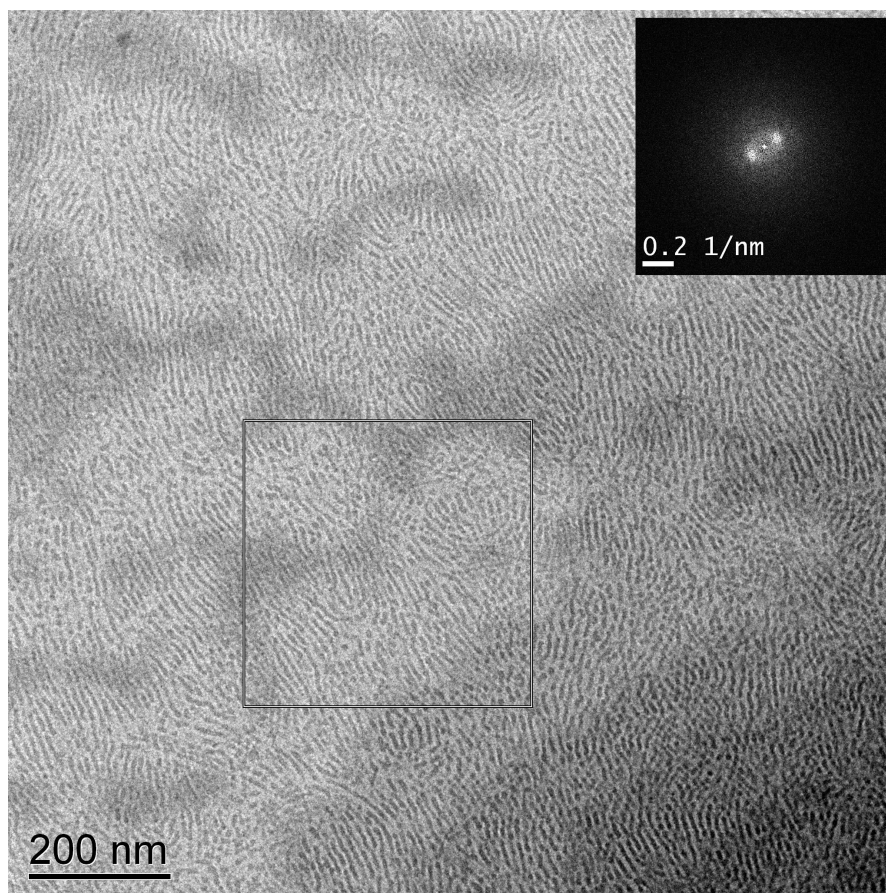


**Figure 4.17** Cryo-TEM image of 0.4 M SDS + 1 wt % MC solution. FFT of selected area is shown in the inner picture. The left bottom corner of image shows the multilayer up to 5 layers. The scale bar corresponds to 200 nm.

With addition of SDS micelles to the MC worm like structures are formed (figure 4.17). The superposition of a few layers of worm like micelles may result in a globular appearance of the structures. This structure may be explained by possible the top views of worm like micelles. In order to understand the distance between worm like chains, fast Fourier transform (FFT) analysis in the selected area was done. The FFT pattern result shows the mean distance between the worm like structure corresponding to approximately is  $10 \pm 2$  nm and the diameter of the chain is approximately 5

## 4. Results and Discussion

nm. Several layers of MC/SDS systems are visible at the bottom of in figure 4.17. The more crowded layers show the mixture of worm like and globular structures.

It is important to realize that the observed increase in diffusion time for part of the dye molecules cannot be explained by the increased overall viscosity. While the viscosity increases by about a factor of 4, the diffusion time of the slower fraction increases by more than a factor of 50. Therefore, even if we normalized the diffusion time of the dye by the (slightly increasing) viscosity, it still would be an order of magnitude larger than in the absence of SDS. We note that a second, considerably faster diffusing fraction of dye molecules is observed along with the large aggregates. The diffusion time of this fraction scatters slightly above the value found for dye molecules bound to SDS micelles. Here, we assume either SDS micelles or aggregates between SDS and single MC chains. The availability of single MC chain varies depending on the bulk aggregation formation with polymer and surfactant. We note that these smaller aggregates are not monitored by macroscopic techniques as they do not significantly influence the solution viscosity. Since the diffusion time is measured over shorter distances and on shorter time scales one can easily determine the relative population of the different fractions 1 and 2. Up to the CAC of SDS 100% of the dye molecules are “free”, i.e. they are not bound to any aggregate. Above the CAC of SDS the population of larger aggregates is increasing and eventually decreases again until almost all dye molecules are bound to freely diffusing MC chains the hydrophobic parts of which are fully decorated with SDS micelles. The relative populations are included in figure 4.7 and 4.9 for fraction 2. The population of fraction 1 can be calculated as the complement to 100%.

## 4. Results and Discussion

**Table 4.1** diffusion coefficients from diffusion time of MC/SDS mixtures.

Con SDS M	No MC		0.25 wt % MC		0.5 wt % MC		1.0 wt % MC	
	fraction 1	fraction 2						
	$\times 10^{-12} \text{ m}^2\text{s}^{-1}$							
$2.0 \times 10^{-3}$	387	--	316	--	432	14.1	243	5.9
$5.0 \times 10^{-3}$	485	121	58	--	231	9.3	49	2.5
$6.0 \times 10^{-3}$	492	95	72	3.6	62	3.0	48	2.3
$8.0 \times 10^{-3}$	131	--	47	4.0	37	2.4	35	2.0
$1.0 \times 10^{-2}$	88	--	40	4.7	29	2.0	38	2.0
$2.0 \times 10^{-2}$	65	--	26	4.0	23	2.1	30	1.0
$2.5 \times 10^{-2}$	60	--	29	7.4	21	2.2	43	1.0
$5.0 \times 10^{-2}$	56	--	37	--	44	8.7	155	1.9
$7.5 \times 10^{-2}$	57	--	39	--	21	--	26	2.3
$1.2 \times 10^{-1}$	51	--	40	--	23	--	138	10.3

From the diffusion times, the diffusion coefficients of SDS micelles and MC/SDS complexes are calculated by using equation 3.19. The diffusion coefficient of SDS micelles at the CMC is  $131 \times 10^{-8} \text{ cm}^2\text{s}^{-1}$  (table 4.1) is close to the literature value of  $96 \times 10^{-8} \text{ cm}^2\text{s}^{-1}$  [109]. The self-diffusion constant of SDS micelles at the CMC as determined with NMR[15] is  $385 \times 10^{-8} \text{ cm}^2\text{s}^{-1}$ . The hydrodynamic radii of the SDS micelles are calculated using the Stokes-Einstein equation (equation 3.20). They coincide with literature value ( $\sim 2.0 \text{ nm}$ ) [109]. Spherical micelles are assumed and the viscosity of the medium is taken as  $0.001 \text{ Pa}\cdot\text{s}$  and temperature  $20 \text{ }^\circ\text{C}$ . The hydrodynamic radii of SDS micelles are included in figure 4.2.

All MC solutions studied here are above the MC overlap concentration. Therefore the MC chains are assumed to be part of an MC/SDS network. We do not expect isolated aggregates and the calculation of hydrodynamic radii seems rather meaningless at concentrations below the EOA.

## 4. Results and Discussion

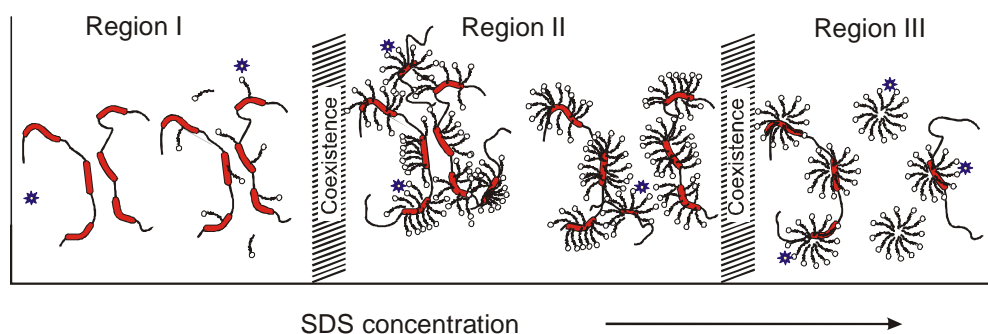


**Figure 4.18** Schematic diagram explaining the MC/SDS complex formation with increasing concentration of SDS. The broader regions in the polymer chains are considered as hydrophobic regions and the remaining part as hydrophilic regions. In Region I, SDS molecules are approaching hydrophobic regions of MC. Maximum aggregation and the polyelectrolyte behavior of the networks is expected in Region II. In Region III the polymer chains are saturated completely with SDS micelles and the network is destroyed. Only selected hydrophobic regions are shown in Region III for clarity.

Above the EOA concentration we can use the Stokes-Einstein equation (equation 3.20) to calculate apparent hydrodynamic radii of freely diffusing MC/SDS aggregates. If we assume a spherical shape of the aggregates and a viscosity of 0.001 Pa.s we find apparent hydrodynamic radii of some 20, 10 and 5 nm for 1.0, 0.5 and 0.25 wt % MC/SDS compositions, respectively. At 1.0 wt % MC we observe a second, slowly diffusing aggregate with an apparent hydrodynamic radius of  $\sim 100$  nm. We note that the solvent viscosity rather than the solution viscosity was used to calculate the hydrodynamic radii. The smaller aggregates are expected to diffuse rather freely in the presence of an immobilized ‘network’ of MC/ SDS complexes. We note that this effect remains unobservable by macroscopic experiments.

We may define a CAC from FCS experiments as the onset of increasing diffusion time. These CAC results happen to exactly match with the results of

#### 4. Results and Discussion

macroscopic techniques. In line with Diamant's theoretical predictions [48], the value of the CAC is lower but close to the CMC and the CAC does not change significantly with the MC concentration.

Our findings can be summarized by a model reported earlier for hydrophobically modified cellulose ethers/SDS systems [45] (figure 4.18). We expect three regions referred to as region I, II and III, respectively. At low SDS concentration (region I) we expect some hydrophobic interaction between the hydrophobic regions on the MC chains with barely any influence of the surfactant. In region II complexes are formed between SDS and the hydrophobic regions of MC leading to a significant strengthening of the physical network. As the dye molecules are known to bind to the SDS aggregates, we observe a fraction of dye molecules which diffuse considerably slower than both the free dye molecules and dye molecules bound to isolated SDS micelles. Finally, at high enough SDS concentrations (region III) the hydrophobic regions of the MC molecules are saturated completely by SDS molecules and the physical network collapse. Consequently, the observed diffusion times decrease considerably, however the final value is found to be longer than the one characteristic of free dye molecules. Thus the macroscopic viscosity first increases from region I to region II and finally (region III) drops to a value lower than in region I as even the weak physical network induced by hydrophobic interactions between MC chains are collapsed.

### 4.2 Temperature dependent studies

Temperature dependent measurements were done for 1 wt % MC with various SDS concentration solutions. The effect of increasing temperature on the structure and dynamics of MC/SDS mixtures has been investigated by FCS, rheology and turbidity.

#### 4.2.1 Fluorescence correlation spectroscopy

The behavior of MC/SDS changes by varying temperatures. To investigate this behavior in detail, the influence or changes in diffusion time of dye alone, and with MC or SDS are verified first. Thus, selected  $c_{\text{SDS}} = 2.0 \times 10^{-3}$ ,  $8.0 \times 10^{-3}$ ,  $2.0 \times 10^{-2}$ ,  $5.0 \times 10^{-2}$ , and  $2.0 \times 10^{-1}$  M which are associated below CAC, around CMC, at maximum aggregation, at EOA and after EOA respectively. These are connected with different regions of MC/SDS systems at room temperature. The results from the effect of temperature between 25 °C to 55 °C are summarized in figure 4.19a for SDS solutions. While fitting FCS data, the measurements resulting triplet fraction of less than 20 % are only considered [95]. For the understanding of the changes in diffusion time of dye with SDS, dye alone is also given. Except  $c_{\text{SDS}} = 8.0 \times 10^{-3}$  M and  $2.0 \times 10^{-2}$  M all other concentrations of SDS show the decreasing trend in the diffusion of dye when increasing the temperature from 25 °C to 55 °C. Diffusion time decreases from 125 to 100  $\mu\text{s}$  when temperature is increased from 25 °C to 35 °C for  $c_{\text{SDS}} = 8.0 \times 10^{-3}$  M. After 45 °C, the diffusion time increases. There is no characteristic difference between the diffusion time of dye alone and with  $c_{\text{SDS}} = 2.0 \times 10^{-3}$  M. By using the viscosity of the medium at different temperature hydrodynamic radii are calculated (figure 4.19b). The  $R_{\text{H},i}$  values almost remain constant until 40 °C.

## 4. Results and Discussion

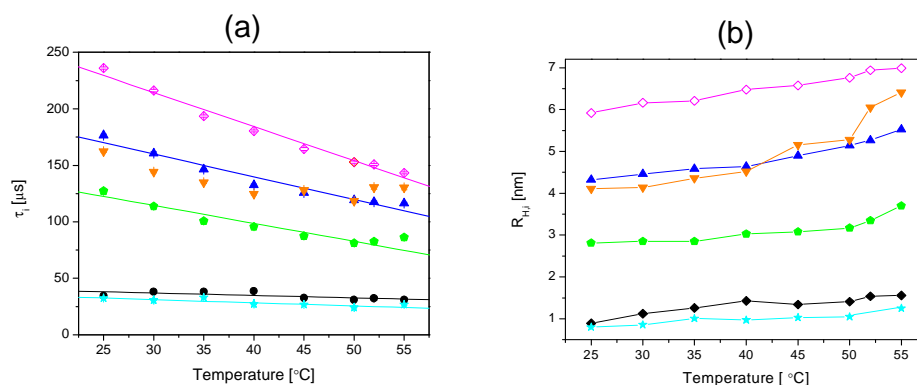


**Figure 4.19** (a) Diffusion time of  $c_{\text{dye}}=10^{-8} \text{ M}$  alone (★ cyan) and with  $c_{\text{SDS}} = 2.0 \times 10^{-3} \text{ M}$  (◆ black),  $8.0 \times 10^{-3} \text{ M}$  (● green),  $2.0 \times 10^{-2} \text{ M}$  (▼ orange),  $5.0 \times 10^{-2} \text{ M}$  (▲ blue), and  $2.0 \times 10^{-1} \text{ M}$  (◇ magenta) at various temperatures. All results are from single-fraction fit. The diffusion time of pure dye and  $c_{\text{SDS}} = 2.0 \times 10^{-3} \text{ M}$  is almost constant irrespective of temperature. Decreasing tendency of diffusion time is observed with all  $c_{\text{SDS}}$  solutions. (b) The hydrodynamic radii of SDS solutions are shown in different temperatures. The changes in  $R_{\text{H},i}$  is significant after 40 °C for  $c_{\text{SDS}} = 8.0 \times 10^{-3} \text{ M}$  (● green) and  $2.0 \times 10^{-2} \text{ M}$  (▼ orange). These results are calculated from single-particle data.

Increasing tendency in  $R_{\text{H},i}$  is predominant for  $c_{\text{SDS}} = 8.0 \times 10^{-3} \text{ M}$  and  $2.0 \times 10^{-2} \text{ M}$ . The change in diffusion time of dye with MC alone is also checked at various temperatures (figure 4.20). The mobility of dye in MC solution decreases to a smaller value until 45 °C. But an increase in diffusion time is observed when temperature increases from 50 °C upwards.

With the surfactant solutions, dye shows decrease in diffusion time when temperature increases. Beyond CMC, we believe that dye is labeled with micelles electrostatically. To calculate the hydrodynamic radius Stokes-Einstein equation is used (equation 3.20). The temperature induced  $R_{\text{H},i}$  infers the changes in the size and assembly of SDS micelles.

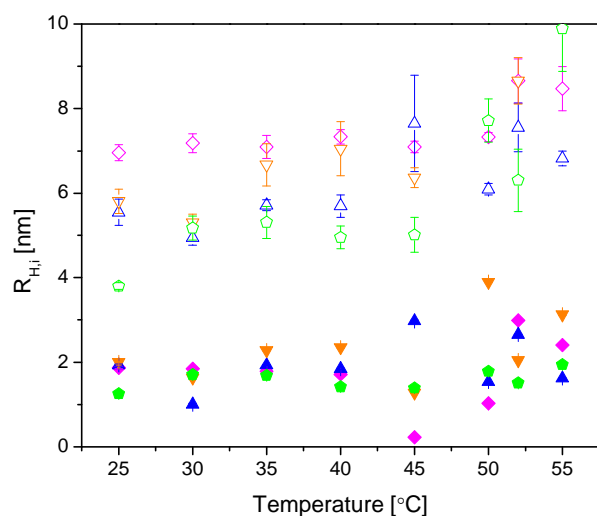


**Figure 4.20** The hydrodynamic radii of SDS solutions are shown in different temperatures. These results are calculated from two-fraction fit data. The symbols are same as figure 4.19. The fraction 1 (closed symbol) and fraction 2 (open symbols) are shown for SDS concentration and temperature. The fraction 1 stays below  $\sim 2$  nm.

At 55 °C all the surfactant solutions above CMC are forming the micelle with higher  $R_{H,i}$ . The increase in temperature is unfavorable for some of SDS monomers which are attached previously with SDS micelles [113]. Therefore the aggregation number drastically reduces at higher temperature [114, 115]. Obviously, SDS micelles are smaller in size at higher temperatures, which would contradict our observations. In order to verify this further, two-fraction fit performed for the same data and results are given in figure 4.20. The fraction 1 corresponds to micelle size approximately 2nm. The per cent of fraction associated with fraction 1 is approximately 50 in all temperatures at CMC. These values reduce with increasing concentration of SDS. At  $c_{SDS} = 2.0 \times 10^{-1}$  M per cent of fraction 1 is approximately 85. Therefore the

## 4. Results and Discussion

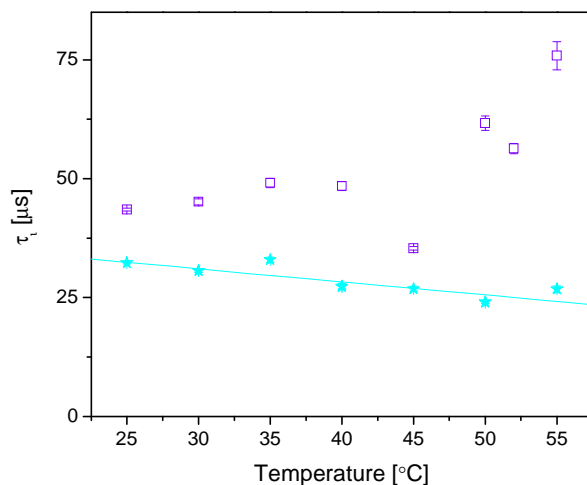


**Figure 4.21** The change in diffusion time of  $c_{\text{dye}}=10^{-8}$  M alone (★ cyan) and with 1 wt % MC (□ violet) is shown. There is a increase in MC diffusion time from 50 °C (gelation temperature). The results are drawn from single-particle fit.

contribution of bigger micelles is less compared to the normal micelles with  $R_{H,i} \sim 2$  nm at very high SDS concentration. FCS is used to follow the dynamics of SDS micelles between bigger and smaller sizes. We note that the increasing per cent of fast diffusing micelles for highest SDS concentration attributes the decreasing aggregation number found in literature at higher temperature. The diffusion time of dye in MC solution increases beyond 50 °C (figure 4.21). Since dye is not covalently attached to MC chains, the mobility of dye molecules in MC solutions does not reach very high value during gelation. Though the environment is highly crowded after gelation, the changes in diffusion time do not experience its macroviscosity. The viscosity experienced by the dye would reach the macroscopic value only when the size of the tracers exceeded the typical size of the water channel (it would correspond roughly to the correlation length of polymer) [116].

## 4. Results and Discussion

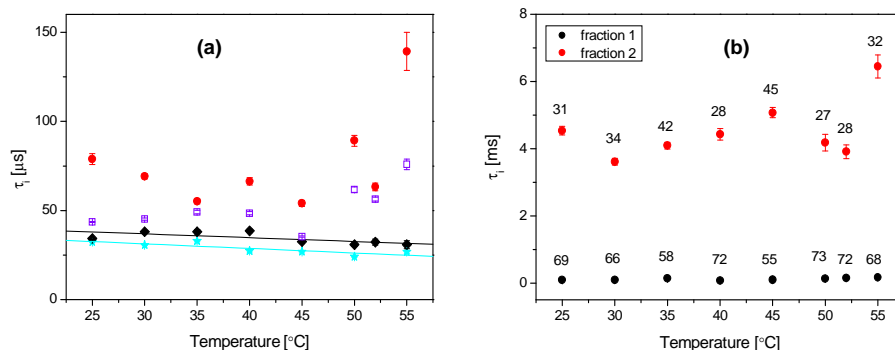


**Figure 4.22** a) Diffusion time of  $c_{\text{dye}}=10^{-8}$  M alone (★cyan) and with  $c_{\text{SDS}}=2.0 \times 10^{-3}$  M (◆black), 1 wt % MC (□violet), and MC/SDS mixture (●red) at various temperatures. All results are from single-fraction fit. No remarkable changes in the diffusion times of MC/SDS mixtures. b) Diffusion time of dye in  $c_{\text{SDS}}=8.0 \times 10^{-3}$  M and 1 wt % MC mixture, and at various temperatures. All results are from two-fraction fit. The increased diffusion time is observed at 55 °C. The per cent of dye fraction associated with fraction 2 varies between 30 and 45.

But the diffusion time obtained from the molecular level coincides with the macroscopic changes. We now discuss the changes in MC/SDS mixtures with varying temperature. Before CAC  $c_{\text{SDS}}=2.0 \times 10^{-3}$  M and 1 wt % MC mixture shows the very small changes in the diffusion time of dye (figure 4.22a). For some temperature values, the diffusion time is comparable with the diffusion time of MC solution alone. Dye molecules do not differ in the diffusion time of dye and in SDS solution alone. Therefore the gelation of MC with  $c_{\text{SDS}}=2.0 \times 10^{-3}$  M does not show significant changes in the diffusion time of dye in FCS measurements. The increase in diffusion time of dye is clearly observed for MC with  $c_{\text{SDS}}=8.0 \times 10^{-3}$  M. Diffusion time of fraction 2 increases up to 6.5 ms at 55 °C. Among the two fractions the slow diffusing fractions (fraction 2) and fast diffusing fraction (fraction 1) attributes to MC/SDS

## 4. Results and Discussion

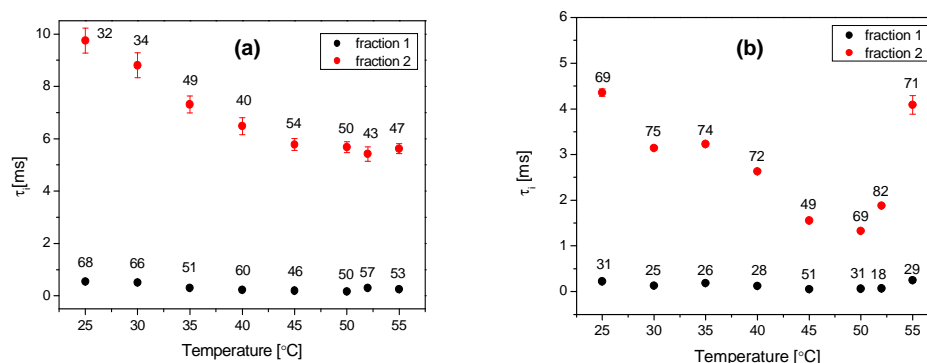


**Figure 4.23** a) FCS measurements of 1 wt% MC and  $c_{\text{SDS}} = 2.0 \times 10^{-2} \text{ M}$  at various temperatures. Results are drawn from two-fraction fit. Diffusion time decreases with increasing temperature until 45 °C without any further characteristic changes beyond. Fraction 1 attributes the smaller size of MC/SDS aggregates. The numerical numbers indicate the per cent of relative fractions b) FCS measurements of 1 wt% MC and  $c_{\text{SDS}} = 5.0 \times 10^{-2} \text{ M}$  at various temperatures. Diffusion time decreases until 50 °C and starts increasing attaining the initial value.

aggregates and SDS micelles respectively. With increasing temperature the gel formation develops slowing the mobility of dye molecules even further.

The maximum aggregates form at  $c_{\text{SDS}} = 2.0 \times 10^{-2} \text{ M}$  with 1 wt MC. By changing the temperature, the diffusion time of fraction 2 is reduced by 50 % at 55 °C (figure 4.23a). Until 45 °C, the diffusion time gradually decreases while further increase in temperature does not induce any further changes in diffusion time. The diffusion time of fraction 1 decreases from 540  $\mu\text{s}$  (25 °C) to 165  $\mu\text{s}$  (50 °C). When temperature further increases the diffusion time increases to 300  $\mu\text{s}$  and 250  $\mu\text{s}$  for 52 °C and 55 °C respectively. Diffusion time of fraction 1 is not comparable with SDS alone and it is attributed to the smaller size of MC/SDS aggregates. The per cent of fraction 2 is nearly 50 after 45 °C. Almost the same behavior like previous is observed with  $c_{\text{SDS}} = 5.0 \times 10^{-2} \text{ M}$  and MC mixtures. But after 50 °C the diffusion time of fraction 2

## 4. Results and Discussion

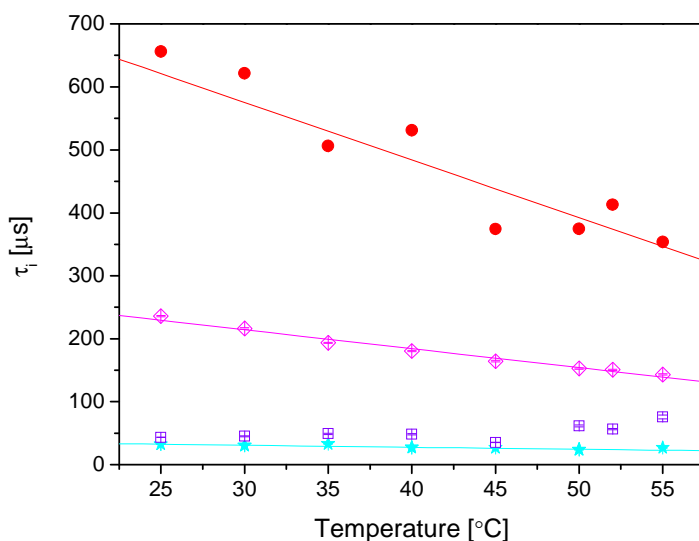


**Figure 4.24** Diffusion time of  $c_{\text{dye}}=10^{-8}$  M alone (★cyan) and with  $c_{\text{SDS}} = 2.0 \times 10^{-1}$  M (◇magenta), 1 wt % MC (□violet), and MC/SDS mixture (●red) at various temperatures. All results are from single-fraction fit. Decreasing tendency of diffusion time is observed with increasing temperature.

increases and attains the diffusion time of room temperature. The diffusion time of fraction 1 is almost in line with SDS alone until 40 °C but in-between 45 °C and 52 °C, it almost two times less than the diffusion time of SDS alone.

At very high concentration  $c_{\text{SDS}} = 2.0 \times 10^{-1}$  M with 1 wt % MC, temperature changes are studied and results are shown in figure 4.24. The data best fit with single-fraction fit. The initial diffusion time 650  $\mu\text{s}$  of dye in MC/SDS mixtures at 25 °C decreases to 350  $\mu\text{s}$  when temperature rises to 55 °C. Even at 55 °C the diffusion time does not equal that of SDS or dye alone. This indicates that the dye is firmly attached to MC/SDS aggregates. Gelation of MC occurs from hydrophobic interactions between MC chains. Since all hydrophobic parts are saturated with SDS micelles, there are no free

## 4. Results and Discussion

hydrophobic parts available in MC chains. Therefore gelation is not observed for MC with very high concentration of SDS.

### 4.2.2 Rheology

Conventional rheometers like Rheometrics RFS II requires more amount of sample, very long measurement time and limited to frequency range (0.01 – 15 Hz). Moreover it has evaporation problems at higher temperatures. Therefore the gelation of MC was analyzed by PAV rheological method. Since it covers the wide frequency range of 0.1 – 3000 Hz a complete study of MC gelation is possible. Gelation of MC is studied before proceeding with the study of MC/SDS mixtures at various temperatures. The elastic modulus ( $G'$ ) and viscous modulus ( $G''$ ) of MC at different temperatures are shown in figure 4.25. After 50 °C, the  $G'$  increases with increasing temperature. The cross over point between  $G'$  and  $G''$  also shifted to higher frequency when temperature increases up to 60 °C. We measured every 30 minutes until the temperature of 45 °C was reached. Then we took measurements only every two hours until 60 °C. When the system is allowed for long time, kinetic effects are possible at higher temperatures. This is similar with the report of Desbrieres et al [78]. Gelation occurs above 50 °C displaying increasing  $G'$  value while at temperatures below 45 °C we observed the characteristic decrease of  $G'$  values. Almost the same behavior is observed for  $c_{\text{SDS}} = 2.0 \times 10^{-3} \text{ M}$  and  $c_{\text{SDS}} = 2.0 \times 10^{-2} \text{ M}$  with 1 wt % MC until 45 °C. But above 45 °C the elastic modulus increases dramatically. With respect to MC, elastic modulus of  $c_{\text{SDS}} = 2.0 \times 10^{-3} \text{ M}$  and 1 wt % MC mixture increased by one order magnitude for 52, 54, 55 °C and by four orders magnitude for 60 °C (figure 4.26). Adding small amount of SDS promotes the gel intensity.

## 4. Results and Discussion

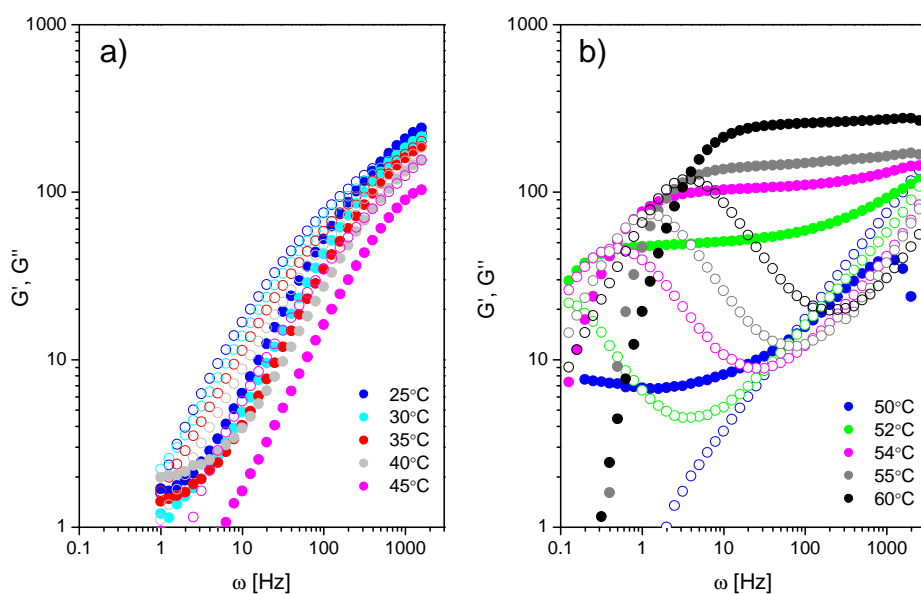


**Figure 4.25** Elastic (full symbols) and loss modulus (open symbols) of 1.0 wt % MC at different temperatures measured with PAV.

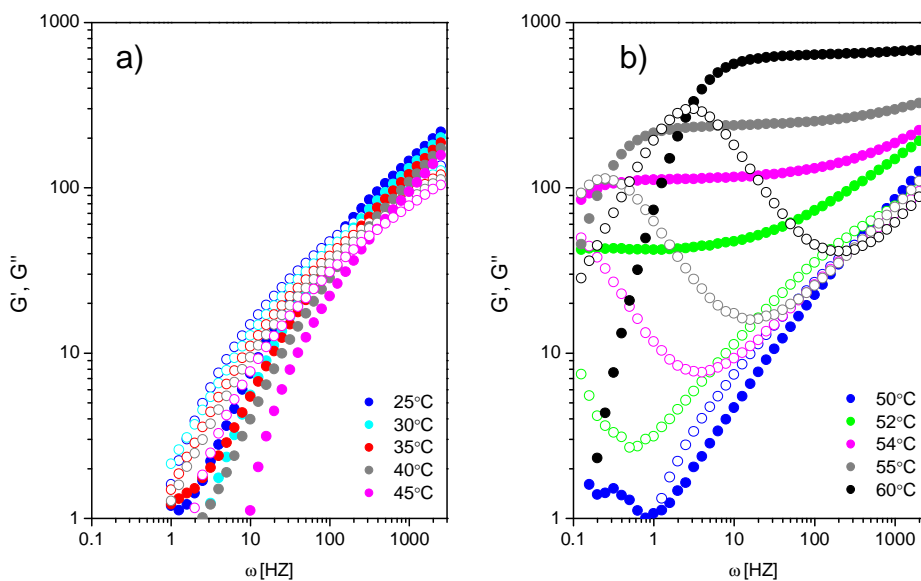


**Figure 4.26** Elastic (full symbols) and loss modulus (open symbols) of  $c_{\text{SDS}} = 2.0 \times 10^{-3} \text{ M}$  and 1.0 wt % MC mixture at different temperatures measured with PAV. Elastic modulus increased one order magnitude for 52, 54, 55 °C and four orders magnitude for 60 °C compared to the 1 wt % MC alone. Addition of small amount of SDS enhances the gelation.

#### 4. Results and Discussion

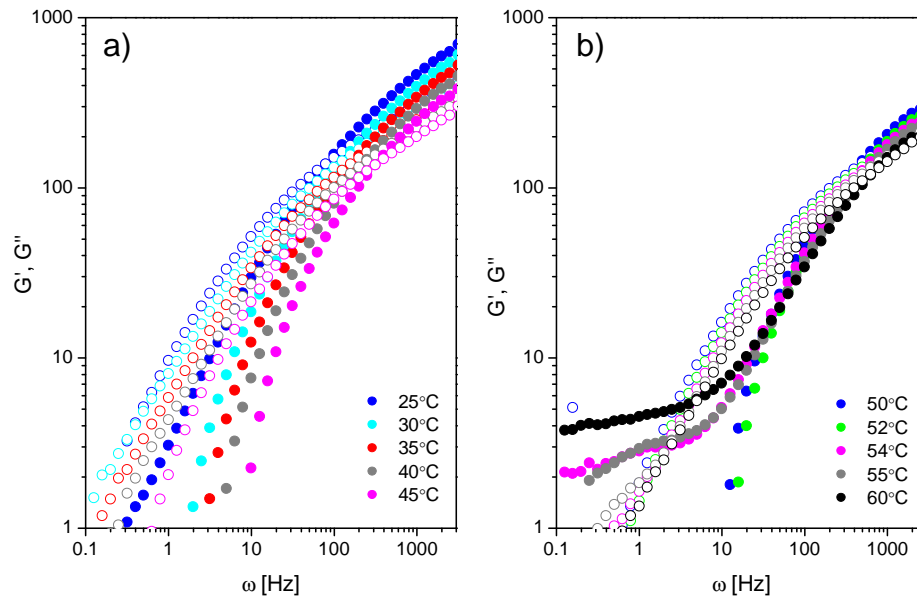


**Figure 4.27** Elastic (full symbols) and loss modulus (open symbols) of  $c_{\text{SDS}} = 2.0 \times 10^{-2} \text{ M}$  and 1.0 wt % MC mixture at different temperatures measured with PAV. Elastic modulus is not shifted to higher value when temperature increases. It shows the absence of gel formation.

The availability of water molecules for MC chains decreases when SDS monomer starts attracting water molecules. This results in intense gel via stabilization of hydrophobic associations between MC chains. The  $G'$  and  $G''$  values of mixtures of  $c_{\text{SDS}} = 2.0 \times 10^{-2} \text{ M}$  and 1 wt % MC are plotted in figure 4.26. There are not any changes in elastic modulus  $G'$  until 52 °C. Even after, there are no significant changes in  $G'$  values compared to MC alone. The temperatures below 45 °C show the decrease in viscosity and the activation energy connected with non associative chains. The gelation of MC and with  $c_{\text{SDS}} = 2.0 \times 10^{-3} \text{ M}$  is predominant between 50-60 °C. It infers the possibility of extensive hydrophobic association. At the same time association time decreases for  $c_{\text{SDS}} = 2.0 \times 10^{-3} \text{ M}$  and 1 wt % MC system compared to MC alone.

## 4. Results and Discussion

The mixture  $c_{\text{SDS}} = 2.0 \times 10^{-2}$  M and 1 wt % MC shows maximum aggregation and almost all hydrophobic areas are occupied with SDS. Hence the gelation formation is not possible with the temperatures applied in our studies (figure 4.27). It would only start at very high temperatures then the SDS cages may be removed from the hydrophobic areas of MC chains and gelation becomes possible.

### 4.2.3 Turbidity

In order to visualize the gel formation, MC and MC/SDS solutions were kept in sealed water bath and temperature was varied to observe the changes. The photographs were taken at different time intervals. The photographs which were taken after 2 hours at each temperature are shown in figure 4.28a. The visual inspection helps to observe the turbid changes of the MC/SDS solutions at different temperatures. The phase diagram of MC solution with the additives SDS is shown in figure 4.28b. The gelation starts at 50 °C for 1 wt % MC and before CMC for MC/SDS mixtures. In order to understand the turbidity quantitatively, turbidity measurements were done. Gelation of MC starts at 50 °C. Decreasing  $U/U_0$  shows a more intense gelation reaching its top at 60 °C.

The turbidity changes are presented for 1 wt % MC with  $c_{\text{SDS}} = 2.0 \times 10^{-3}$  M in figure 4.30. There is no characteristic huge change in the values of  $U/U_0$  until 50 °C. The deep decrease in  $U/U_0$  value at 50 °C shows the intense gel formation. Since the intensity of gelation reaches its top at 60 °C little light is transmitted so the value gets close to the resolution of the instrument not allowing any further measurements. The turbidity curve supports the rheology data which is shown in figure 4.26b.

#### 4. Results and Discussion

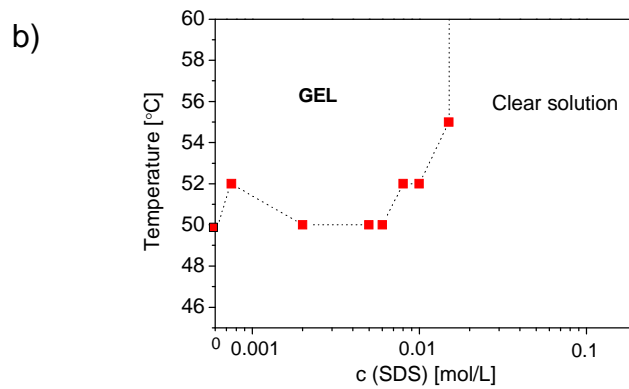
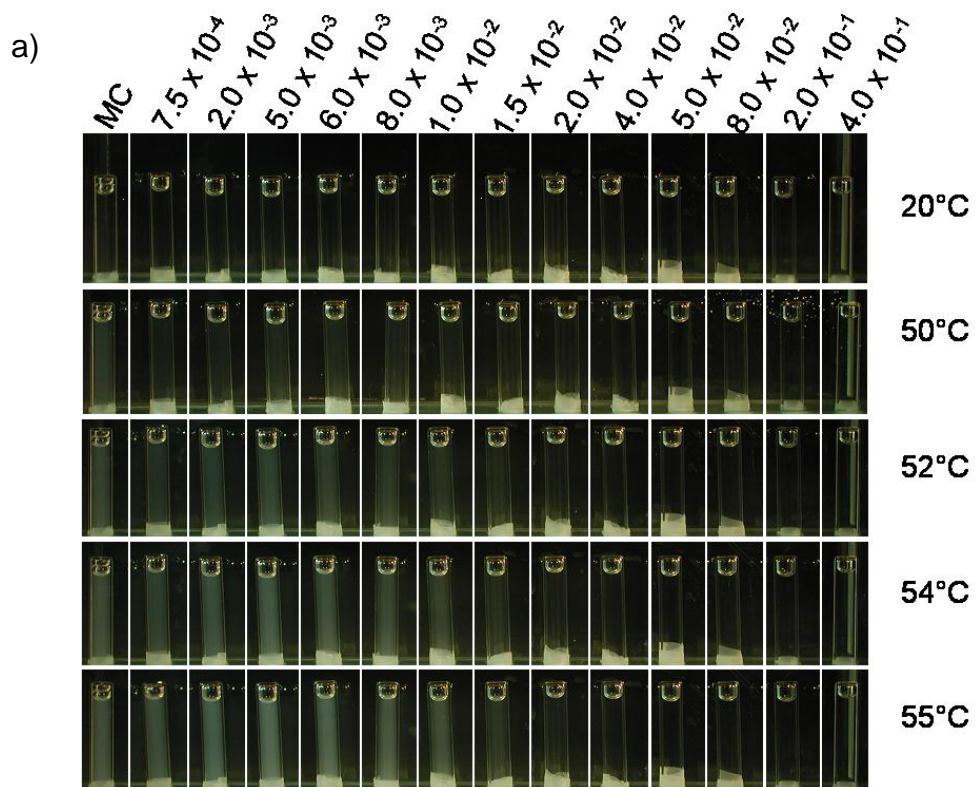


**Figure 4.28** Visual inspection of 1 wt % MC and SDS mixtures at different temperatures. Addition of small amount of SDS with MC promotes the gelation. No gelation is observed with the maximum aggregate forming MC/SDS mixture ( $c_{MC}=1\text{wt \%}$  &  $c_{SDS}=2.0 \times 10^{-2}\text{ M}$ ). The same is observed with high concentrations of SDS and MC mixtures. b) Phase diagram of 1 wt % MC with SDS.

## 4. Results and Discussion

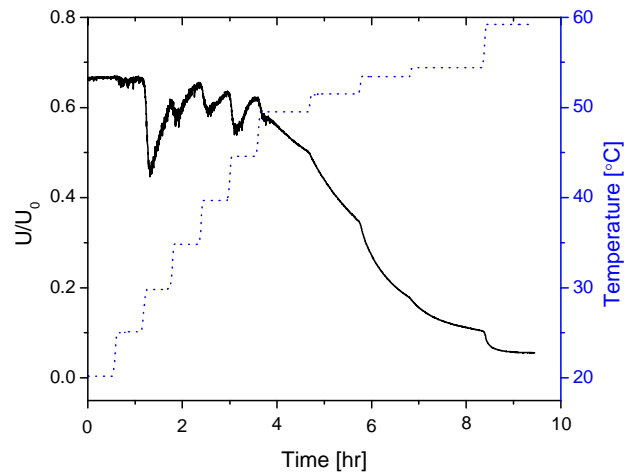


**Figure 4.29** Turbidity measurement of 1 wt % MC alone (—). Gelation starts at 50 °C and more turbidity is observed at 55 °C. Temperature profile (....) is given in y-scale (blue curve).

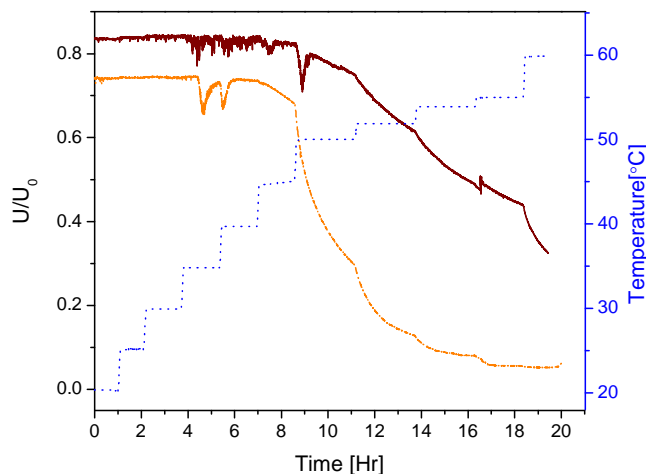


**Figure 4.30** Turbidity curve for the mixtures of  $c_{\text{SDS}} = 2.0 \times 10^{-2} \text{ M}$  and 1 wt % MC (— wine),  $c_{\text{SDS}} = 2.0 \times 10^{-3} \text{ M}$  and 1 wt % MC (--- orange). The temperature profile (....) is shown in blue in color. The deep decrease in  $U/U_0$  of orange curve shows the intense gel formation. With minimum amount of SDS more gelation is observed for MC. Beyond 52 °C it crosses the resolution of the turbidity instrument. Therefore the changes are not observed well.

#### 4. Results and Discussion

Increased elastic modulus and decreased  $U/U_0$  give some direct information about the intense gel formation of MC with the addition of very small amounts of SDS. The next turbidity curve focuses on the mixture of 1 wt % MC with  $c_{SDS} = 2.0 \times 10^{-2}$  M which shows maximum aggregation at room temperature. There is a slight decrease in  $U/U_0$  value beyond 50 °C and the value decreases steadily with increasing temperature. The final value is not close to zero. FCS measurements show that the decreasing diffusion of time dye, correlates with the turbidity curve. When temperature is increased for the mixture of  $c_{SDS} = 2.0 \times 10^{-1}$  M and 1 wt %MC, the solution gets clearer. Increase in temperature promotes the transmission of light and leads to higher  $U/U_0$  value. The turbidity curve shows no turbid formation with increasing temperature in figure 4.31. The combined view of turbidity curve for MC and with SDS solution is show in figure 4.32.

The effect of temperature on MC/SDS mixtures are studied with FCS, rheology and turbidity measurements. The effect of temperature on individual components of MC/SDS mixtures is studied by FCS before analyzing the MC/SDS mixtures. The diffusion time of dye decreases with increasing temperatures. The same behavior is observed for SDS solutions, too. The dynamics of SDS micelles between big and small sizes is predominant after CMC at various temperatures. Microscopic level changes of MC gelation coincide with the macroscopic rheological studies.

We discuss the above results based on the schematic diagram figure 4.18. Region I focuses on the strategy of before CAC. The hydrophobic regions of MC come close by eliminating surrounded water molecules to form association when temperature increases. With the addition of small amounts of SDS, the gel intensity increases.

## 4. Results and Discussion

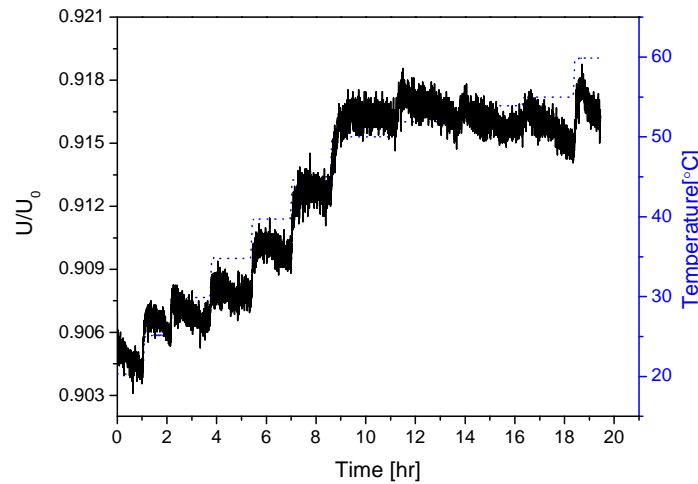


**Figure 4.31** Turbidity curve for the mixtures of  $c_{\text{SDS}} = 2.0 \times 10^{-1} \text{ M}$  and 1 wt %MC. The increasing  $U/U_0$  value with increasing temperature shows the clear solution formation. It accords with FCS and visual temperature inspection measurements. Temperature profile (.....) is shown in blue curve.

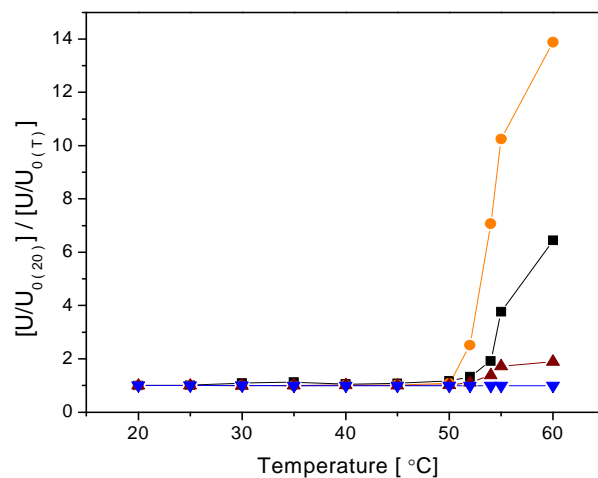


**Figure 4.32** Selected data of Turbidity curve between 20 and 60 °C for the mixtures of  $c_{\text{SDS}} = \text{no SDS}$  (■)  $2.0 \times 10^{-3} \text{ M}$  (●),  $2.0 \times 10^{-2} \text{ M}$  (▲),  $2.0 \times 10^{-1} \text{ M}$  (▼), with 1 wt %MC. There are no remarkable changes in  $[U/U_{0(20)}]/[U/U_{0(T)}]$  values until 50 °C. The gelation changes notably directly beyond 50 °C. The MC/SDS belong to region III doesn't show gelation.

#### 4. Results and Discussion

We note that during the hydrophobic association process of MC, SDS monomers are attracted towards hydrophobic regions and other cross linked net works. Therefore the intensity of gel grows with the addition of very small amounts of SDS to MC. This is effectively supported by the rheology and turbidity measurements. Wang et al claim that the mechanism is based on the modification of water's hydrophobicity by SDS [90]. The region II covers the concentration between CAC and EOA.

The diffusion time of dye in the mixture of  $c_{\text{SDS}} = 8.0 \times 10^{-3}$  M and 1 wt % MC increases high at 55 °C (figure 4.22b). But at the maximum aggregation, linearly decreasing diffusion time is observed until 50 °C and then remains constant in diffusion time value. At EOA, the same behavior is observed until 50 °C and then heads for the initial diffusion time value with increasing temperature. In this region II, the hydrophobic areas of MC are shielded with SDS micelles. With increasing temperature, gelation is possible only at temperatures higher than the MC gelation temperature. Hydrophobic areas of MC are highly shielded for highly aggregated MC/SDS (region II, figure 4.18). Therefore it requires more heat to move away the SDS cages from the hydrophobic zones. Thus the gelation point shifts to higher temperature when the charge of SDS in a mixture of MC/SDS is increased. The region III focuses beyond EOA. At very high concentrations, the highly SDS occupied MC chains, looses the SDS cages from the MC chains at increasing temperature. Therefore linearly decreasing diffusion time is observed. Though the increase in temperature is required to knock out the SDS micelles from MC chains gelation is not observed before 55 °C. This may be due to the high population of single SDS micelles around the MC chains. It may prevent the hydrophobic association between MC chains.

# 5

## Summary

The interactions between the anionic surfactant sodium dodecyl sulfate (SDS) and a hydrophobically modified non ionic polymer, methylcellulose (MC), have been investigated in aqueous solution by fluorescence correlation spectroscopy (FCS), cryo-TEM, turbidity and rheology. The micelle formation of SDS is followed with cationic Cresyl Violet perchlorate dye via diffusion time. The opposite polarity of dye is suitable to aggregate with micelles and act as a labeled dye. Two major studies focused in the research work are concentration dependent and temperature measurements to understand the interactions of MC/SDS aggregates. The concentration of SDS is varied to a wide range in the mixture by fixing the concentration of MC. By this approach, the changes in the aggregation and the conformations of MC chains are being studied. Similar studies have been repeated at various temperatures in the range of 25-60 °C to understand the changes in gelation properties of MC. To understand the results of the above mentioned studies of MC/SDS, the behavior of MC and SDS is analyzed individually. In this line, the critical micelle concentration (CMC) of SDS has found with FCS

## 5. Summary

measurements is in good agreement with literature value obtained from 'classical methods'. The two-fraction fit confirms the pre-micellar effect and is explained in detail. The hydrodynamic radius of SDS micelle around CMC is found to be  $\sim 2.0$  nm. The shape of the autocorrelation curves and number of dye particles in the focal volume also supports to follow the SDS micelle. When varying the concentration of MC, slight changes in the diffusion time of dye are observed. The MC/SDS mixtures show huge increase in the diffusion time compared to the individual components MC and SDS. At constant MC concentration the diffusion time of single aggregates increases gradually up to a certain SDS concentration and decreases to a minimum when the SDS concentration is further increased. This behavior coincides with the behavior of the zero shear viscosity. Two different fractions viz fast diffusing fraction of dye molecule along with the larger aggregates are observed in between the critical aggregation concentration (CAC) and end of aggregation (EOA). FCS is used to follow the dynamics of single aggregates of the different populations. At very high concentration of SDS, MC/SDS mixtures show the worm like structure in cryoTEM measurements. A model is proposed based on FCS, cryoTEM and rheology measurements to explain the effect of surfactant concentration on polymer conformation and aggregation size.

While varying the temperature, MC/SDS mixtures show changes in the diffusion time only at room temperature. MC has the tendency to form thermoreversible gel upon heated above  $50$  °C. The presence of SDS alter the intensity of MC gelation. Before CAC, the addition of SDS promotes the MC gelation. The MC-SDS mixture giving maximum aggregation at room temperature shows decreasing tendency in its diffusion time upon increasing the temperature.

## 5. Summary

We have shown that a single molecule technique like FCS can be successfully used to follow the dynamics of single aggregates in polymer/surfactant systems. We can identify single inter-chain aggregates, the hydrodynamic size of which changes in a characteristic way as a function of surfactant concentration. These changes are reflected in the behavior of the macroscopic viscosity. The present results show the large potential of single molecule experiments as a complement to the classical macroscopic techniques for a characterization of polymer solutions and polymer/surfactant mixtures. In addition to the large aggregates dominating the macroscopic rheology of the system, the single molecule approach can identify considerably faster aggregates as well, which are not accessible by conventional techniques. Thereby the single molecule approach is able to monitor what may be called a micro viscosity of the solution, i.e. the potential of small aggregates to diffuse rather fast through a network of slowly diffusing chains. This study also shows that the diffusion behavior of polymer-surfactant systems can be followed by FCS without covalent labeling with dye molecules. Moreover, FCS is only sensitive to the dye concentration; therefore these investigations can be applied over a wide range of polymer concentrations.

## 5. Summary

# 6

## Zusammenfassung

Die Wechselwirkungen zwischen dem anionischen Tensid Natriumdodecylsulfat (SDS) und einem hydrophob modifizierten, nicht-ionischen Polymer, Methylcellulose (MC), wurde in wäßriger Lösung durch Fluoreszenzkorrelationsspektroskopie (FCS), Kryotransmissionselektronenmikroskopie (Kryo-TEM), Trübung und Rheologie untersucht. Die Bildung von SDS-Mizellen wurde über die Diffusionszeit durch den kationischen Farbstoff Kresylviolett-perchlorat verfolgt. Durch die gegensätzliche Polarität des Farbstoffs kann dieser mit den Mizellen aggregieren und als Fluoreszenz-Markierung dienen. Diese Arbeit konzentriert sich im Wesentlichen auf konzentrations- und temperaturabhängige Messungen, um die Wechselwirkungen in den MC-SDS-Aggregaten zu verstehen. Dabei wurde die Konzentration von SDS in einem großen Bereich variiert, während die MC-Konzentration konstant gehalten wurde. So wurden die Aggregation und die Konformation der MC-Ketten studiert. Weitere Untersuchungen wurden bei verschiedenen

## 6. Zusammenfassung

Temperaturen zwischen 25 °C und 60 °C durchgeführt, um Unterschiede in den Gelierungseigenschaften der Methylcellulose festzustellen.

Zur Erklärung der Ergebnisse der oben genannten Untersuchungen wurde das Verhalten von MC und SDS getrennt analysiert. So wurde herausgefunden, dass die kritische Mizellbildungskonzentration (CMC) von SDS, die durch FCS-Messungen bestimmt wurde, gut mit dem Literaturwert übereinstimmt, der mit klassischen Methoden bestimmt wurde. Das Auftreten von Aggregaten vor Erreichen der CMC (pre-micellar effect) konnte mit einem Modell, das zwei Fraktionen berücksichtigt, und dessen Anpassung an die Korrelationskurve bestätigt und detailliert erklärt werden. Der hydrodynamische Radius der SDS-Mizellen wurde zu 2,0 nm bestimmt. Durch die Form der Autokorrelationskurve und die Anzahl der Farbstoffteilchen im konfokalen Volumen wurde die Bildung von Mizellen belegt. Wird die Konzentration der MC variiert, konnten geringe Änderungen in der Diffusionszeit beobachtet werden. Mischungen von MC mit SDS zeigten einen starken Anstieg in der Diffusionszeit verglichen mit den Lösungen der einzelnen Komponenten. Bei konstanter MC-Konzentration stieg die Diffusionszeit von einzelnen Aggregaten bis zu einer bestimmten SDS-Konzentration beständig an und sank dann auf ein Minimum, wenn die SDS-Konzentration weiter erhöht wurde. Diese Beobachtung stimmt mit der Null-Viskosität (zero-shear viscosity) überein. Es konnten zwei verschiedene Fraktionen, eine schnell diffundierende Fraktion von Farbstoffmolekülen zusammen mit größeren Aggregaten, die zwischen der kritischen Aggregationskonzentration (CAC) und dem Ende der Aggregation (EOA) auftreten, beobachtet werden. Die Dynamik von einzelnen Aggregaten der verschiedenen Populationen wurde mit FCS beobachtet. Bei sehr hohen Konzentrationen von SDS zeigten MC-SDS-Mischungen in der Kryo-TEM

## 6. Zusammenfassung

wurmartige Strukturen. Um den Effekt der Tensid-Konzentration auf die Polymerkonformation und die Größe der Aggregate zu erklären, wurde ein Model vorgeschlagen, das auf FCS, Kryo-TEM und Rheologie-Messungen beruht.

Wird die Temperatur verändert, zeigten die MC-SDS-Mischungen Änderungen in der Diffusionszeit. Methylcellulose hat die Tendenz, bei Temperaturen über 50 °C thermoreversible Gele zu bilden. In Anwesenheit von SDS ändert sich die Stärke der MC-Gelierung. Das Hinzufügen von SDS vor der CAC förderte die MC-Gelierung. Die MC-SDS-Mischung, die bei Raumtemperatur am stärksten aggregiert ist, zeigte mit ansteigender Temperatur abnehmende Diffusionszeit.

Es wird gezeigt, dass mit einer Einzelmolekültechnik wie FCS die Dynamik von einzelnen Aggregaten in Polymer-Tensid-Systemen erfolgreich verfolgt werden kann. Einzelne Aggregate zwischen verschiedenen Polymerketten können identifiziert werden, deren hydrodynamische Größe sich auf charakteristische Weise als Funktion der Tensid-Konzentration ändert. Diese Änderungen spiegeln das Verhalten der makroskopischen Viskosität wieder. Die vorliegenden Ergebnisse zeigen das große Potential von Einzelmolekülexperimenten als Ergänzung zu klassischen Techniken zur makroskopischen Charakterisierung von Polymer-Lösungen und Polymer-Tensid-Mischungen. In Ergänzung zu den großen Aggregaten, die die makroskopischen rheologischen Eigenschaften des Systems dominieren, können durch die eingesetzte Einzelmolekültechnik auch deutlich schnellere Aggregate, die nicht über die konventionellen Techniken zugänglich sind, identifiziert werden. Daher kann durch Einzelmolekülspektroskopie eine so genannte Mikroviskosität beobachtet werden, das heißt, die schnelle

## 6. Zusammenfassung

Bewegung kleiner Aggregate durch ein Netzwerk vergleichsweise langsam diffundierender Polymerketten. In dieser Arbeit wird ebenfalls gezeigt, dass die Beobachtung des Diffusionsverhaltens von Polymer-Tensid-Systemen mit FCS ohne kovalente Anknüpfung von Farbstoffen möglich ist. Darüber hinaus ist FCS nur auf die Farbstoffkonzentration empfindlich. Daher können diese Untersuchungen auf einen großen Bereich von Polymerkonzentrationen ausgedehnt werden.

# 7

## Bibliography

- (1) Kwak, J. C. T. *Polymer-Surfactant Systems*; Marcel Dekker: New York, 1998; Vol. 77.
- (2) Goddard, E. D. *Interactions of Surfactants with Polymers and Proteins*; CRC Press: Boca Raton, 1993.
- (3) Evertsson, H.; Nilsson, S.; Welch, C. J.; Sundelof, L. O. "Molecular dynamics in dilute aqueous solutions of ethyl(hydroxyethyl)cellulose and sodium dodecyl sulfate as investigated by proton NMR relaxation". *Langmuir* **1998**, *14*, 6403-6408.
- (4) Kulicke, W. M.; Arendt, O.; Berger, M. "Rheological characterization of the dilatant flow behavior of highly substituted hydroxypropylmethylcellulose solutions in the presence of sodium lauryl sulfate". *Colloid Polym. Sci.* **1998**, *276*, 617-626.
- (5) Loeffroth, J. E.; Johansson, L.; Norman, A. C.; Wettstroem, K. "Interactions between surfactants and polymers. I: HPMC". *Prog. Colloid Polym. Sci.* **1991**, *84*, 73-77.

## 7. Bibliography

- (6) Nystroem, B.; Thuresson, K.; Lindman, B. "Rheological and dynamic light-scattering studies on aqueous solutions of a hydrophobically modified nonionic cellulose ether and its unmodified analog". *Langmuir* **1995**, *11*, 1994-2002.
- (7) Lochhead, R. Y.; Huisinga, L. R. "A brief review of polymer/surfactant interaction". *Cosmetics & Toiletries* **2004**, *119*, 37-38,40-42,44-46.
- (8) Evertsson, H.; Nilsson, S. "Microviscosity in clusters of ethyl hydroxyethyl cellulose and sodium dodecyl sulfate formed in dilute aqueous solutions as determined with fluorescence probe techniques". *Macromolecules* **1997**, *30*, 2377-2385.
- (9) Hoff, E.; Nystroem, B.; Lindman, B. "Polymer-Surfactant Interactions in Dilute Mixtures of a Nonionic Cellulose Derivative and an Anionic Surfactant". *Langmuir* **2001**, *17*, 28-34.
- (10) Persson, B.; Nilsson, S.; Sundelof, L. O. "On the characterization principles of some technically important water-soluble nonionic cellulose derivatives .2. Surface tension and interaction with a surfactant". *Carbohydr. Polym.* **1996**, *29*, 119-127.
- (11) Alli, D.; Bolton, S.; Gaylord, N. G. "Hydroxypropyl methyl cellulose-anionic surfactant interactions in aqueous systems". *J. Appl. Polym. Sci.* **1991**, *42*, 947-956.
- (12) Singh, S. K.; Nilsson, S. "Thermodynamics of interaction between some cellulose ethers and SDS by titration microcalorimetry - II. Effect of polymer hydrophobicity". *J. Colloid Interface Sci.* **1999**, *213*, 152-159.
- (13) Bai, D.; Khin, C. C.; Chen, S. B.; Tsai, C.-C.; Chen, B.-H. "Interaction between a Nonionic Surfactant and a Hydrophobically Modified 2-Hydroxyethyl Cellulose". *J. Phys. Chem. B* **2005**, *109*, 4909-4916.
- (14) Carlsson, A.; Karlstroem, G.; Lindman, B. "Characterization of the interaction between a nonionic polymer and a cationic surfactant by

## 7. Bibliography

- the Fourier transform NMR self-diffusion technique". *J. Phys. Chem.* **1989**, *93*, 3673-3677.
- (15) Hammarstroem, A.; Sundeloef, L. O. "NMR study of polymer surfactant interaction in the system HPMC/SDS/water". *Colloid Polym. Sci.* **1993**, *271*, 1129-1133.
- (16) Nilsson, S.; Thuresson, K.; Lindman, B.; Nystroem, B. "Associations in Mixtures of Hydrophobically Modified Polymer and Surfactant in Dilute and Semidilute Aqueous Solutions. A Rheology and PFG NMR Self-Diffusion Investigation". *Macromolecules* **2000**, *33*, 9641-9649.
- (17) Morawetz, H. "Some Applications of Fluorimetry to Synthetic-Polymer Studies". *Science* **1979**, *203*, 405-410.
- (18) Winnik, M. A. "End-to-End Cyclization of Polymer-Chains". *Acc. Chem. Res.* **1985**, *18*, 73-79.
- (19) Winnik, F. M.; Regismond, S. T. A. In *Polymer-surfactant systems*; Kwak, J. C. T., Ed.; Marcel Dekker: New York, 1998; Vol. 77, pp 267-315.
- (20) Erhardt, R.; Boker, A.; Zettl, H.; Kaya, H.; Pyckhout-Hintzen, W.; Krausch, G.; Abetz, V.; Mueller, A. H. E. "Janus micelles". *Macromolecules* **2001**, *34*, 1069-1075.
- (21) Bowden, N. B.; Willets, K. A.; Moerner, W. E.; Waymouth, R. M. "Synthesis of fluorescently labeled polymers and their use in single-molecule imaging". *Macromolecules* **2002**, *35*, 8122-8125.
- (22) Zettl, H.; Hafner, W.; Boker, A.; Schmalz, H.; Lanzendorfer, M.; Muller, A. H. E.; Krausch, G. "Fluorescence correlation spectroscopy of single dye-labeled polymers in organic solvents". *Macromolecules* **2004**, *37*, 1917-1920.
- (23) Liu, R. G.; Gao, X.; Adams, J.; Oppermann, W. "A fluorescence correlation spectroscopy study on the self-diffusion of polystyrene

## 7. Bibliography

- chains in dilute and semidilute solution". *Macromolecules* **2005**, *38*, 8845-8849.
- (24) Humpolickova, J.; Prochazka, K.; Hof, M.; Tuzar, Z.; Spirkova, M. "Fluorescence correlation spectroscopy using octadecylrhodamine B as a specific micelle-binding fluorescent tag; Light scattering and tapping mode atomic force microscopy studies of amphiphilic water-soluble block copolymer micelles". *Langmuir* **2003**, *19*, 4111-4119.
- (25) Matejicek, P.; Humpolickova, J.; Prochazka, K.; Tuzar, Z.; Spirkova, M.; Hof, M.; Webber, S. E. "Hybrid block copolymer micelles with partly hydrophobically modified polyelectrolyte shells in polar and aqueous media: Experimental study using fluorescence correlation spectroscopy, time-resolved fluorescence, light scattering, and atomic force microscopy". *J. Phys. Chem. B* **2003**, *107*, 8232-8240.
- (26) Matejicek, P.; Podhajecka, K.; Humpolickova, J.; Uhlik, F.; Jelinek, K.; Limpouchova, Z.; Prochazka, K.; Spirkova, M. "Polyelectrolyte behavior of polystyrene-block-poly(methacrylic acid) micelles in aqueous solutions at low ionic strength". *Macromolecules* **2004**, *37*, 10141-10154.
- (27) Zhao, J.; Granick, S. "Polymer lateral diffusion at the solid-liquid interface". *J. Am. Chem. Soc.* **2004**, *126*, 6242-6243.
- (28) Sukhishvili, S. A.; Chen, Y.; Muller, J. D.; Gratton, E.; Schweizer, K. S.; Granick, S. "Surface diffusion of poly(ethylene glycol)". *Macromolecules* **2002**, *35*, 1776-1784.
- (29) Loos, K.; Boker, A.; Zettl, H.; Zhang, A. F.; Krausch, G.; Muller, A. H. E. "Micellar aggregates of amylose-block-polystyrene rod-coil block copolymers in water and THF". *Macromolecules* **2005**, *38*, 873-879.
- (30) Erhardt, R.; Zhang, M. F.; Boker, A.; Zettl, H.; Abetz, C.; Frederik, P.; Krausch, G.; Abetz, V.; Muller, A. H. E. "Amphiphilic Janus micelles with polystyrene and poly(methacrylic acid) hemispheres". *J. Am. Chem. Soc.* **2003**, *125*, 3260-3267.

## 7. Bibliography

- (31) Pristinski, D.; Kozlovskaya, V.; Sukhishvili Svetlana, A. "Fluorescence correlation spectroscopy studies of diffusion of a weak polyelectrolyte in aqueous solutions". *J. Chem. Phys.* **2005**, *122*, 14907.
- (32) Norenberg, R.; Klingler, J.; Horn, D. "Study of the interactions between poly(vinyl pyrrolidone) and sodium dodecyl sulfate by fluorescence correlation spectroscopy". *Angew. Chem., Int. Ed.* **1999**, *38*, 1626-1629.
- (33) Yu, L. L.; Tan, M. Y.; Ho, B.; Ding, J. L.; Wohland, T. "Determination of critical micelle concentrations and aggregation numbers by fluorescence correlation spectroscopy: Aggregation of a lipopolysaccharide". *Anal. Chim. Acta* **2006**, *556*, 216-225.
- (34) Zettl, H.; Portnoy, Y.; Gottlieb, M.; Krausch, G. "Investigation of Micelle Formation by Fluorescence Correlation Spectroscopy". *J. Phys. Chem. B* **2005**, *109*, 13397-13401.
- (35) Arisz, P. W.; Kauw, H. J. J.; Boon, J. J. "Substituent Distribution Along the Cellulose Backbone in O-Methylcelluloses Using Gc and Fab-Ms for Monomer and Oligomer Analysis". *Carbohydr. Res.* **1995**, *271*, 1-14.
- (36) Sarkar, N. "Thermal Gelation Properties of Methyl and Hydroxypropyl Methylcellulose". *J. Appl. Polym. Sci.* **1979**, *24*, 1073-1087.
- (37) Mayers, D. *Surfactant Science and Technology*; VCH Publishers: New York, 1988.
- (38) Evans, D. F. *The Colloidal Domain : Where Physics, Chemistry, biology, and Technology Meet*, Second ed.; Wiley-VCH: New York, 1999.
- (39) Israelachvili, J. N. *Intermolecular and surface forces*, Second ed.; Academic Press: New York, 1991.

## 7. Bibliography

- (40) Lange, R. K. *Surfactants A Practical Handbook*; Hanser Publishers: Munich, 1999; Vol. 237.
- (41) Zimin, D. *Synergetic Effects of Polymer-Surfactant Mixtures on Solid-Liquid Interfaces*, Ph.D. Thesis, Universitaet Regensburg, Regensburg, Germany, 2003.
- (42) Schramm, L. L. *Surfactants: Fundamentals and Applications in the Petroleum Industry*; Cambridge University Press: Cambridge, 2000.
- (43) Tadros, T. F. *Surfactants*; Academic Press: London, 1984.
- (44) Benrraou, M.; Bales, B. L.; Zana, R. "Effect of the nature of the counterion on the properties of anionic surfactants. 1. Cmc, ionization degree at the cmc and aggregation number of micelles of sodium, cesium, tetramethylammonium, tetraethylammonium, tetrapropylammonium, and tetrabutylammonium dodecyl sulfates". *J. Phys. Chem. B* **2003**, *107*, 13432-13440.
- (45) Holmberg, K.; Joensson, B.; Kronberg, B.; Lindman, B. *Surfactants and polymers in aqueous solution*, Second ed.; John Wiley & Sons Ltd., 2002.
- (46) Shinoda, K.; Yamaguchi, N.; Carlsson, A. "Physical Meaning of the Krafft Point - Observation of Melting Phenomenon of Hydrated Solid Surfactant at the Krafft Point". *J. Phys. Chem.* **1989**, *93*, 7216-7218.
- (47) Holmberg, K., Ed. *Handbook of Applied Surface and Colloid Chemistry*; John Wiley & Sons, Ltd.: West Sussex, 2002; Vol. 1.
- (48) Diamant, H.; Andelman, D. "Self-assembly in mixtures of polymers and small associating molecules". *Macromolecules* **2000**, *33*, 8050-8061.
- (49) Zimmerman, S. B.; Murphy, L. D. "Electrophoresis of polyethylene glycols and related materials as sodium dodecyl sulfate complexes". *Anal. Biochem.* **1996**, *234*, 190-193.

## 7. Bibliography

- (50) Stefansson, M. "Surfactant-induced electrophoretic mobility of intact cellulose polymer derivatives". *Anal. Chem.* **2003**, *75*, 281-287.
- (51) Wittgren, B.; Stefansson, M.; Porsch, B. "Interactions between sodium dodecyl sulphate and non-ionic cellulose derivatives studied by size exclusion chromatography with online multi-angle light scattering and refractometric detection". *Journal of Chromatography, A* **2005**, *1082*, 166-175.
- (52) Stilbs, P. In *Polymer-surfactant systems*; Kwak, J. C. T., Ed.; Marcel Dekker: New York, 1998; Vol. 77, pp 239-266.
- (53) Pettersson, E.; Topgaard, D.; Stilbs, P.; Soederman, O. "Surfactant/Nonionic Polymer Interaction. A NMR Diffusometry and NMR Electrophoretic Investigation". *Langmuir* **2004**, *20*, 1138-1143.
- (54) Griffith, P. C.; Stilbs, P.; Howe, A. M.; Cosgrove, T. "A self-diffusion study of the complex formed by sodium dodecyl sulfate and gelatin in aqueous solutions". *Langmuir* **1996**, *12*, 2884-2893.
- (55) Soederman, O.; Stilbs, P.; Price, W. S. "NMR studies of surfactants". *Concepts Magn. Reson., Part A* **2004**, *23A*, 121-135.
- (56) Witte, F. M.; Buwalda, P. L.; Engberts, J. B. F. N. "Micelle-polymer complexes as studied by the ESR spin probe technique". *Colloid & Polymer Science* **1987**, *V265*, 42-44.
- (57) Shirahama, K.; Tohdo, M.; Murahashi, M. "The interaction between surfactant and polymer as observed by a spin probe method". *J. Colloid Interface Sci.* **1982**, *86*, 282-283.
- (58) Nilsson, S.; Goldraich, M.; Lindman, B.; Talmon, Y. "Novel organized structures in mixtures of a hydrophobically modified polymer and two oppositely charged surfactants". *Langmuir* **2000**, *16*, 6825-6832.
- (59) Goldraich, M.; Schwartz, J. R.; Burns, J. L.; Talmon, Y. "Microstructures formed in a mixed system of a cationic polymer and an anionic surfactant". *Coll. Surfaces A Phy Engn* **1997**, *125*, 231-244.

## 7. Bibliography

- (60) Talmon, Y. In *Modern Characterization Methods of Surfactant Systems*; Binks, B. P., Ed.; Marcel Dekker, Inc.: New York, 1999; Vol. 83, pp 148-177.
- (61) Romani, A. P.; Gehlen, M. H.; Itri, R. "Surfactant-Polymer Aggregates Formed by Sodium Dodecyl Sulfate, Poly(N-vinyl-2-pyrrolidone), and Poly(ethylene glycol)". *Langmuir* **2005**, *21*, 127-133.
- (62) Goldraich, M.; Talmon, Y. In *Amphiphilic Block Copolymers Self-Assembly and Applications*; Alexandridis, P.; Lindman, B., Eds.; Elsevier: Amsterdam, 2000; pp 253-280.
- (63) Sesta, B.; La Mesa, C. "Interactions between surfactants and polymers". *Curr. Top. Col. Inte. Sci.* **2002**, *5*, 261-270.
- (64) Soderman, O.; Stilbs, P. "Nmr-Studies of Complex Surfactant Systems". *Prog. Nucl. Magn. Reson. Spectrosc.* **1994**, *26*, 445-482.
- (65) Stilbs, P. "Fourier transform pulsed-gradient spin-echo studies of molecular diffusion". *Prog. Nucl. Magn. Reson. Spectrosc.* **1987**, *19*, 1-45.
- (66) Breuer, M. M.; Robb, I. D. "Interactions between macromolecules and detergents". *Chemistry & Industry* **1972**, 530-535.
- (67) Lewis, K. E.; Robinson, C. P. "Interaction of Sodium Dodecyl Sulfate with Methyl Cellulose and Polyvinyl Alcohol". *J. Colloid Interface Sci.* **1970**, *32*, 539-546.
- (68) Sakamoto, N. "Viscometric Studies on the Methyl Cellulose Sodium Dodecyl-Sulfate Complex in Aqueous-Solution". *Polymer* **1987**, *28*, 288-292.
- (69) Dhara, D.; Shah, D. O. "Stability of sodium dodecyl sulfate micelles in the presence of a range of water-soluble polymers: A pressure-jump study". *J. Phys. Chem. B* **2001**, *105*, 7133-7138.

## 7. Bibliography

- (70) Evertsson, H.; Nilsson, S. "Microviscosity in dilute aqueous solutions of SDS and non-ionic cellulose derivatives of different hydrophobicity: fluorescence probe investigations". *Carbohydr. Polym.* **1998**, *35*, 135-144.
- (71) Kundu, P. P.; Kundu, M. "Effect of salts and surfactant and their doses on the gelation of extremely dilute solutions of methyl cellulose". *Polymer* **2001**, *42*, 2015-2020.
- (72) Kobayashi, K.; Huang, C. I.; Lodge, T. P. "Thermoreversible gelation of aqueous methylcellulose solutions". *Macromolecules* **1999**, *32*, 7070-7077.
- (73) Takahashi, M.; Shimazaki, M.; Yamamoto, J. "Thermoreversible gelation and phase separation in aqueous methyl cellulose solutions". *J. Polym. Sci., Part B: Polym. Phys.* **2001**, *39*, 91-100.
- (74) Ibbett, R. N.; Philp, K.; Price, D. M. "C-13 Nmr-Studies of the Thermal-Behavior of Aqueous-Solutions of Cellulose Ethers". *Polymer* **1992**, *33*, 4087-4094.
- (75) Desbrieres, J.; Hirrien, M.; Rinaudo, M. "A calorimetric study of methylcellulose gelation". *Carbohydr. Polym.* **1998**, *37*, 145-152.
- (76) Nishinari, K.; Hofmann, K. E.; Kohyama, K.; Nishinari, N. "Gel-sol transition of methylcellulose". *Macromol. Chem. Physic.* **1997**, *198*, 1217-1226.
- (77) Li, L. "Thermal gelation of methylcellulose in water: Scaling and thermoreversibility". *Macromolecules* **2002**, *35*, 5990-5998.
- (78) Desbrieres, J.; Hirrien, M.; Ross-Murphy, S. B. "Thermogelation of methylcellulose: rheological considerations". *Polymer* **2000**, *41*, 2451-2461.
- (79) Li, L.; Thangamathesvaran, P. M.; Yue, C. Y.; Tam, K. C.; Hu, X.; Lam, Y. C. "Gel network structure of methylcellulose in water". *Langmuir* **2001**, *17*, 8062-8068.

## 7. Bibliography

- (80) Sekiguchi, Y.; Sawatari, C.; Kondo, T. "A gelation mechanism depending on hydrogen bond formation in regioselectively substituted O-methylcelluloses". *Carbohydr. Polym.* **2003**, *53*, 145-153.
- (81) Takahashi, M.; Shimazaki, M. "Formation of junction zones in thermoreversible methylcellulose gels". *J Polym Sci Pol Phys* **2001**, *39*, 943-946.
- (82) Hirrien, M.; Chevillard, C.; Desbrieres, J.; Axelos, M. A. V.; Rinaudo, M. "Thermogelation of methylcelluloses: new evidence for understanding the gelation mechanism". *Polymer* **1998**, *39*, 6251-6259.
- (83) Banks, S. R.; Sammon, C.; Melia, C. D.; Timmins, P. "Monitoring the thermal gelation of cellulose ethers in situ using attenuated total reflectance fourier transform infrared spectroscopy". *Appl. Spectrosc.* **2005**, *59*, 452-459.
- (84) Liang, H. F.; Hong, M. H.; Ho, R. M.; Chung, C. K.; Lin, Y. H.; Chen, C. H.; Sung, H. W. "Novel method using a temperature-sensitive polymer (methylcellulose) to thermally gel aqueous alginate as a pH-sensitive hydrogel". *Biomacromolecules* **2004**, *5*, 1917-1925.
- (85) Xu, Y.; Li, L. "Thermoreversible and salt-sensitive turbidity of methylcellulose in aqueous solution". *Polymer* **2005**, *46*, 7410-7417.
- (86) Xu, Y.; Wang, C.; Tam, K. C.; Li, L. "Salt-assisted and salt-suppressed sol-gel transitions of methylcellulose in water". *Langmuir* **2004**, *20*, 646-652.
- (87) Xu, Y. R.; Li, L.; Zheng, P. J.; Lam, Y. C.; Hu, X. "Controllable gelation of methylcellulose by a salt mixture". *Langmuir* **2004**, *20*, 6134-6138.
- (88) Wang, Q.; Li, L. "Effects of molecular weight on thermoreversible gelation and gel elasticity of methylcellulose in aqueous solution". *Carbohydr. Polym.* **2005**, *62*, 232-238.

## 7. Bibliography

- (89) Savage, A. B. "Temperature-Viscosity Relationships for Water-Soluble Cellulose Ethers". *Ind Eng Chem* **1957**, *49*, 99-103.
- (90) Wang, Q.; Li, L.; Liu, E.; Xu, Y.; Liu, J. "Effects of SDS on the sol-gel transition of methylcellulose in water". *Polymer* **2006**, *47*, 1372-1378.
- (91) Holmberg, C.; Nilsson, S.; Singh, S. K.; Sundelof, L. O. "Hydrodynamic and Thermodynamic Aspects of the Sds Ehec Water-System". *J. Phys. Chem.* **1992**, *96*, 871-876.
- (92) Elson, E. L.; Magde, D. "Fluorescence correlation spectroscopy. I. Conceptual basis and theory". *Biopolymers* **1974**, *13*, 1-27.
- (93) Magde, D.; Elson, E. L.; Webb, W. W. "Fluorescence correlation spectroscopy. II. Experimental realization". *Biopolymers* **1974**, *13*, 29-61.
- (94) Rigler, R.; Elson, E. S. *Fluorescence Correlation Spectroscopy: Theory and Applications*; Springer: Berlin, 2001; Vol. 65.
- (95) Zeiss, *Application Manual LSM 510 - Confocor 2*, Carl Zeiss Advanced Imaging Microscopy, 2001.
- (96) Schwille, P. "Fluorescence correlation spectroscopy and its potential for intracellular applications". *Cell Biochem. Biophys.* **2001**, *34*, 383-408.
- (97) Koppel, D. E.; Axelrod, D.; Schlessinger, J.; Elson, E. L.; Webb, W. W. "Dynamics of Fluorescence Marker Concentration as a Probe of Mobility". *Biophys. J.* **1976**, *16*, 1315-1329.
- (98) Schwille, P.; Haustein, E. *Fluorescence Correlation Spectroscopy: An Introduction to its Concepts and Applications*; Biophysics Textbook Online (BTOL), 2002.
- (99) Krichevsky, O.; Bonnet, G. "Fluorescence correlation spectroscopy: the technique and its applications". *Rep. Prog. Phys.* **2002**, *65*, 251-297.

## 7. Bibliography

- (100) Widengren, J.; Mets, U.; Rigler, R. "Fluorescence Correlation Spectroscopy of Triplet-States in Solution - A Theoretical and Experimental-Study". *J. Phys. Chem.* **1995**, *99*, 13368-13379.
- (101) Zettl, H. *Labview program for FCS analysis*, Physical Chemistry II, University of Bayreuth, Bayreuth, 2001.
- (102) Meseth, U.; Wohland, T.; Rigler, R.; Vogel, H. "Resolution of fluorescence correlation measurements". *Biophys. J.* **1999**, *76*, 1619-1631.
- (103) Milon, S.; Hovius, R.; Vogel, H.; Wohland, T. "Factors influencing fluorescence correlation spectroscopy measurements on membranes: simulations and experiments". *Chem Phys* **2003**, *288*, 171-186.
- (104) Saffarian, S.; Elson, E. L. "Statistical analysis of fluorescence correlation spectroscopy: The standard deviation and bias". *Biophys. J.* **2003**, *84*, 2030-2042.
- (105) Wohland, T.; Rigler, R.; Vogel, H. "The standard deviation in fluorescence correlation spectroscopy". *Biophys. J.* **2001**, *80*, 2987-2999.
- (106) Zettl, H. *Setup of temperature dependent FCS measurements*, Physical Chemistry II, University of Bayreuth, Bayreuth, 2004.
- (107) Shenoy, V. A. *Rheology of Filled Polymer Systems*; Kluwer Academic Publishers: London, 1999.
- (108) Crassous, J. J.; Regisser, R.; Ballauff, M.; Willenbacher, N. "Characterization of the viscoelastic behavior of complex fluids using the piezoelastic axial vibrator". *J Rheol* **2005**, *49*, 851-863.
- (109) van Os, N. M.; Haak, J. R.; Rupert, L. A. M., Eds. *Physico-chemical properties of selected anionic, cationic and nonionic surfactants*; Elsevier: Amsterdam, 1993.
- (110) Winnik, M. A.; Li, X. B.; Guillet, J. E. "Cyclization Dynamics of Polymers .13. Effects of Added Polymer on the Conformation and

## 7. Bibliography

Dynamics of Polystyrene Containing Evenly Spaced Pyrene Groups". *Macromolecules* **1984**, *17*, 699-702.

- (111) Irondi, K.; Zhang, M. Z.; Duhamel, J. "Study of the semidilute solutions of poly(N,N-dimethylacrylamide) by fluorescence and its implications to the kinetics of coil-to-globule transitions". *J. Phys. Chem. B* **2006**, *110*, 2628-2637.
- (112) Jimenez-Regalado, E.; Selb, J.; Candau, F. "Effect of surfactant on the viscoelastic behavior of semidilute solutions of multisticker associating polyacrylamides". *Langmuir* **2000**, *16*, 8611-8621.
- (113) Bezzabotnov, V. Y.; Borbely, S.; Cser, L.; Farago, B.; Gladkih, I. A.; Ostanovich, Y. M.; Vass, S. "Temperature and concentration dependence of properties of sodium dodecyl sulfate micelles determined from small angle neutron scattering experiments". *J. Phys. Chem.* **1988**, *92*, 5738-5743.
- (114) Malliaris, A.; Lemoigne, J.; Sturm, J.; Zana, R. "Temperature-Dependence of the Micelle Aggregation Number and Rate of Intramicellar Excimer Formation in Aqueous Surfactant Solutions". *J. Phys. Chem.* **1985**, *89*, 2709-2713.
- (115) Shah, S. S.; Jamroz, N. U.; Sharif, Q. M. "Micellization parameters and electrostatic interactions in micellar solution of sodium dodecyl sulfate (SDS) at different temperatures". *Colloids and Surfaces A: Physicochemical and Engineering Aspects* **2001**, *178*, 199-206.
- (116) Szymanski, J.; Patkowski, A.; Wilk, A.; Garstecki, P.; Holyst, R. "Diffusion and Viscosity in a Crowded Environment: from Nano- to Macroscale". *J. Phys. Chem. B* **2006**, *110*, 25593-25597.
- (117) John Bosco, S.; Zettl, H.; Crassous, J. J.; Ballauff, M.; Krausch, G. "Interactions between Methyl Cellulose and Sodium Dodecyl Sulfate in Aqueous Solution Studied by Single Molecule Fluorescence Correlation Spectroscopy". *Macromolecules* **2006**, *39*, 8793-8798.

## 7. Bibliography

# 8

## List of publications

During the course of this thesis the following papers have been published (/in preparation):

 John Bosco, S.; Zettl, H.; Crassous, J.J; Ballauff, M.; Krausch, G. “Interactions between Methyl Cellulose and Sodium Dodecyl Sulfate in Aqueous Solution Studied by Single Molecule Fluorescence Correlation Spectroscopy” *Macromolecules*, **2006**, 39, 8793-8798.

 John Bosco, S.; Zettl, H.; Crassous, J.J; Ballauff, M.; Krausch, G. “Effect of Additives on Gelation of Methyl Cellulose in Aqueous Solution studied by Fluorescence Correlation Spectroscopy” (Manuscript in preparation).

 John Bosco, S.; Zettl, H.; Crassous, J.J; Ballauff, M.; Krausch, G. “Effect of temperature on the dynamics of micelle A single molecule study of the interactions between methyl cellulose and sodium dodecyl sulfate in

aqueous solution by fluorescence correlation spectroscopy” (Manuscript in preparation).

# Acknowledgements

With the support of the following people I could finish this thesis successfully and would like to express my gratitude to all of them.

It is my great pleasure to thank Prof. Georg Krausch for giving an opportunity to do research in this interesting field under his supervision. His immense guidance especially in the critical situations always motivated me to work hard towards my project. I thank him for his outstanding ideas, discussion, and optimistic approach for my thesis work. I am extremely proud to have such a noble and friendly person as my Ph.D supervisor.

I thank Prof. M. Mathias Balluaff for his excellent co-operation and fruitful discussions to publish my results. He introduced me to several relevant experts to tackle the research problems in an easier way and I should especially thank him for his great support.

## Acknowledgements

I am also thankful to Dr. Frank Schubert for his excellent co-operation at the start of my research at PC II by helping me in getting acquainted with all the available facilities. With his moral support and timely help, I had lot of opportunities to learn new things in short time. I consider myself to be fortunate to have a nice friend like him.

I thank Jérôme Crassous for his constructive suggestions and novel ideas to build up on my research project whenever required.

Dr. Markus Drechsler, Prof. Ishi Talmon are gratefully acknowledged for their patience, invaluable contributions and tireless enumerable attempts to get very nice Cryo-TEM images.

I thank Dr. Heiko Zettl for helping me to handle FCS and relevant software at the start. I acknowledge Markus Ruppel and Markus Burkhardt for their great help in using SLS and turbidity instruments respectively.

I thank Günther Jutz for his great help to translate the summary into German. His co-operation to organize the things in lab is gratefully acknowledged. I thank Kristin Schmidt and Heiko Schoberth for their timely help to solve my computer problems.

I thank the complete crew of PCII, Dr. Wolfgang Häfner, Prof. Alexander Böker, Prof. Andreas Fery, Dr. Arnaud Chiche, Dr. Helmut Hänsel, Dr. Armin Knoll, Dr. Marina Lysetska, Dr. Larisa Tsorkova, Dr. Chun Wang, Dr. Denis Zimin, Thomas Czubak, Nicole Glaser, Anne Horn, Andriana Hovert, Sebastian Hoffmann, Markus Hund, Sven Hüttner, Christian Karl, Carmen Kunert, Sergej Kutuzov, Eva Max, Adriana Mihut, Nathelie Mougine, Violetta Olszowka, Melanie Pretzl, Gustav Sauer, Kerstin Schindler, Stephan Schmidt,

## Acknowledgements

Alexandra Schweikart, Alexandra Sperschneider, Christa Weber and Ute Zettl for a very nice working atmosphere.

Last but not the least; I thank Mrs. Sybille Zimmermann for her bureaucratic work with lot patience and kindness. With her strong support and caring, I always felt at home.

I express my gratitude to my family members for their strong support, motivation and encouragement which always inspired me to work meticulously.

## Acknowledgements

## Curriculum Vitae

Name : John Bosco Stanislaus

Date of Birth : 2<sup>nd</sup> May 1977, in Kalugumalai, TN / India

School Education : 1987 – 1992 R.C. Susai High School,  
Kalugumalai, TN, India.

1992 – 1994 Govt. Hr. Sec. School,  
Kalugumalai, TN, India.

Scientific Background : 1994 – 1997 Bachelor of Science (Chemistry)  
Maduri Kamaraj University, India  
(A.N.J.A College, Sivakasi, India)

1997 – 1999 Master of Science (Chemistry)  
Bharathidhasan University, India.  
(St Joseph's College, Trichy, India)

1999 – 2000 Master of Philosophy (Chemistry)  
University of Madras, Chennai, India  
(Loyola College, Chennai, India)

2001 – 2002 Bachelor of Education (B.Ed)  
University of Madras, Chennai, India  
(Institute of Advanced Studies in  
Education, Chennai, India.)

Teaching : 2000 - 2003 Loyola College, Chennai, TN, India.

Ph.D : 2003 March – 2007 May  
University of Bayreuth, Bayreuth.  
Supervisor: Prof. G. Krausch  
Topic: Single Molecule Study of  
Polymer-Surfactant Interactions.

Homepage : <http://johnbosco.tk>

## Curriculum Vitae

## **Erklärung**

Die vorliegende Arbeit wurde von mir selbstständig verfasst und ich habe dabei keine anderen als die angegebenen Hilfsmittel und Quellen benutzt.

Ferner habe ich nicht versucht, anderweitig mit oder ohne Erfolg eine Dissertation einzureichen oder mich der Doktorprüfung zu unterziehen.

Bayreuth, den 16.05.2007

John Bosco Stanislaus